

# **Behavior of Field-Cast Ultra-High Performance Concrete Bridge Deck Connections Under Cyclic and Static Structural Loading**

**November 2010**

**NTIS Accession No. PB2011-101995**

**FHWA Publication No. FHWA-HRT-11-023**



U.S. Department of Transportation  
**Federal Highway Administration**

## FOREWORD

With the ever increasing congestion and deterioration of our nation's highway system, a need exists to develop highly durable and rapidly constructed infrastructure systems. Durable bridge structures that would require less intrusive maintenance and would exhibit longer life spans thus maximizing the use of the facility are highly desirable. Expediting bridge construction can minimize traffic flow disruptions. Ultra-high performance concrete (UHPC) is an advanced construction material which affords new opportunities to envision the future of the highway infrastructure. The Federal Highway Administration has been engaged in research on the optimal uses of UHPC in the highway bridge infrastructure since 2001 through its Bridge of the Future initiative. This report presents results of a study aimed at assessing the performance of field-cast UHPC connections for modular bridge deck components. Connections between modular components are necessary, but have also been widely recognized to have performance shortcomings. The connection systems investigated herein facilitate simplified construction while simultaneously allowing the bridge deck to emulate or supersede cast-in-place deck performance.

This report corresponds to the TechBrief titled "Field-Cast UHPC Connections for Modular Bridge Deck Elements" (FHWA-HRT-11-022). This report is being distributed through the National Technical Information Service for informational purposes. The content in this report is being distributed "as is" and may contain editorial or grammatical errors.

### **Notice**

This document is disseminated under the sponsorship of the U.S. Department of Transportation in the interest of information exchange. The U.S. Government assumes no liability for the use of the information contained in this document.

The U.S. Government does not endorse products or manufacturers. Trademarks or manufacturers' names appear in this report only because they are considered essential to the objective of the document.

### **Quality Assurance Statement**

The Federal Highway Administration (FHWA) provides high-quality information to serve Government, industry, and the public in a manner that promotes public understanding. Standards and policies are used to ensure and maximize the quality, objectivity, utility, and integrity of its information. FHWA periodically reviews quality issues and adjusts its programs and processes to ensure continuous quality improvement.

## TECHNICAL REPORT DOCUMENTATION PAGE

1. Report No. FHWA-HRT-11-023	2. Government Accession No. NTIS PB2011-101995	3. Recipient's Catalog No.	
4. Title and Subtitle Behavior of Field-Cast Ultra-High Performance Concrete Bridge Deck Connections Under Cyclic and Static Structural Loading		5. Report Date November 2010	
		6. Performing Organization Code:	
7. Author(s) Benjamin A. Graybeal		8. Performing Organization Report No.	
9. Performing Organization Name and Address Office of Infrastructure Research & Development Federal Highway Administration 6300 Georgetown Pike McLean, VA 22101-2296		10. Work Unit No.	
		11. Contract or Grant No.	
12. Sponsoring Agency Name and Address Office of Infrastructure Research & Development Federal Highway Administration 6300 Georgetown Pike McLean, VA 22101-2296		13. Type of Report and Period Covered Final Report: 2009-2010	
		14. Sponsoring Agency Code HRDI-40	
15. Supplementary Notes			
<p>16. Abstract</p> <p>The use of modular bridge deck components has the potential to produce higher quality, more durable bridge decks; however, the required connections have often proved lacking, resulting in less than desirable overall system performance. Advanced cementitious composite materials whose mechanical and durability properties far exceed those of conventional concretes present an opportunity to significantly enhance the performance of field-cast connections thus facilitating the wider use of modular bridge deck systems. Ultra-high performance concrete (UHPC) represents a class of such advanced cementitious composite materials. Of particular interest here, UHPCs can exhibit both exceptional bond when cast against previously cast concrete and can significantly shorten the development length of embedded discrete steel reinforcement. These properties allow for a redesign of the modular component connection, facilitating simplified construction and enhanced long-term system performance.</p> <p>This study investigated the structural performance of field-cast UHPC connections for modular bridge deck components. The transverse and longitudinal connection specimens simulated the connections between precast deck panels and the connections between the top flanges of deck-bulb-tee girders, respectively. Testing included both cyclic and static loadings. The results demonstrated that the field-cast UHPC connection facilitates the construction of an emulative bridge deck system whose behaviors should meet or exceed those of a conventional cast-in-place bridge deck.</p> <p>This report corresponds to the TechBrief titled "Field-Cast UHPC Connections for Modular Bridge Deck Elements" (FHWA-HRT-11-022).</p>			
17. Key Words Ultra-high performance concrete, UHPC, fiber-reinforced concrete, bridges, accelerated construction, durable infrastructure systems, non-contact lap splice, precast deck panel connection, adjacent decked-girder connection, cyclic testing		18. Distribution Statement No restrictions. This document is available through the National Technical Information Service, Springfield, VA 22161.	
19. Security Classif. (of this report) Unclassified	20. Security Classif. (of this page) Unclassified	21. No. of Pages 106	22. Price N/A

# SI\* (MODERN METRIC) CONVERSION FACTORS

## APPROXIMATE CONVERSIONS TO SI UNITS

Symbol	When You Know	Multiply By	To Find	Symbol
<b>LENGTH</b>				
in	inches	25.4	millimeters	mm
ft	feet	0.305	meters	m
yd	yards	0.914	meters	m
mi	miles	1.61	kilometers	km
<b>AREA</b>				
in <sup>2</sup>	square inches	645.2	square millimeters	mm <sup>2</sup>
ft <sup>2</sup>	square feet	0.093	square meters	m <sup>2</sup>
yd <sup>2</sup>	square yard	0.836	square meters	m <sup>2</sup>
ac	acres	0.405	hectares	ha
mi <sup>2</sup>	square miles	2.59	square kilometers	km <sup>2</sup>
<b>VOLUME</b>				
fl oz	fluid ounces	29.57	milliliters	mL
gal	gallons	3.785	liters	L
ft <sup>3</sup>	cubic feet	0.028	cubic meters	m <sup>3</sup>
yd <sup>3</sup>	cubic yards	0.765	cubic meters	m <sup>3</sup>
NOTE: volumes greater than 1000 L shall be shown in m <sup>3</sup>				
<b>MASS</b>				
oz	ounces	28.35	grams	g
lb	pounds	0.454	kilograms	kg
T	short tons (2000 lb)	0.907	megagrams (or "metric ton")	Mg (or "t")
<b>TEMPERATURE (exact degrees)</b>				
°F	Fahrenheit	5 (F-32)/9 or (F-32)/1.8	Celsius	°C
<b>ILLUMINATION</b>				
fc	foot-candles	10.76	lux	lx
fl	foot-Lamberts	3.426	candela/m <sup>2</sup>	cd/m <sup>2</sup>
<b>FORCE and PRESSURE or STRESS</b>				
lbf	poundforce	4.45	newtons	N
lbf/in <sup>2</sup>	poundforce per square inch	6.89	kilopascals	kPa
<b>APPROXIMATE CONVERSIONS FROM SI UNITS</b>				
Symbol	When You Know	Multiply By	To Find	Symbol
<b>LENGTH</b>				
mm	millimeters	0.039	inches	in
m	meters	3.28	feet	ft
m	meters	1.09	yards	yd
km	kilometers	0.621	miles	mi
<b>AREA</b>				
mm <sup>2</sup>	square millimeters	0.0016	square inches	in <sup>2</sup>
m <sup>2</sup>	square meters	10.764	square feet	ft <sup>2</sup>
m <sup>2</sup>	square meters	1.195	square yards	yd <sup>2</sup>
ha	hectares	2.47	acres	ac
km <sup>2</sup>	square kilometers	0.386	square miles	mi <sup>2</sup>
<b>VOLUME</b>				
mL	milliliters	0.034	fluid ounces	fl oz
L	liters	0.264	gallons	gal
m <sup>3</sup>	cubic meters	35.314	cubic feet	ft <sup>3</sup>
m <sup>3</sup>	cubic meters	1.307	cubic yards	yd <sup>3</sup>
<b>MASS</b>				
g	grams	0.035	ounces	oz
kg	kilograms	2.202	pounds	lb
Mg (or "t")	megagrams (or "metric ton")	1.103	short tons (2000 lb)	T
<b>TEMPERATURE (exact degrees)</b>				
°C	Celsius	1.8C+32	Fahrenheit	°F
<b>ILLUMINATION</b>				
lx	lux	0.0929	foot-candles	fc
cd/m <sup>2</sup>	candela/m <sup>2</sup>	0.2919	foot-Lamberts	fl
<b>FORCE and PRESSURE or STRESS</b>				
N	newtons	0.225	poundforce	lbf
kPa	kilopascals	0.145	poundforce per square inch	lbf/in <sup>2</sup>

\*SI is the symbol for the International System of Units. Appropriate rounding should be made to comply with Section 4 of ASTM E380. (Revised March 2003)

## TABLE OF CONTENTS

<b>CHAPTER 1. INTRODUCTION .....</b>	<b>1</b>
INTRODUCTION .....	1
OBJECTIVE .....	1
SUMMARY OF APPROACH .....	1
OUTLINE OF REPORT .....	2
<b>CHAPTER 2. BACKGROUND.....</b>	<b>3</b>
INTRODUCTION .....	3
ULTRA-HIGH PERFORMANCE CONCRETE.....	3
FIELD-CAST ULTRA-HIGH PERFORMANCE CONCRETE CONNECTIONS .....	4
<i>Ontario Bridge Projects</i> .....	5
<i>New York State Department of Transportation Bridge Projects</i> .....	7
RECENT MODULAR BRIDGE DECK COMPONENT CONNECTION RESEARCH.....	12
<b>CHAPTER 3. SPECIMEN DESIGN, FABRICATION, AND MATERIAL PROPERTIES</b> <b>.....</b>	<b>14</b>
INTRODUCTION .....	14
SPECIMEN DESIGN .....	14
SPECIMEN FABRICATION .....	22
UHPC MATERIAL PROPERTIES .....	22
HPC MATERIAL PROPERTIES .....	23
MILD STEEL REINFORCEMENT MECHANICAL PROPERTIES .....	23
REINFORCEMENT PULLOUT TEST RESULTS.....	24
<b>CHAPTER 4. TEST PROGRAM, RESULTS, AND ANALYSES.....</b>	<b>27</b>
INTRODUCTION .....	27
TRANSVERSE CONNECTION TEST PROGRAM AND RESULTS.....	27
<i>Specimen 8H</i> .....	33
Cyclic Testing .....	33
Static Testing.....	38
<i>Specimen 8E</i> .....	42
Cyclic Testing .....	42
Static Testing.....	45
<i>Specimen 8G</i> .....	50
Cyclic Testing .....	50
Static Testing.....	54
<i>Specimen 8B</i> .....	58
Cyclic Testing .....	58
Static Testing.....	63
SUMMARY OF TRANSVERSE CONNECTION TEST RESULTS .....	67
LONGITUDINAL CONNECTION TEST PROGRAM AND RESULTS .....	69
<i>Specimen 6H</i> .....	74
Cyclic Testing .....	74

Static Testing .....	80
<i>Specimen 6B</i> .....	84
Cyclic Testing .....	84
LONGITUDINAL CONNECTION TEST COMPILATION OF RESULTS.....	96
<b>CHAPTER 5. CONCLUSIONS .....</b>	<b>99</b>
INTRODUCTION .....	99
CONCLUSIONS .....	99
ONGOING AND FUTURE RESEARCH .....	101
<b>REFERENCES .....</b>	<b>105</b>

## LIST OF FIGURES

Figure 1. Photograph. Longitudinal connections prior to field-casting of UHPC in Route 31 Bridge in Lyons, New York. (Photo courtesy of NYSDOT.) .....	8
Figure 2. Photograph. Placement of UHPC into longitudinal connections between deck-bulb-tee girders in Route 31 Bridge in Lyons, New York. (Photo courtesy of NYSDOT.).....	9
Figure 3. Photograph. Longitudinal connections after field-casting of UHPC in Route 31 Bridge in Lyons, New York. (Photo courtesy of NYSDOT.) .....	10
Figure 4. Photograph. Completed Route 31 Bridge in Lyons, New York. (Photo courtesy of NYSDOT.).....	10
Figure 5. Photograph. Transverse connectin prior to field-casting of UHPC in Route 23 Bridge in Oneonta, New York. (Photo courtesy of NYSDOT.).....	11
Figure 6. Photograph. Field-casting of UHPC for Route 23 Bridge in Oneonta, New York. ....	11
Figure 7. Photograph. Elevation view of Route 23 Bridge in Oneonta, New York. ....	12
Figure 8. Illustration. Layout and rebar plan for panel 8H. ....	17
Figure 9. Illustration. Layout and rebar plan for panel 8E.....	18
Figure 10. Illustration. Layout and rebar plan for panels 8G and 8B. ....	19
Figure 11. Illustration. Layout and rebar plan for panels 6H.....	20
Figure 12. Illustration. Layout and rebar plan for panels 6B. ....	21
Figure 13. Photo. Placement of UHPC into connection. (Photo courtesy of NYSDOT) .....	22
Figure 14. Illustration. Specimen design for reinforcement pullout tests. ....	25
Figure 15. Illustration. Test setup for cyclic loading of panels 8H, 8E, 8G, and 8B. ....	30
Figure 16. Illustration. Test setup for static loading of panels 8H, 8E, 8G, and 8B. ....	31
Figure 17. Photograph. Oblique view of cyclic test setup for panels 8H, 8E, 8G, and 8B.....	31
Figure 18. Illustration. Cyclic loading program for panels 8H, 8E, 8G, and 8B. ....	32
Figure 19. Illustration. Instrumentation for cyclic testing of panels 8H, 8E, 8G, and 8B. ....	32
Figure 20. Illustration. Instrumentation for static testing of panels 8H, 8E, 8G, and 8B. ....	33
Figure 21. Graph. Cyclic test results for panel 8H.....	35
Figure 22. Graph. Strain response for panel 8H after 462,000 cycles. ....	36
Figure 23. Graph. Strain response for panel 8H after 7,137,000 cycles. ....	37
Figure 24. Illustration. Cracking pattern observed on underside of panel 8H after the conclusion of 2.063 million cycles to 71 kN (16 kips), and additional cracks occurring during first cycle to 95 kN (21.3 kips).....	37
Figure 25. Illustration. Cracking pattern observed on underside of panel 8H after 687,000 cycles to 95 kN (21.3 kips) and at the conclusion of cyclic testing.....	38
Figure 26. Graph. Load-deflection response of panel 8H under step-wise loading to failure. ....	39
Figure 27. Graph. Load-strain response of panel 8H under step-wise loading to failure. ....	40
Figure 28. Photograph. Underside of panel 8H near midspan after 40 mm (1.6 inch) of midspan centerline deflection.....	40
Figure 29. Photograph. Top of panel 8H after flexural failure. ....	41
Figure 30. Photograph. Underside of panel 8H at midspan centerline location after flexural failure. ....	41

Figure 31. Illustration. Cracking pattern observed on underside of panel 8H after conclusion of static test. ....	42
Figure 32. Graph. Cyclic test results for panel 8E. ....	44
Figure 33. Graph. Strain response for panel 8E after 5,824,000 cycles. ....	45
Figure 34. Graph. Load-deflection response of panel 8E under step-wise loading to failure. ....	47
Figure 35. Graph. Load-strain response of panel 8E under step-wise loading to failure. ....	47
Figure 36. Photograph. East side and top of panel 8E after 53 mm (2.1 inch) of midspan centerline deflection. ....	48
Figure 37. Photograph. Top of panel 8E after flexural failure. ....	48
Figure 38. Photograph. Underside of panel 8E near midspan centerline location after flexural failure. ....	49
Figure 39. Illustration. Cracking pattern observed on underside of panel 8E after conclusion of static test. ....	50
Figure 40. Graph. Cyclic test results for panel 8G. ....	52
Figure 41. Graph. Strain response for panel 8G after 1,694,000 cycles. ....	53
Figure 42. Graph. Strain response for panel 8G after 7,791,000 cycles. ....	54
Figure 43. Illustration. Cracking pattern observed on underside of panel 8G after the conclusion of cyclic testing. ....	54
Figure 44. Graph. Load-deflection response of panel 8G under step-wise loading to failure. ....	56
Figure 45. Graph. Load-strain response of panel 8G under step-wise loading to failure. ....	56
Figure 46. Photograph. Top of panel 8G after flexural failure. ....	57
Figure 47. Photograph. Underside of panel 8G near midspan centerline location after flexural failure. ....	57
Figure 48. Illustration. Cracking pattern observed on underside of panel 8G after conclusion of static test. ....	58
Figure 49. Graph. Cyclic test results for panel 8B. ....	60
Figure 50. Graph. Strain response for panel 8B after 1,608,000 cycles. ....	61
Figure 51. Graph. Strain response for panel 8B after 7,372,000 cycles. ....	62
Figure 52. Illustration. Cracking pattern observed on underside of panel 8B after the conclusion of cyclic testing. ....	63
Figure 53. Graph. Load-deflection response of panel 8B under step-wise loading to failure. ....	65
Figure 54. Graph. Load-strain response of panel 8B under step-wise loading to failure. ....	65
Figure 55. Photograph. Top of panel 8B after flexural failure. ....	66
Figure 56. Photograph. Underside of panel 8B at midspan centerline location after flexural failure. ....	66
Figure 57. Illustration. Cracking pattern observed on underside of panel 8B after conclusion of static test. ....	67
Figure 58. Illustration. Test setup for cyclic loading of panels 6B and 6H. ....	71
Figure 59. Illustration. Test setup for static loading of panel 6H. ....	72
Figure 60. Photograph. Overhead view showing cyclic test setup for panels 6B and 6H. ....	73
Figure 61. Illustration. Instrumentation for cyclic testing of panels 6H and 6B. ....	73
Figure 62. Illustration. Instrumentation for static testing of panel 6H. ....	74

Figure 63. Graph. Cyclic test results for panel 6H.....	76
Figure 64. Graph. Strain response for panel 6H after 1,555,000 cycles. ....	77
Figure 65. Graph. Strain response for panel 6H after 8,969,000 cycles. ....	78
Figure 66. Illustration. Cracking pattern observed on underside of panel 6H after conclusion of cyclic testing. ....	79
Figure 67. Illustration. Cracking pattern observed on east face of panel 6H after conclusion of cyclic testing. ....	79
Figure 68. Illustration. Cracking pattern observed on west face of panel 6H after conclusion of cyclic testing. ....	80
Figure 69. Graph. Load-deflection response of panel 6H under step-wise loading to failure. ....	81
Figure 70. Graph. Load-strain response of panel 6H under step-wise loading to failure. ....	82
Figure 71. Photograph. Top of panel 6H after flexural failure. ....	82
Figure 72. Photograph. Underside of panel 6H along midspan after failure. ....	83
Figure 73. Illustration. Cracking pattern observed on underside of panel 6H after conclusion of static test. ....	83
Figure 74. Illustration. Cyclic test program for panel 6B. ....	87
Figure 75. Illustration. Cracking pattern observed on underside of panel 6B after the first cycle from 9 to 71 kN (2 to 16 kips). ....	88
Figure 76. Illustration. Cracking pattern observed on underside of panel 6B both after the initial overload and again after 10.1 million cycles of loading from 13 to 95 kN (3 to 21.3 kips). ....	89
Figure 77. Photograph. East side and top of panel 6B after the conclusion of cyclic loading.....	90
Figure 78. Graph. Cyclic test results for panel 6B.....	91
Figure 79. Graph. Strain response for panel 6B after 9,743,000 cycles to 95 kN (21.3 kips). ....	92
Figure 80. Graph. Strain response for panel 6B after 1,118,000 cycles to 142 kN (32 kips). ....	93
Figure 81. Graph. Strain response for panel 6B after 190,000 cycles to 178 kN (40 kips). ....	94
Figure 82. Illustration. Cross section at rebar failure plane for panel 6B including photographs of twelve of the rebar. ....	95

## LIST OF TABLES

Table 1. Typical field-cast UHPC mix composition. ....	3
Table 2. Typical field-cast UHPC material properties. ....	4
Table 3. Test specimens.....	14
Table 4. Cylinder density, compressive strength, and modulus of elasticity test results. ....	23
Table 5. Rebar pullout test results. ....	25

## **CHAPTER 1. INTRODUCTION**

### **INTRODUCTION**

There is a growing need for durable and resilient highway bridge construction/reconstruction systems which facilitate rapid completion of on-site activities in order to minimize the impact on the traveling public. Modular components can provide higher quality, accelerated, and safer construction; however, greater offsite prefabrication of bridge components necessitates an increased reliance on the long-term performance of field-installed connections between these components. Connections have often proved lacking, resulting in less than desirable overall system performance.

Bridge decks are heavily stressed throughout their lives by both structural and environmental loadings. Bridge decks are traditionally constructed with cast-in-place conventional concrete, creating a monolithic slab which effectively transmits structural loads but has also frequently been shown to be susceptible to accelerated degradation due to a myriad of factors. The use of modular bridge deck components can facilitate the use of higher quality and likely more durable components in the bridge deck; however, these components are smaller than the entirety of the bridge deck and thus require field-applied connections. Advanced cementitious composite materials whose mechanical and durability properties far exceed those of conventional concretes present the opportunity to significantly enhance the performance of these field-applied connections thus facilitating the wider use of modular bridge deck systems.

Ultra-high performance concrete (UHPC) is an advanced cementitious composite material which has been developed in recent decades. When compared to more conventional cement-based concrete materials, UHPCs tend to exhibit superior properties such as increased strength, durability, and long-term stability. Of particular interest here, UHPCs can exhibit both exceptional bond when cast against previously cast concrete and can significantly shorten the development length of embedded discrete steel reinforcement. These properties allow for a redesign of the modular component connection, facilitating simplified construction and enhanced long-term system performance.

### **OBJECTIVE**

The objective of this research program was to evaluate the structural response of field-cast UHPC connections linking precast concrete bridge deck components.

### **SUMMARY OF APPROACH**

The research discussed herein focuses on assessing the structural performance of field-cast UHPC connections for bridge deck components. Bridge deck components simulating both longitudinal and transverse connections were fabricated and tested under both cyclic and static wheel patch loadings. Four transverse connection specimens simulated the connections between precast deck panels. These specimens were identical aside from the different discrete reinforcing details, which included straight lapped bars, headed bars, and intersecting hoop bars. The two longitudinal connection specimens simulated the connections between the top flanges of deck-

bulb-tee girders. These two specimens were identical aside from the inclusion of two different discrete reinforcing details, namely straight lapped bars and lapped headed bars.

The tested components simulated a portion of a bridge deck, each 2.4 by 2.152 m (94.5 by 84.7 inch), with a 152-mm (6-inch) wide field-cast UHPC connection at midspan. The specimens were loaded on a simple span with the load applied through a simulated wheel patch placed adjacent to the connection near midspan. Cyclic loads were applied first, with the test program including at least 2 million cycles to a load just below the cracking strength of the specimen, followed by at least 5 million cycles to a load larger than the cracking strength of the specimen. After the completion of the cyclic testing, the test specimen was statically loaded to failure.

This loading program was designed to allow for the assessment of three critical behaviors. First, the cyclic loading below the cracking load allowed for the assessment of the cracking performance of the field-cast UHPC and the bonding performance of the UHPC to precast concrete interface. Second, the cyclic loading which generated stresses above the static cracking stress of the specimen allowed for the assessment of the cracking performance of the system, including whether there was any uncontrolled, progressive cracking or any interface debonding. Finally, this loading program allowed for the assessment of the static overload performance of the system, thus providing an indication of whether the system effectively emulated the performance anticipated from a monolithic concrete deck.

## **OUTLINE OF REPORT**

This report is divided into five chapters. Chapters 1 and 2 provide an introduction to the study and relate relevant background information necessary in understanding the study's results. Chapter 3 presents the geometric details of the test specimens along with the mechanical properties of the UHPC and precast concrete included in the study. Chapter 4 presents the test results and an analysis thereof. Finally, Chapter 5 presents the conclusions of this research program.

## CHAPTER 2. BACKGROUND

### INTRODUCTION

This chapter provides background information relevant to the focus of the research effort. A general discussion of UHPC constituent materials and material properties is presented first. Next, prior deployments of field-cast UHPC connection technology are presented. These include early work on this topic completed in Denmark and Sweden, as well as recent deployments in Ontario and New York. Finally, a few significant research efforts pertaining to the use of field-cast connections between precast concrete modular bridge components are presented.

### ULTRA-HIGH PERFORMANCE CONCRETE

The term UHPC refers to a class of advanced cementitious composite materials. Many of the technological advances in the field of cement and concrete science have been brought together in the development of this set of concretes. In general terms, these concretes can be classified as high strength, fiber-reinforced cementitious composites with discontinuous pore structures and enhanced durability properties. These concretes tend to have exceptionally low water-to-cementitious materials ratios and an optimized gradation of granular materials.

Although the general concepts which lead to the advanced performance characteristics of UHPC are well known, the commercial availability of UHPC and the development of locally-sourced UHPC mixes has been limited in the United States. The availability of UHPC has developed differently in other parts of the world, most notably Europe, where multiple prebagged and locally-sourced UHPCs are available. The specific UHPC investigated in this study is a product of a major worldwide construction materials manufacturer and supplier. It is currently the only product of this type that is widely available in the U.S. in the quantities necessary for large scale infrastructure applications. Table 1 provides a typical UHPC composition<sup>(1)</sup>.

**Table 1. Typical field-cast UHPC mix composition.**

<b>Material</b>	<b>Amount (kg/m<sup>3</sup> (lb/yd<sup>3</sup>))</b>	<b>Percent by Weight</b>
Portland Cement	712 (1,200)	28.5
Fine Sand	1,020 (1,720)	40.8
Silica Fume	231 (390)	9.3
Ground Quartz	211 (355)	8.4
Superplasticizer	30 (51)	1.2
Steel Fibers	156 (263)	6.2
Water	130 (218)	5.2

As reported in reference (1), the constituent material proportions were determined, in part, based on an optimization of the granular mixture. This method allows for a finely graded and highly homogeneous concrete matrix. Fine sand, generally between 150 and 600 micrometers (0.006 and 0.024 inch), is dimensionally the largest granular material. The next largest particle is cement with an average diameter of approximately 15  $\mu\text{m}$  (0.0006 inch). Of similar size is the

crushed quartz with an average diameter of 10  $\mu\text{m}$  (0.0004 inch). The smallest particle, the silica fume, has a diameter small enough to fill the interstitial voids between the cement and the crushed quartz particles. Dimensionally, the largest constituent in the mix is the steel fiber reinforcement. In this study, the fibers in the mix had a diameter of 0.2 mm (0.008 inch), a length of 12.7 mm (0.5 inch), and a minimum tensile strength of 2600 MPa (377 ksi). The fibers were included in the mix at two percent by volume. Given the relative sizes of the sand and the fibers, the steel fibers are able to reinforce the concrete matrix on the micro level.

The research program associated with reference (1) characterized the material properties of the same UHPC investigated in this study. A brief summary of the relevant results is presented in Table 2. Note that, as with the UHPC in the specimens tested in this study, these results pertain to UHPC which was cast and cured in an ambient environment.

**Table 2. Typical field-cast UHPC material properties.**

<b>Material Characteristic</b>	<b>Average Result</b>
Density	2,480 kg/m <sup>3</sup> (155 lb/ft <sup>3</sup> )
Compressive Strength (ASTM C39; 28-day strength)	126 MPa (18.3 ksi)
Modulus of Elasticity (ASTM C469; 28-day modulus)	42.7 GPa (6200 ksi)
Split Cylinder Cracking Strength (ASTM C496)	9.0 MPa (1.3 ksi)
Prism Flexure Cracking Strength (ASTM C1018; 305-mm (12-in.) span)	9.0 MPa (1.3 ksi)
Mortar Briquette Cracking Strength (AASHTO T132)	6.2 MPa (0.9 ksi)
Direct Tension Cracking Strength (Axial tensile load)	5.5–6.9 MPa (0.8–1.0 ksi)
Prism Flexural Tensile Toughness (ASTM C1018; 305-mm (12-in.) span)	$I_{30} = 48$
Long-Term Creep Coefficient (ASTM C512; 77 MPa (11.2 ksi) load)	0.78
Long-Term Shrinkage (ASTM C157; initial reading after set)	555 microstrain
Total Shrinkage (Embedded vibrating wire gage)	790 microstrain
Coefficient of Thermal Expansion (AASHTO TP60–00)	$14.7 \times 10^{-6}$ mm/mm/°C ( $8.2 \times 10^{-6}$ in./in./°F)
Chloride Ion Penetrability (ASTM C1202; 28-day test)	360 coulombs
Chloride Ion Permeability (AASHTO T259; 12.7-mm (0.5-in.) depth)	< 0.06 kg/m <sup>3</sup> (< 0.10 lb/yd <sup>3</sup> )
Scaling Resistance (ASTM C672)	No Scaling
Abrasion Resistance (ASTM C944 2x weight; ground surface)	0.73 grams lost (0.026 oz. lost)
Freeze-Thaw Resistance (ASTM C666A; 600 cycles)	RDM = 112%
Alkali-Silica Reaction (ASTM C1260; tested for 28 days)	Innocuous

## **FIELD-CAST ULTRA-HIGH PERFORMANCE CONCRETE CONNECTIONS**

The concept of using the advanced properties of UHPC to significantly modify the design of connections between precast concrete components is not new. In fact, research and deployments in this area date back to at least 1995. At that time, a commercially available UHPC was used as a closure pour material in the connection of slab elements in a building being constructed at Aalborg University. A few years later, a second project at the same university resulted in the use of field-cast UHPC connections both between slab elements and between slabs and columns. In

support and association with these two projects, a series of research projects were completed to assess the bonding performance between the UHPC and straight lengths of mild steel reinforcement<sup>(2,3,4,5)</sup>. Additional research, focused specifically on field-cast UHPC connections for precast bridge deck panels, was completed at Chalmers University<sup>(6,7,8)</sup>.

More recently, the concept of using the properties of UHPC to redesign the connections between modular bridge components has been recognized in North America. Field-cast UHPC connections between prefabricated bridge components have now been implemented in nine bridges in Canada and two in the U.S. A general overview of these deployments is provided below.

### **Ontario Bridge Projects**

The Ministry of Transportation of Ontario (MTO) has been a leader in deployment of field-cast UHPC connection technology. As of late 2010, the MTO had completed construction of nine bridges with UHPC in the connections between precast concrete elements, and had scheduled the completion of an additional seven bridges by the end of 2011. The use of field-cast UHPC in connections between precast concrete modular components has become commonplace in Northwestern Ontario. This region has come to rely on modular bridge construction systems partly due to the remote locations and difficulty in receiving acceptable ready-mix concrete on-site. The use of field-cast UHPC allows for simplified connection details which are anticipated to prove more durable than those constructed with conventional connecting systems. In all cases, the type of UHPC used in the Ontario bridge projects was the same as that used in the research program discussed in this report.

The first bridge, the Rainy Lake Bridge, was constructed on Highway 11 between Fort Frances and Atikokan, Ontario in 2006. This project used precast bridge deck panels to rehabilitate the deck on a single span steel stringer bridge. UHPC was used in the connections between adjacent deck panels as well as in the composite connection between the panels and the girders. The transverse connections between deck panels were 210-mm (8.3-inch) wide and included straight, lapped fiber reinforced polymer (FRP) reinforcing bars. The composite connection between the deck panels and the girders was a series of 210-mm (8.3-inch) wide pockets above each of the five girder lines through which the FRP deck reinforcement passed and into which the shear studs emanated.

The next project, the Sunshine Creek Bridge, was constructed on Highway 11/17 near Thunder Bay, Ontario in 2007. This project included the removal of the existing simple span superstructure and the replacement with 10 adjacent box beams. The longitudinal connections between the beams were completed with a field-cast UHPC detail. The detail included hairpin-shaped FRP reinforcing bars extending into the diamond-shaped shear keys.

In 2008, the Hawk Lake Bridge was completed on Highway 17 near Hawk Lake, Ontario. This project again included a UHPC connection detail between adjacent box beams. The 12 simple span beams were connected via a diamond-shaped shear keys into which straight lengths of FRP reinforcing bars extended.

The Buller Creek Bridge was constructed on Highway 105 over the Buller Creek near Vermillion Bay, Ontario in 2009. This project included UHPC in the diamond-shaped shear keys between the 10 simple span adjacent box beams. The straight lengths of FRP reinforcing bar extended approximately 100-mm (4-inch) into the field-cast UHPC and created an approximately 25-mm (1-inch) lap length between bars from adjacent beams. This project also included three field-cast UHPC longitudinal connections between four precast approach slabs on each end of the bridge. The 150-mm (6-inch) wide female-female shear key detail included straight lengths of lapped FRP reinforcing bars.

The Log River Bridge was constructed on Highway 71 near Nestor Falls, Ontario in 2009. It also used a UHPC connection detail in the diamond-shaped shear keys between 8 simple span adjacent box beams. In this bridge, the straight lengths of FRP reinforcing bars extended into the connection creating an approximately 50-mm (2-inch) lap length between bars from adjacent beams. This project also included three field-cast UHPC longitudinal connections between four precast approach slabs on each end of the bridge. The 20-mm (0.8-inch) wide exposed gap between panels included a female-female shear key with a middepth width of 70-mm (2.8-inch) and threaded inserts for hex-head bolts which lapped across the connection.

In 2009/2010, the Eagle River Bridge was constructed on Highway 17 near Eagle River, Ontario. This multi-span bridge includes 36 adjacent box beams, with 12 in each of 3 spans. The bridge was reconstructed in two stages, with traffic remaining on half of the bridge throughout the project. The longitudinal connections between the adjacent box girders were similar to that used in the Log River Bridge. The design also included two other UHPC connections: a continuous for live load transverse connection linking the ends of the beams above the interior supports and a set of longitudinal and transverse connections between precast concrete approach slabs. The continuous for live load connections were full depth and included FRP reinforcement extending from the precast beams as well as additional FRP bars tied into the connection. The approach slabs also included straight FRP bars extending into the connections. Finally, the nosing material for the strip seal expansion joint on each end of the bridge was field-cast UHPC.

The Wabigoon River Bridge was constructed on Highway 105 over the Wabigoon River near Vermillion Bay, Ontario in 2010. This project included UHPC in the diamond-shaped shear keys between the 10 simple span adjacent box beams. The straight length of FRP reinforcing bar extended approximately 100-mm (4-inch) into the field-cast UHPC and created an approximately 25-mm (1-inch) lap length between bars from adjacent beams. This project also included three field-cast UHPC longitudinal connections between four precast approach slabs on each end of the bridge. The 150-mm (6-inch) wide female-female shear key detail included straight lengths of lapped FRP reinforcing bars. Finally, the nosing material for the strip seal expansion joint on the south end of the bridge was field-cast UHPC.

Also in 2010, the Chukuni River Bridge was constructed on Highway 105 over the Chukuni River near Red Lake, Ontario. This project included the construction of an 83.5-m (274-foot) long single span steel plate girder bridge. A total of 54 half-width conventional concrete precast deck panels were used to construct the deck on the project. The bridge had four girders, resulting in a centerline longitudinal deck connection not situated over a girder line. The longitudinal and transverse connections were constructed with field-cast UHPC. The discrete reinforcement in these connections included straight lengths of lapped FRP reinforcement. The

field-cast UHPC also completed the composite connections to the girders in the periodic shear pockets and provided the bedding under the deck panels. Each 3.6-m (11.8-foot) wide panel contained two shear pockets into which 24 shear studs projected.

A fourth bridge was reconstructed in 2010 over the La Vallee River near La Vallee, Ontario. This bridge project, on Highway 11 just west of Fort Frances, Ontario, involved replacing the single span superstructure with adjacent concrete box beams. The longitudinal connection detail between precast box beams included hairpin FRP bars and was similar to the detail deployed on the Sunshine Creek Bridge in 2007. Field-cast UHPC completed the connection. This project also included three field-cast UHPC longitudinal connections between four precast approach slabs at each end of the bridge. The 150-mm (6-inch) wide connection included straight lengths of lapped FRP reinforcing bars.

Three additional bridges projects are under construction in Northwestern Ontario and are scheduled to be finished by the end of 2010. Another four projects have been awarded for construction in Ontario in 2011. Each of these projects engages field-cast UHPC technology in the construction/reconstruction of a highway bridge.

### **New York State Department of Transportation Bridge Projects**

The New York State Department of Transportation (NYSDOT) has played a significant role in advancing the use of field-cast UHPC connections for deck-level connections between modular bridge components. They, along with many other bridge owners in the U.S., have begun deploying precast bridge deck technology in certain circumstances wherein the benefits are clear. Not unlike other owners, NYSDOT has experience with many varied technologies of this type and has a strong interest in facilitating further development. As relevant to the scope of this report, NYSDOT has a strong interest in using full-depth precast deck panels and deck-bulb-tee prestressed girders for use in constructing/reconstructing bridges. In both bridge types, the precast concrete elements must be connected together at the deck level via a permanent, durable connection. This connection is heavily stressed both structurally and environmentally, meaning that the long-term performance of the bridge is dependent on acceptable performance of the connection.

During the summer of 2009, NYSDOT completed two bridge projects using field-cast UHPC connections between the prefabricated elements. In both cases, the specific UHPC was the same as that tested within the research program discussed in this report. The first project was the Route 31 Bridge in Lyons, New York. In this bridge superstructure replacement, newly fabricated 1.04-m (41-inch) deep prestressed concrete deck-bulb-tee girders were installed in the bridge over the Canandaigua Outlet. The connection detail geometry was similar to specimen 6B which is presented later in this report. In the bridge, straight lengths of epoxy-coated bars projected from precast girder decks into the connection. After adjusting the girder cambers and forming the connections, the UHPC was mixed and cast. After casting, the exposed surfaces were covered to prevent dehydration and the UHPC was then allowed to cure under the natural environmental conditions. After curing, the bridge deck surface was ground and a waterproof membrane and asphalt overlay were installed. Figure 1 provides a photograph showing the longitudinal connections prior to UHPC casting. Figure 2 provides a photograph showing the placing of the UHPC into a connection. Figure 3 provides a photograph showing the connections

after casting and before surface grinding. Finally, Figure 4 provides a photograph of the completed bridge structure.

The second project was the replacement of the Route 23 Bridge in Oneonta, New York. This steel stringer integral abutment bridge spans the Otego Creek. The bridge deck construction included the use of precast deck panels and field-cast UHPC connections. The connection detail geometry was similar to specimen 8E which is presented later in this report. After setting the precast panels on the girders and forming the connections, the UHPC was mixed and cast. After casting, exposed surfaces were covered to prevent dehydration and the UHPC was then allowed to cure under the natural environmental conditions. After curing, a 40 mm (1.6 inch) minimum thickness concrete overlay was installed so as to provide a smooth riding surface. Figure 5 provides a photograph of a transverse connection prior to UHPC casting. Figure 6 provides a photograph of the field-casting of a transverse connection. Finally, Figure 7 provides a photograph of the completed bridge.



**Figure 1. Photograph. Longitudinal connections prior to field-casting of UHPC in Route 31 Bridge in Lyons, New York. (Photo courtesy of NYSDOT.)**



**Figure 2. Photograph. Placement of UHPC into longitudinal connections between deck-bulb-tee girders in Route 31 Bridge in Lyons, New York. (Photo courtesy of NYSDOT.)**



**Figure 3. Photograph. Longitudinal connections after field-casting of UHPC in Route 31 Bridge in Lyons, New York. (Photo courtesy of NYSDOT.)**



**Figure 4. Photograph. Completed Route 31 Bridge in Lyons, New York. (Photo courtesy of NYSDOT.)**



**Figure 5. Photograph. Transverse connectin prior to field-casting of UHPC in Route 23 Bridge in Oneonta, New York. (Photo courtesy of NYSDOT.)**



**Figure 6. Photograph. Field-casting of UHPC for Route 23 Bridge in Oneonta, New York.**



**Figure 7. Photograph. Elevation view of Route 23 Bridge in Oneonta, New York.**

## **RECENT MODULAR BRIDGE DECK COMPONENT CONNECTION RESEARCH**

Modular bridge deck components have been investigated in many studies over the past decades. The basic design of full depth concrete deck panels emulates the design of conventional cast-in-place concrete bridge decks. From a performance standpoint, the innovative aspect of these modular components is the connections and thus this is the system aspect which has been most heavily investigated.

In the U.S., degradation of bridge decks in combination with construction related traffic congestion and concern for worker safety have combined to provide impetus behind initiatives aimed at facilitating the accelerated construction/reconstruction of bridge decks. At the national level, the American Association of State Highway Transportation Officials (AASHTO) has moved this concept forward through three recent research programs. These programs, coordinated through the National Cooperative Highway Research Program, have focused specifically on advancing the state-of-the-art with regard to non-post-tensioned deck-level connections details between prefabricated concrete components.

The first project, titled “Full-Depth Precast Concrete Bridge Deck Panel Systems” and frequently referred to as NCHRP 12-65, resulted in the publication of NCHRP Report 584 in 2008<sup>9</sup>. A primary focus of this project was to develop an economical, non-post-tensioned transverse connection detail capable of developing the yield strength of straight lengths of mild steel reinforcement in a short length. This concept allows for smaller connections and a reduced volume of field-cast grout. Two concepts were developed and tested, both of which rely on shortening the development length of the mild steel through confinement provided by confining steel tubes. In one case the tubes cast into each side of the mating panels are slotted to allow for

the top-down insertion of each individual splice bar across the connection. In the other case, the tube is cast into one panel while the mating rebar extends from the adjacent panel. Structural testing of these systems demonstrated the acceptability of the structural performance. However, concerns about the complexity, the expense, and the constructability of the connection system in the field have led to limited deployment.

Of particular interest, the cyclic testing of the two connection concepts was completed in a fashion generally similar to that used in the test program discussed in this report. A trio of precast deck panels supported on two girders was connected by the two connection details. The span between girders was 6.1 m (20 feet) and wheel patch loads were applied at the quarter points adjacent to the connections. Surface-mounted strain gages oriented to capture the transverse flexure at midspan recorded strain ranges of up to 65 microstrain on the compression face and 50 microstrain on the tension face under a total applied load ranging from 17.8 to 189 kN (4 to 42.6 kip). The load was cycled for 2,000,000 repetitions on each connection. This structural load application did not cause any cracking or other degradation of the precast panels or the connections either initially or during the cyclic loading.

The second project, titled “Design and Construction Guidelines for Long-Span Decked Precast, Prestressed Concrete Girder Bridges” and frequently referred to as NCHRP 12-69, was also recently completed. Of particular interest to the research presented herein, two journal papers emanating from this study present results and recommendations for advancing the state-of-the-practice in regard to longitudinal connections between decked girders<sup>(10,11)</sup>. This research demonstrated that redesign of the traditional connection systems used in the longitudinal connections between decked girders could allow for a simpler connection thus increasing the feasibility of this construction system. This research recommends a connection design consisting of a 204-mm (8-inch) wide female-female shear key field-cast connection which contains headed rebar extending from each adjacent precast member and lapping over a 152-mm (6-inch) length. The research was based on the use of a magnesium phosphate grout in the connection.

The third project, titled “Cast-in-Place Concrete Connections for Precast Deck Systems” and frequently referred to as NCHRP 10-71, was initiated in 2006. The draft final report resulting from this project is under review and its publication is anticipated in 2011<sup>12</sup>. This project focused on both transverse and longitudinal connections between precast concrete components. Significant consideration was given to bridge systems identified in the 2004 Prefabricated Bridge Elements and Systems International Scan sponsored by FHWA. Of note, the physical testing program in this project included fatigue and static testing of bridge deck element subcomponents emulating the stresses imparted on longitudinal and transverse connections. The longitudinal connection test setup included similar specimen dimensions and support conditions to those engaged in the study presented in this report.

## CHAPTER 3. SPECIMEN DESIGN, FABRICATION, AND MATERIAL PROPERTIES

### INTRODUCTION

The physical details of the deck panel specimens and the fabrication of these specimens are described in this chapter. The material properties for the UHPC and the HPC are also presented. Finally, the results obtained by NYSDOT in an associated test program focused on pullout testing of mild-steel reinforcement embedded into UHPC cylinders are presented.

### SPECIMEN DESIGN

The test program included six specimens, representing connections between two different types of elements. Four of the specimens emulated the types of transverse connections being considered for use between full-depth precast deck panels. The remaining two specimens emulated the types of longitudinal connections being considered for use between adjacent deck-bulb-tee girders. Within each of the two sets of specimens, multiple reinforcement configurations were tested. Table 3 provides a brief summary of the six test specimens.

**Table 3. Test specimens.**

<b>Name</b>	<b>Orientation</b>	<b>Depth</b>	<b>Reinforcement</b>
8H	Transverse	200 mm	Alternating 16M (#5) <b>headed black</b> reinforcement with 90 mm lap length and 450 mm (top) and 180 mm (bottom) spacings
8E	Transverse	200 mm	Alternating 13M (#4) <b>hairpin epoxy-coated</b> bars with 100 mm lap length and 55 mm spacing
8G	Transverse	200 mm	Alternating 16M (#5) <b>galvanized straight</b> bars with 150 mm lap length and 450 mm (top) and 180 mm (bottom) spacings
8B	Transverse	200 mm	Alternating 16M (#5) <b>black straight</b> bars with 150 mm lap length and 450 mm (top) and 180 mm (bottom) spacings
6H	Longitudinal	150 mm	Alternating 16M (#5) <b>headed black</b> reinforcement with 90 mm lap length and 450 mm (top) and 180 mm (bottom) spacings
6B	Longitudinal	150 mm	Alternating 16M (#5) <b>black straight</b> bars with 150 mm lap length and 450 mm (top) and 180 mm (bottom) spacings

1 in. = 25.4 mm

The details for each of the six specimens are provided in Figure 8 through Figure 12. In all cases, the test specimens were 2.4 by 2.152 m (94.5 by 84.7 inch) with the connection running the length of the panel. Each of the specimens included a female-female diamond-shaped shear key with a 152 mm (6 inch) nominal minimum width at the top and bottom exposed surfaces. The connection reinforcement extends from the adjacent faces of the precast panels into the connection. All connections were passively reinforced, with no post-tensioning included in any of the specimens. Panels 8H, 8E, 8G, and 8B simulate transverse connections between full-depth

precast deck panels. Panels 6H and 6B simulate longitudinal connections between adjacent decked girders.

Figure 8 presents the reinforcement details for specimen 8H. The connection reinforcement consisted of headed 16M (#5) mild-steel reinforcement. The Dayton Superior D-158-B Plain End Anchor was used. The head on this bar has a diameter of 50.5 mm (1.987 inch) and a thickness of 12.7 mm (0.5 inch). The reinforcement had no supplemental corrosion protection. The minimum lap length for the two layers of reinforcement in the connection was 90 mm (3.54 inch). Two additional 16M (#5) bars were threaded along the length of the connection between the heads. At the interface between the precast panel and the field-cast UHPC, this reinforcement configuration resulted in a 180 mm (7.1 inch) spacing of the bottom mat of reinforcement. In the middle of the connection, the spacing between any two adjacent non-contact lap spliced headed bars was 90 mm (3.5 inch).

Figure 9 presents the reinforcement details for specimen 8E. The connection reinforcement consisted of epoxy-coated hairpin 13M (#4) mild-steel reinforcement. The minimum lap length for the reinforcement in the connection was 100 mm (3.9 inch). Two additional 16M (#5) bars were threaded through the confined region created by the lapped hairpins. At the interface between the precast panel and the field-cast UHPC, this reinforcement configuration resulted in a 110 mm (4.3 inch) spacing of the top and bottom mats of reinforcement. In the center of the connection, this configuration resulted in a 55 mm (2.2 inch) spacing between adjacent hairpins emanating from alternating sides of the connection.

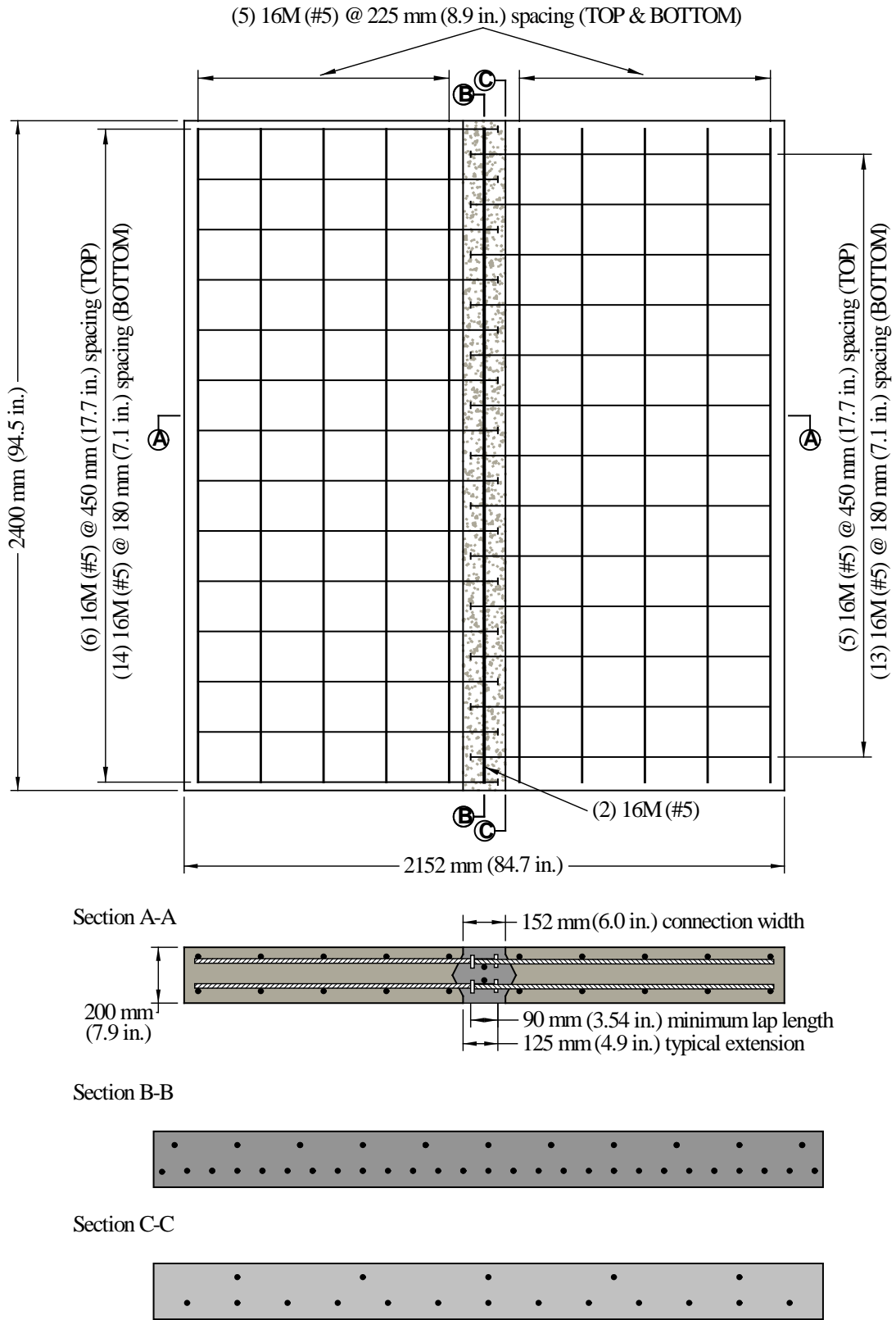
Figure 10 presents the reinforcement details for specimen 8G. The connection reinforcement consisted of straight, lapped 16M (#5) mild-steel reinforcement. All reinforcement in this test specimen was galvanized. The minimum lap length for the reinforcement in the connection was 150 mm (5.9 inch). Two additional 16M (#5) bars were oriented along the length of the connection between the top and bottom mats. At the interface between the precast panel and the field-cast UHPC, this reinforcement configuration resulted in a 180 mm (7.1 inch) spacing of the bottom mat of reinforcement. In the middle of the connection, the spacing between any two adjacent non-contact lap spliced bars was 90 mm (3.5 inch).

Figure 10 also presents the reinforcement details for specimen 8B. The connection reinforcement again consisted of straight, lapped 16M (#5) mild-steel reinforcement. The reinforcement in this specimen did not have any supplemental corrosion protection. The minimum lap length for the reinforcement in the connection was 150 mm (5.9 inch). Two additional 16M (#5) bars were oriented along the length of the connection between the top and bottom mats. At the interface between the precast panel and field-cast UHPC, this reinforcement configuration resulted in a 180 mm (7.1 inch) spacing of the bottom mat of reinforcement. In the middle of the connection, the spacing between any two adjacent non-contact lap spliced bars was 90 mm (3.5 inch).

Figure 11 presents the reinforcement details for specimen 6H. The connection reinforcement consisted of headed 16M (#5) mild-steel reinforcement. The Dayton Superior D-158-B Plain End Anchor was used. The head on this bar had a diameter of 50.5 mm (1.987 inch) and a thickness of 12.7 mm (0.5 inch). The reinforcement had no supplemental corrosion protection. The minimum lap length for the bottom layer of reinforcement in the connection was 90 mm

(3.54 inch). Two additional 16M (#5) bars were threaded along the length of the connection between the heads. At the interface between the precast panel and the field-cast UHPC, this reinforcement configuration resulted in a 180 mm (7.1 inch) spacing of the bottom mat of reinforcement. In the middle of the connection, the spacing between any two adjacent non-contact lap spliced headed bars was 90 mm (3.5 inch).

Figure 12 presents the reinforcement details for specimen 6B. The connection reinforcement consisted of straight, lapped 16M (#5) mild-steel reinforcement. The reinforcement had no supplemental corrosion protection. The minimum lap length for the reinforcement in the connection was 150 mm (5.9 inch). Two additional 16M (#5) bars were threaded along the length of the connection between the heads. At the interface between the precast panel and the field-cast UHPC, this reinforcement configuration resulted in a 180 mm (7.1 inch) spacing of the bottom mat of reinforcement. In the middle of the connection, the spacing between any two adjacent non-contact lap spliced bars was 90 mm (3.5 inch).



**Figure 8. Illustration. Layout and rebar plan for panel 8H.**

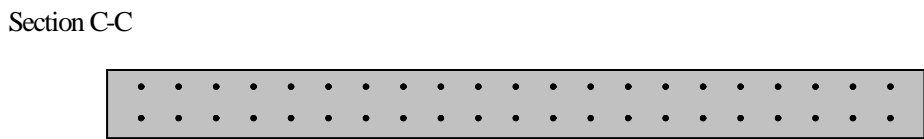
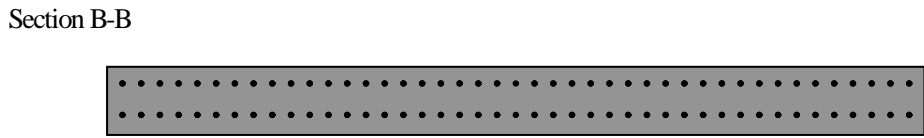
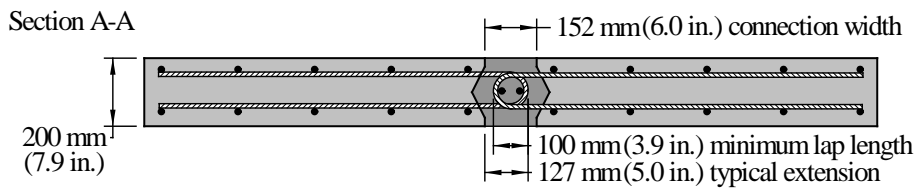
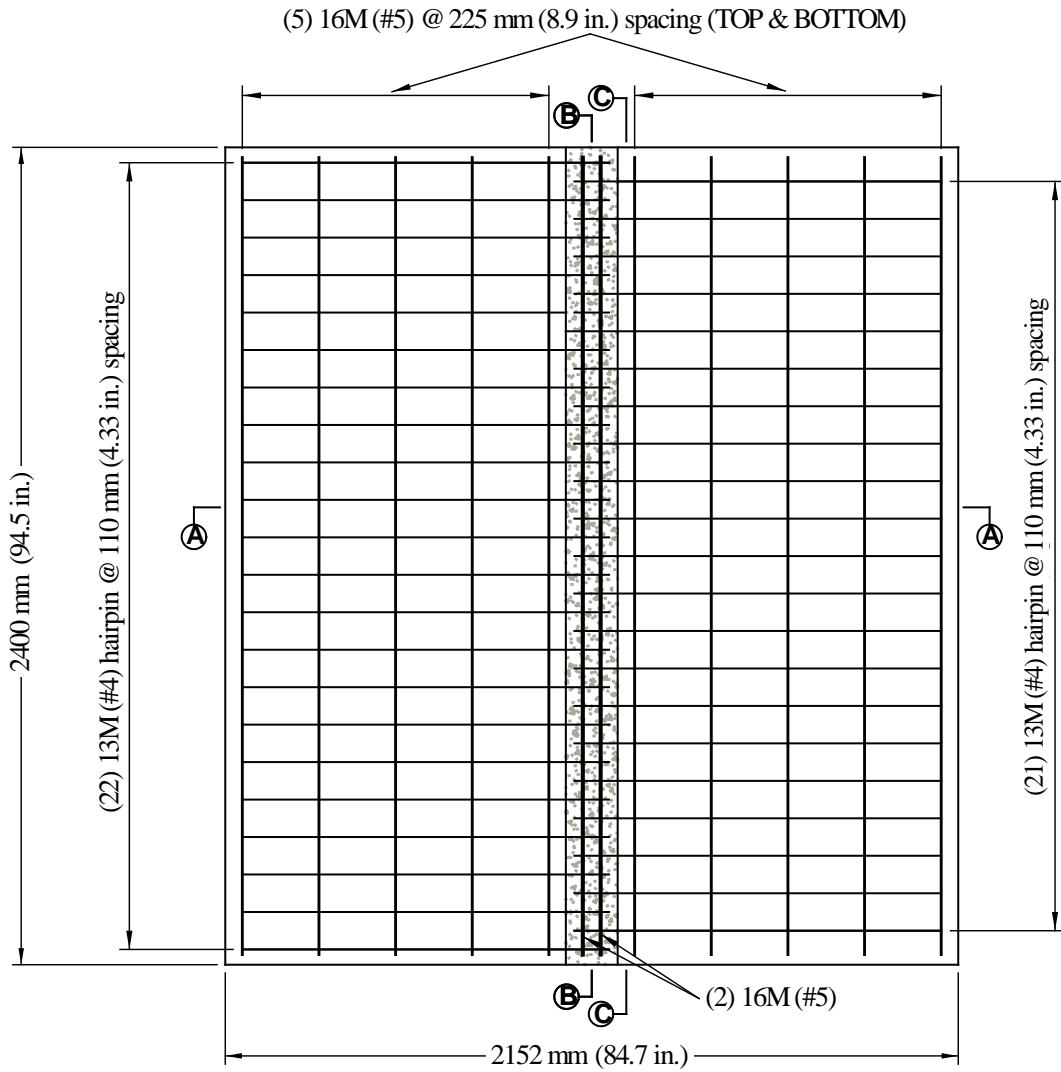


**Figure 9. Illustration. Layout and rebar plan for panel 8E.**

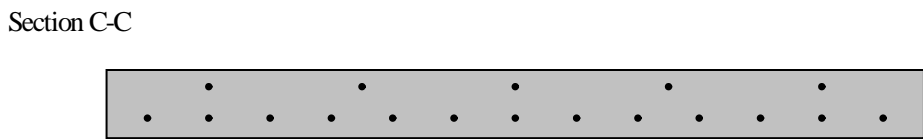
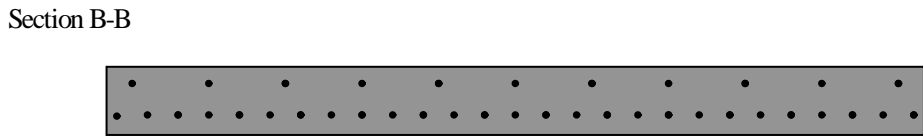
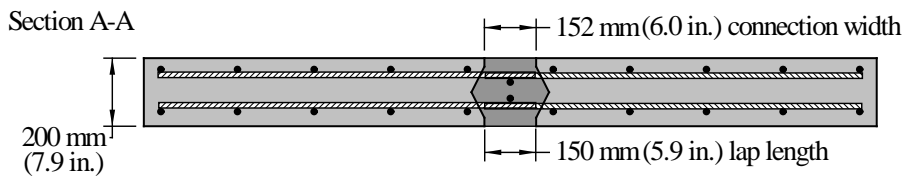
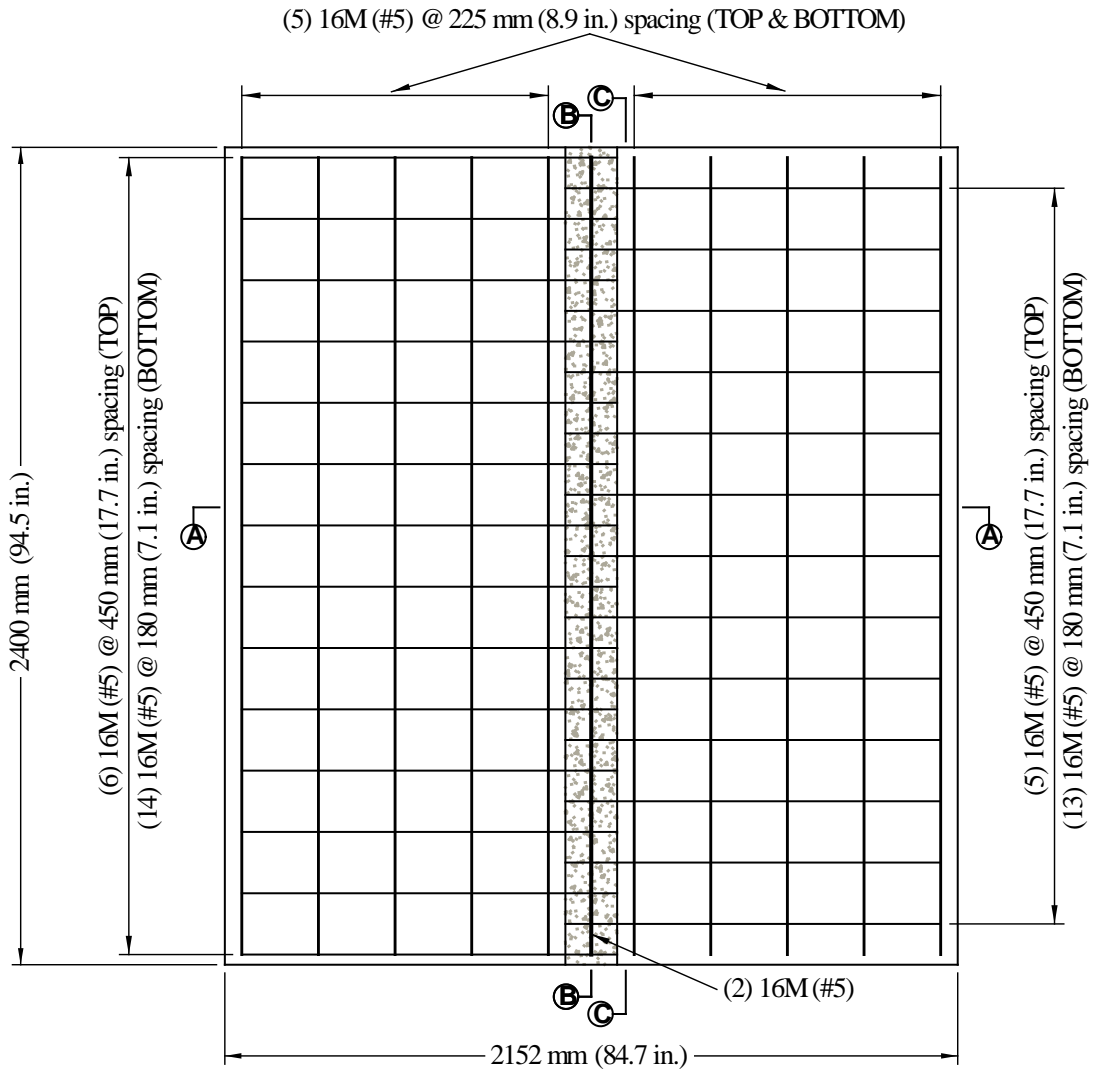


**Figure 10. Illustration. Layout and rebar plan for panels 8G and 8B.**

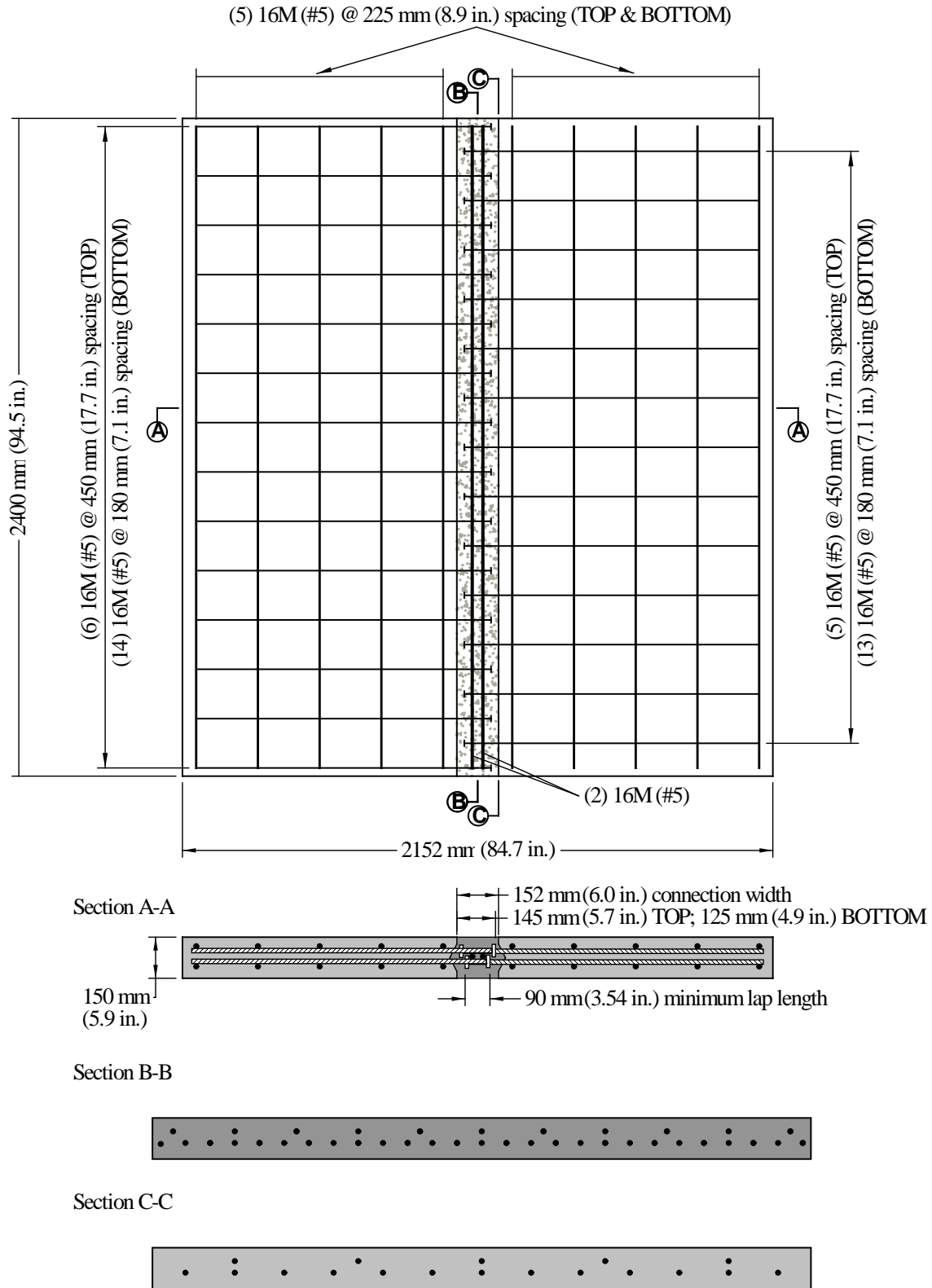
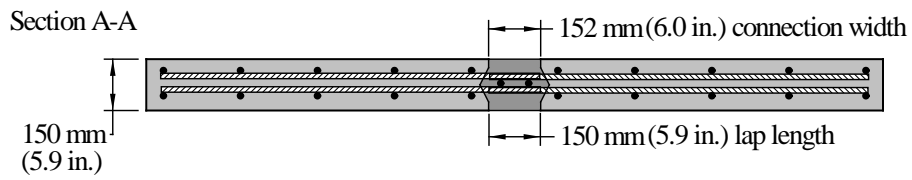
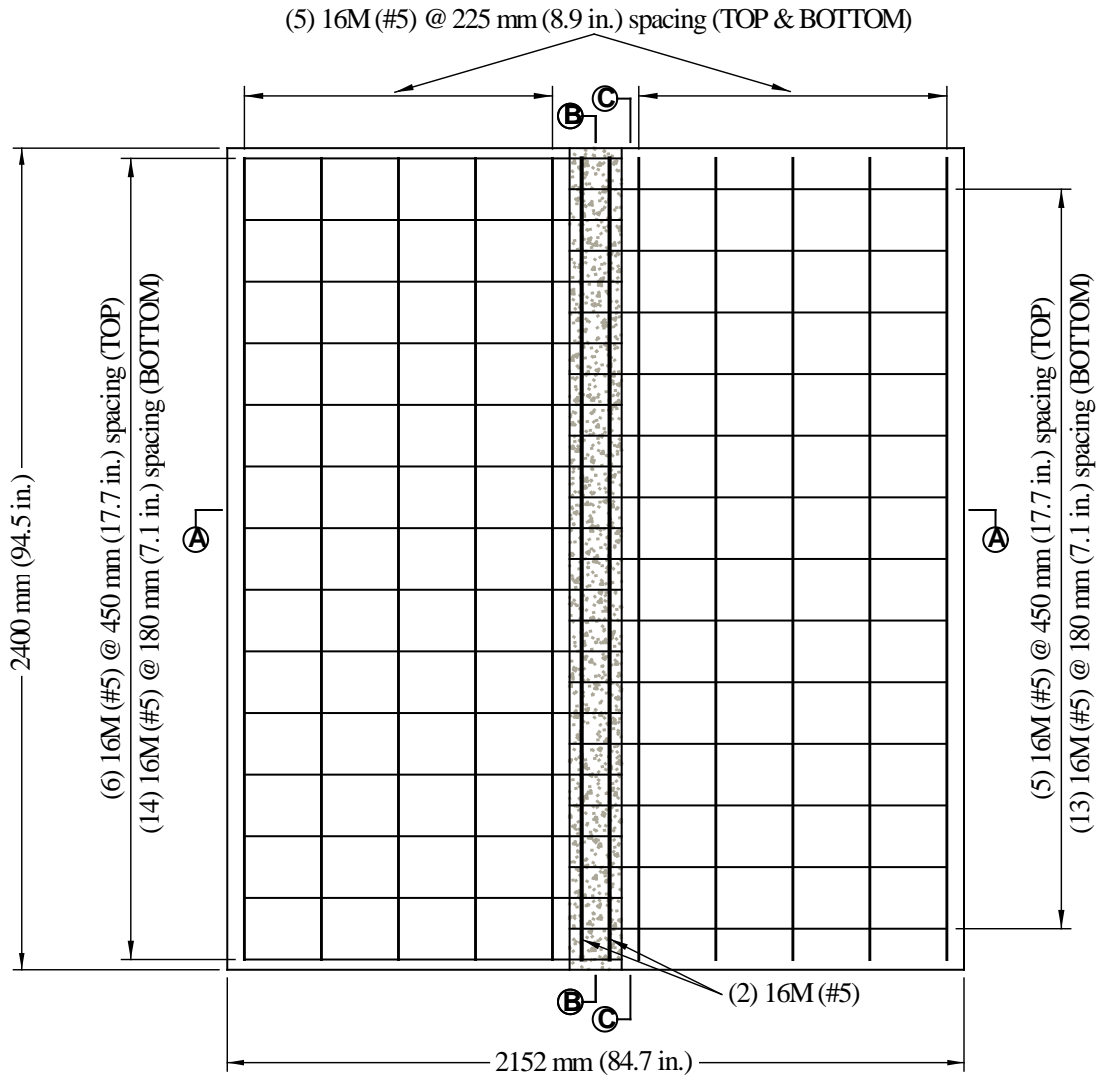


**Figure 11. Illustration. Layout and rebar plan for panels 6H.**



Section B-B



Section C-C



**Figure 12. Illustration. Layout and rebar plan for panels 6B.**

## SPECIMEN FABRICATION

The specimens were fabricated by a precast concrete component manufacturer, The Fort Miller Co., Inc., of Schuylerville, New York. As each specimen is composed of two precast half-panels joined by a field-cast UHPC connection, the half-panels were fabricated first. The 12 half-panels were fabricated in mid-January 2009. After curing for approximately three weeks, each of the six pairs of half-panels was arranged into the appropriate configuration for fabrication of the six specimens. The UHPC connections were cast sequentially from a single batch of UHPC on February 11, 2009. The pre-bagged UHPC was mixed according to the manufacturer's recommendation. The casting of one of the UHPC connections is shown in the photo in Figure 13. The completed specimens were then cured at the precast facility in the ambient environment for two weeks, after which they were shipped to the Turner-Fairbank Highway Research Center's Structural Testing Laboratory.



**Figure 13. Photo. Placement of UHPC into connection. (Photo courtesy of NYSDOT)**

## UHPC MATERIAL PROPERTIES

During the placing of the UHPC into the six test panel specimen connections, 76-mm (3-inch) diameter cylinder specimens were cast in order to allow for material property characterization. Three cylinders were cast and stored with the test panels.

The cylinders were prepared for testing by grinding both ends to create parallel surfaces through the use of a fixed end grinder. After preparation, the cylinders exhibited length to diameter ratios

of approximately 1.9. Three tests were carried out on the cylinders: density, compressive strength, and modulus of elasticity. Density measurements were obtained through conventional means by measuring weight of each cylinder and dividing by the volume. The average density of the UHPC was 2540 kg/m<sup>3</sup> (159 lb/ft<sup>3</sup>).

The compressive strength and modulus of elasticity tests were completed simultaneously according to ASTM C39<sup>(13)</sup> and ASTM C469<sup>(14)</sup>. Minor modifications to these test methods included the continuation of the loading and data collection through failure without the removal of the strain measurement device and the increase in load rate to 1 MPa/sec (150 psi/sec). Also, the load was not cycled as described in ASTM C469; instead, each cylinder was loaded via a continually increasing load to failure. Strains were measured via a trio of linear variable displacement transducers (LVDTs) attached to a pair of parallel rings which engaged a 51-mm (2-inch) gage length on the cylinder. The modulus of elasticity was calculated based on a best fit approximation of the stress-strain response between ten and thirty percent of the failure load for each cylinder.

The test results for the three cylinders are presented in Table 4. The tests were completed fifteen months after casting of the panel specimens, which was near the conclusion of the cyclic testing of the panels. Overall, the average compressive strength of the UHPC was 219 MPa (31.8 ksi). The average modulus of elasticity was 61.3 GPa (8900 ksi).

**Table 4. Cylinder density, compressive strength, and modulus of elasticity test results.**

<b>Cylinder Number</b>	<b>Density, kg/m<sup>3</sup> (lb/ft<sup>3</sup>)</b>	<b>Compressive Strength, MPa (ksi)</b>	<b>Modulus of Elasticity, GPa (ksi)</b>
1	2535 (158.3)	217 (31.5)	61.3 (8890)
2	2550 (159.2)	218 (31.8)	60.8 (8810)
3	2535 (158.3)	222 (32.3)	61.9 (8970)

## **HPC MATERIAL PROPERTIES**

A self-consolidating high-performance concrete was used to fabricate the precast panels. The concrete had a minimum 28-day compressive strength of 35 MPa (5 ksi). The precaster reported an average slump spread for the concrete of 660 mm (26 inch) and an average air content of 6.1 percent. The average reported 1-day compressive strength of the concrete was 27 MPa (3.9 ksi). The 7-day strength averaged 40 MPa (5.8 ksi), and the 28-day strength averaged 45 MPa (6.5 ksi).

## **MILD STEEL REINFORCEMENT MECHANICAL PROPERTIES**

No mechanical testing was completed on the mild steel reinforcement used in the test specimens. The reinforcement was specified to meet standard New York State Department of Transportation requirements for structural concrete reinforcement.

## **REINFORCEMENT PULLOUT TEST RESULTS**

The development length of mild-steel reinforcement embedded into UHPC was investigated through a series of tensile pullout tests. A total of nine tests were completed in which a 13M, 16M, or 19M (#3, #4, or #5) bar was cast into a cylinder of UHPC then pulled out after a specified curing regime had been applied. These tests were completed by the New York State Department of Transportation Materials Bureau and were first reported in an internal document dated March 11, 2009.

The specimen design for these tests is shown in Figure 14. Each of the nine tested rebar were cast into 400-mm (15.74-inch) diameter UHPC cylinders. A 300-mm (11.81-inch) diameter, 19-mm (0.75-inch) deep recess was cast into the surface from which the rebar emerged. The embedment length of the rebar varied depending on the size of the bar. The 13M (#4) bars were embedded 75 mm (2.9 inch) into the UHPC. The 16M (#5) bars were embedded 100 mm (3.9 inch) into the UHPC. 19M (#6) bars were embedded 125 mm (4.9 inch) into the UHPC.

The tests were completed by applying an axial tensile force on the free end of the rebar. The force was resisted by the 50-mm (2-inch) wide annulus of concrete which bore against the load frame through which the rebar was being pulled. Tests were completed at two UHPC ages after casting, namely 7 days and 28 days.

The results of the tests are shown in Table 5. In all nine cases, the rebar failed via rebar fracture within the length of exposed rebar. The peak stress in the rebar prior to failure was always greater than 690 MPa (100 ksi), a stress level at which rebar of these types would be expected to reach ultimate tensile capacity.

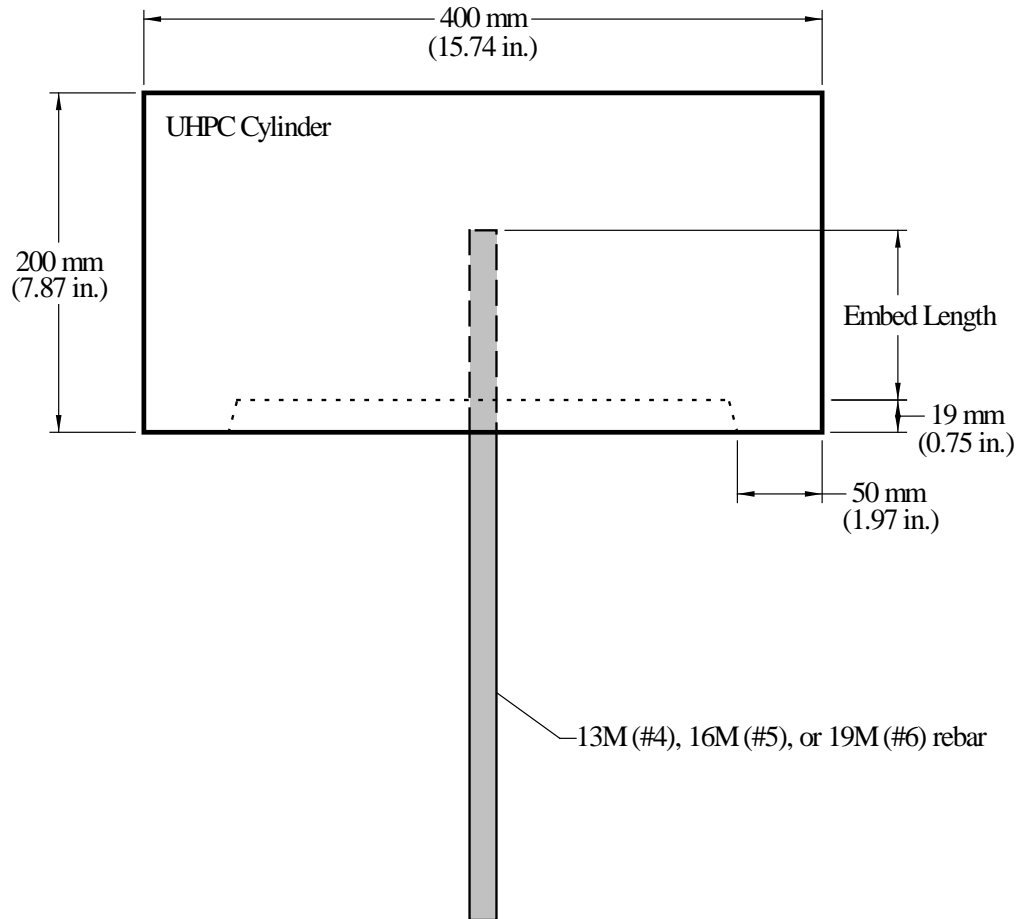


**Figure 14. Illustration. Specimen design for reinforcement pullout tests.**

**Table 5. Rebar pullout test results.**

Bar Type	Bar Size	UHPC Age, days	Peak Bar Stress, MPa (ksi)	Mode of Failure
Black	13M (#4)	7	697 (101.1)	Rebar Fracture
Black	16M (#5)	7	723 (104.8)	Rebar Fracture
Black	19M (#6)	7	724 (105.0)	Rebar Fracture
Epoxy-Coated	13M (#4)	7	703 (102.0)	Rebar Fracture
Epoxy-Coated	16M (#5)	7	743 (107.7)	Rebar Fracture
Epoxy-Coated	19M (#6)	7	730 (105.9)	Rebar Fracture
Epoxy-Coated	13M (#4)	28	692 (100.4)	Rebar Fracture
Epoxy-Coated	16M (#5)	28	740 (107.3)	Rebar Fracture
Epoxy-Coated	19M (#6)	28	731 (106.0)	Rebar Fracture



## CHAPTER 4. TEST PROGRAM, RESULTS, AND ANALYSES

### INTRODUCTION

The test results and observations from the physical testing of the deck panel connection specimens are presented in this chapter. The tests on specimens which simulated the transverse connections between full-depth deck panels are discussed first. The tests on specimens which simulated the longitudinal connections between adjacent decked girders then follow.

### TRANSVERSE CONNECTION TEST PROGRAM AND RESULTS

Four of the deck panels were designed to simulate the transverse connection between adjacent full-depth bridge deck panels. In order to simulate the types of stresses normally imparted into this type of connection, the test setup was arranged so that the panels were loaded in three-point bending with a load adjacent to the connection. This setup allowed for primary flexural stresses oriented parallel to the connection to be imparted into each panel. Simultaneously, this setup required the transmission of shear forces across the connection in order to allow the locally applied load to be distributed across the panel. The implemented test setup focused on local transverse flexural behaviors in the bridge deck, not on global flexural behaviors experienced by the composite deck/girder system. Transverse connections in negative moment regions can experience nearly uniform tensile forces throughout the depth of the connection. Although not explicitly tested, these types of forces were more closely replicated by the testing completed on the longitudinal connections specimens discussed later in this report.

Figure 15 shows the test setup that was used for the cyclic testing of the four test panels. Figure 16 shows the test setup used for the static testing to failure of these same panels. The cyclic and static setups were identical aside from the change in the hydraulic jack and the type of cylindrical bearing attached thereto. The load application point was offset from the center of the panel toward the north such that the load was applied immediately adjacent to the connection. The load patch measured 254 x 508 mm (10 x 20 inch) and was oriented to mimic a truck wheel load driving on a bridge deck. Loads were applied to the deck through a 25 mm (1 inch) thick elastomeric pad which was backed by a 25 mm (1 inch) thick steel plate. Each specimen was supported by a 25 mm (1 inch) thick, 51 x 1524 mm (2 x 60 inch) elastomeric strip on each end of the span. Figure 17 provides a photograph showing specimen 8E being subjected to cyclic loading.

It is recognized that, given the boundary conditions, this test setup does not simulate a subcomponent of a bridge which spans the full distance transversely between two girders. In a bridge structure, the precast components span across multiple girders to which they are fixed, thus allowing for limited rotations of the component at the support points. The test setup employed here more closely represents the portion of the modular component system which spans transversely between two adjacent inflection points in the flexural response of the bridge deck. Additionally, this test setup did not emulate the axial restraint (i.e., “arching action”) which also contributes a portion of the load carrying capacity of a bridge deck.

The cyclic loads were applied through the use of a servo-hydraulic controlled actuator operated under load control. The maximum achievable frequency of loading was influenced by the

stiffness of the specimen and reaction system. Prior to structural cracking of the deck panel specimen, the loading frequency was 6 Hz. After cracking, the frequency was decreased such that the load peaks were reached and objectionable movement of the load frame did not occur.

The sinusoidal cyclic loading of each panel was initially programmed to achieve peak applied loads of 9 and 71 kN (2 and 16 kips). This loading was continued for at least 2 million cycles. Subsequently, the load level was increased to achieve peak applied loads of 9 and 95 kN (2 and 21.3 kips). This loading was continued for at least 5 million cycles. An illustration of the cyclic loading program is shown in Figure 18. The 71 kN (16 kip) load level was selected as this load level generated tensile stresses which were near but below the anticipated first cracking strength of the precast deck panels. The 95 kN (21.3 kip) load level, which is 1.33 times the earlier load, was selected as this load level generated tensile stresses which were above the anticipated cracking strength of the precast panels. The number of load cycles within the test program was selected based on a consideration of prior experience with cyclic loading of concrete structures and recognition of the time constraints inherent in any cyclic test program.

After the completion of the cyclic testing, an estimation of the type of bridge system which the tested subcomponents most closely resemble was completed through the use of an elastic finite element model. The elastic loading of the tested subcomponent was modeled first in order to facilitate calibration. Then the subcomponent was inserted into the middle of the deck of a four girder simple span bridge model. The deck was fully composite with the torsionally rigid girders. This model demonstrated that, in order to mimic the elastic surface strain range observed on the top and bottom of the deck under the loading from 9 to 71 kN (2 to 16 kips), the girder spacing would need to be approximately 5.3 m (17.5 feet). A second analysis was then completed to determine the wheel patch load which would be needed to cause similar strain response in a bridge with a girder spacing of 3 m (10 feet). It was found that an applied wheel patch load peaking at 125 kN (28 kips), or 1.75 times the load applied in this portion of the test program, would create a similar strain range in the real bridge as was observed here in the test program. In summary, the analytical modeling demonstrated that the tested transverse connection configuration with an applied load of 71 kN (16 kips) was a reasonable simulation of a transverse connection in a bridge with a 3 m (10 foot) girder spacing and an applied wheel load of 125 kN (28 kips).

The structural response during the cyclic loading of the specimens was captured through the use of electronic instrumentation and visual/audible observations. The electronic instrumentation included six electrical resistance strain gages mounted on the concrete, one LVDT monitoring the opening of the underside of the connection, a load cell on the actuator to measure load, and an LVDT on the actuator to measure stroke. The locations for the six strain gages and the connection-opening LVDT are shown in Figure 19. The electronic data was captured during cyclic load application by a high speed data acquisition system. The rate of structural loading was not modified during the periodic data collection events. The initiation of each periodic data collection was manually triggered and can be deduced from inspection of the cycle versus strain response plot generated for each specimen. The gages were applied to the midspan cross section in order to assess the response at this highly stressed area, and were spaced across the specimen to allow for assessment of the load transfer across the connection.

The performance of the connection was also monitored through visual observations of water leakage through the connection. Water was ponded on the top of the connection throughout the cyclic tests, and the underside of each specimen was periodically checked for signs of water leakage. The leakage inspection occurred at least as frequently as the electronic data capture. The ponding setup is shown in Figure 17.

The static loading of the panels to failure was completed through the use of a pressure-actuated static hydraulic jack. The initial loading of each specimen was completed in a stair-step fashion with temporary holds occurring at approximately 22.2 kN (5 kip) intervals. After the initiation of inelastic behaviors, the steps were incremented on midspan displacement of the specimen.

The structural response during the static loading of the specimens was captured through the use of electronic instrumentation and visual/audible observations. The electronic instrumentation included six electrical resistance strain gages mounted on the concrete, six string potentiometers to measure vertical deflection of the underside of the specimen, one LVDT monitoring the opening of the underside of the connection, a load cell on the actuator to measure load, and an LVDT on the actuator to measure stroke. The locations for the strain gages, potentiometers, and the connection-opening LVDT are shown in Figure 20. As with the cyclic tests, the gages were applied so as to allow for assessment of highly stressed regions and load transfer across the connection.

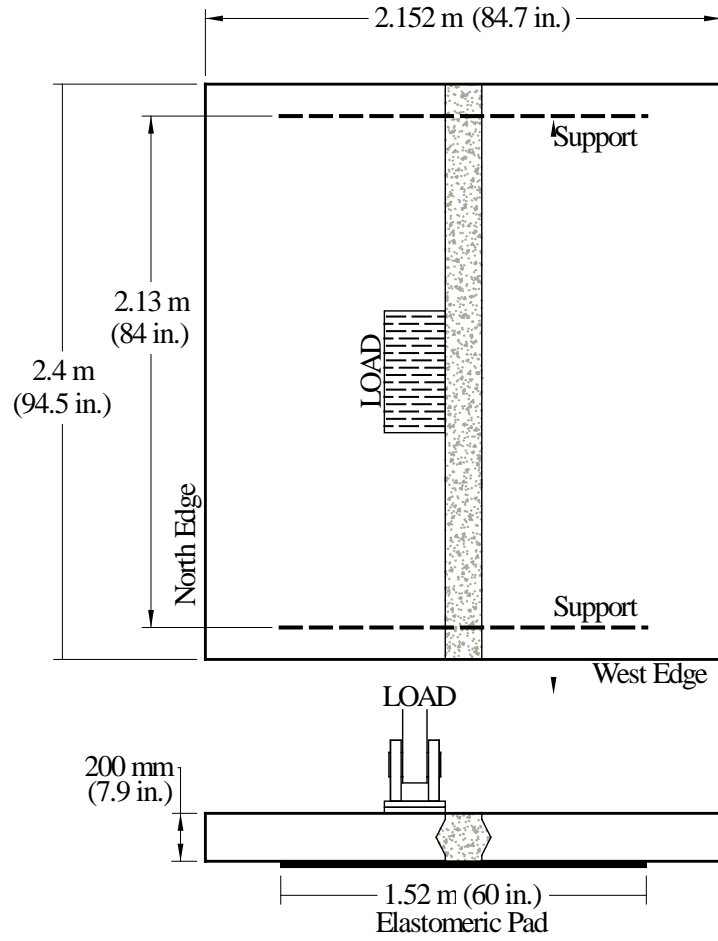


**Figure 15. Illustration. Test setup for cyclic loading of panels 8H, 8E, 8G, and 8B.**

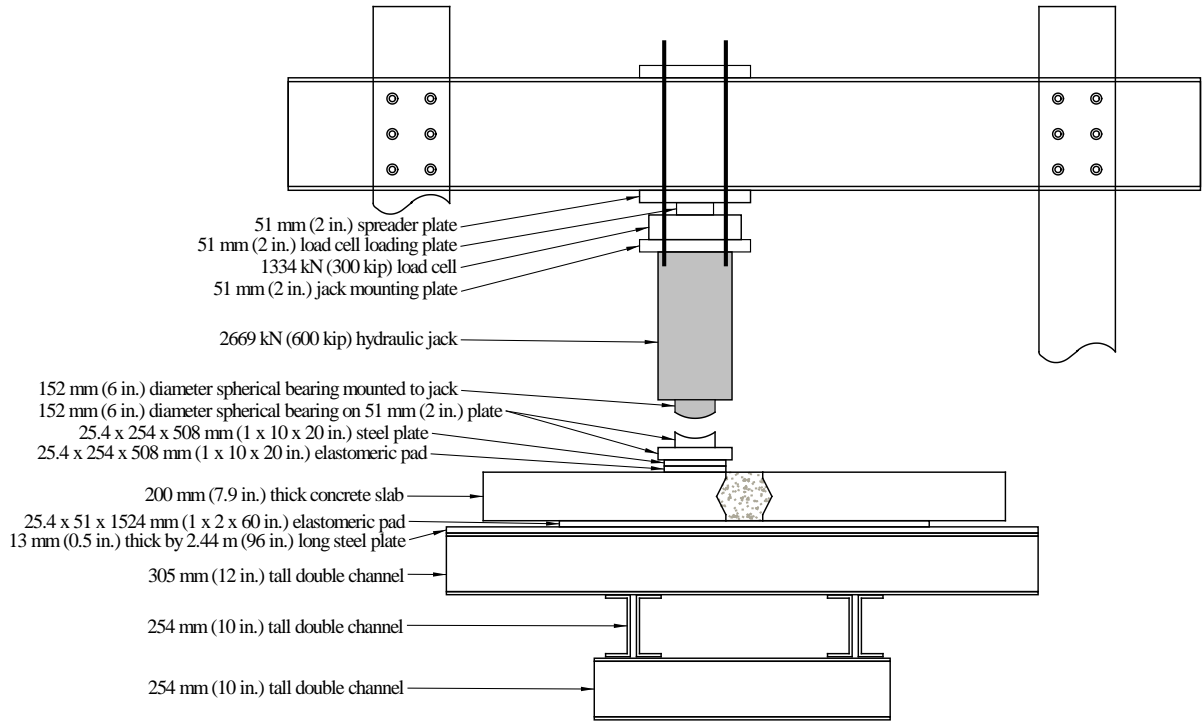


**Figure 16. Illustration. Test setup for static loading of panels 8H, 8E, 8G, and 8B.**



**Figure 17. Photograph. Oblique view of cyclic test setup for panels 8H, 8E, 8G, and 8B.**

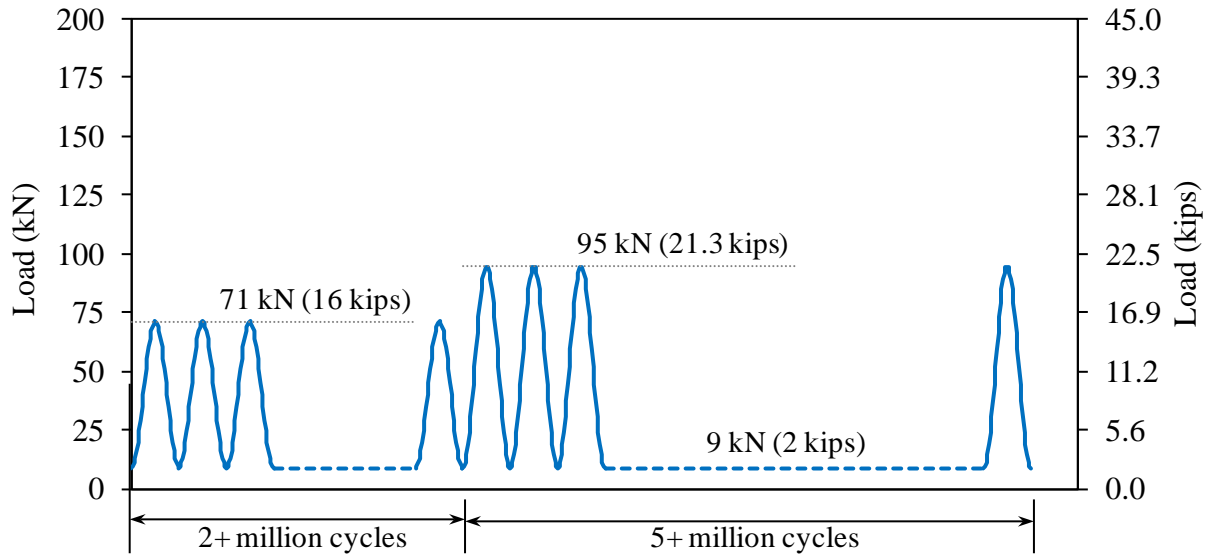


**Figure 18. Illustration. Cyclic loading program for panels 8H, 8E, 8G, and 8B.**

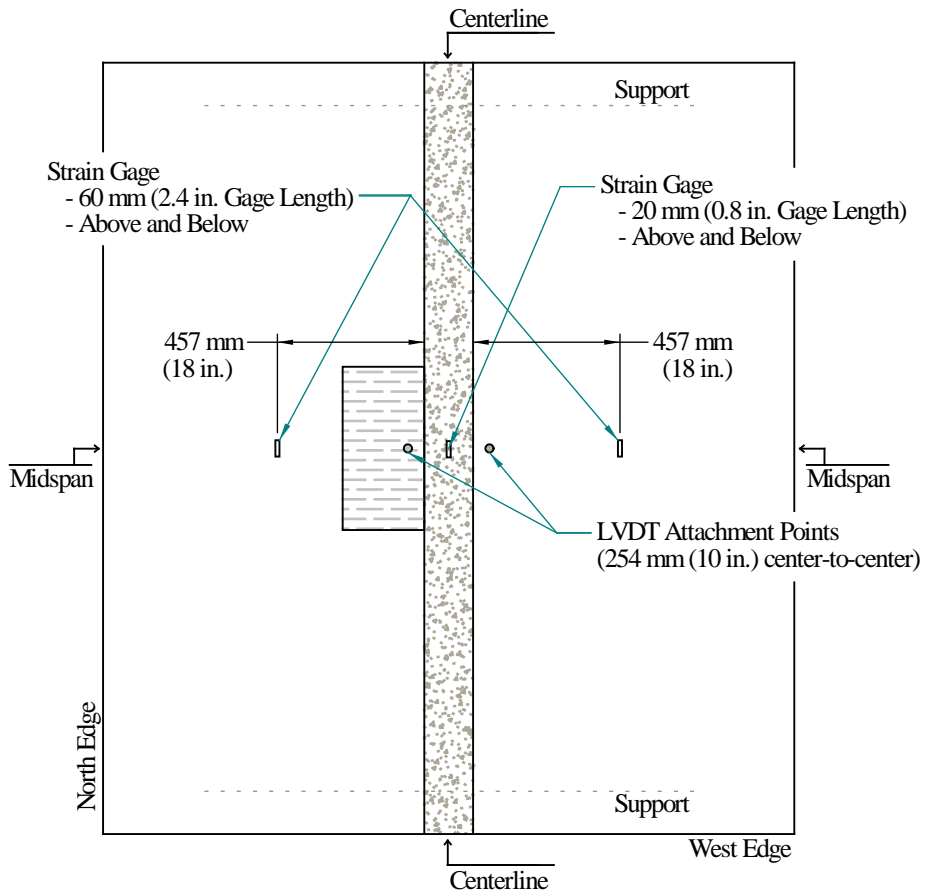


**Figure 19. Illustration. Instrumentation for cyclic testing of panels 8H, 8E, 8G, and 8B.**

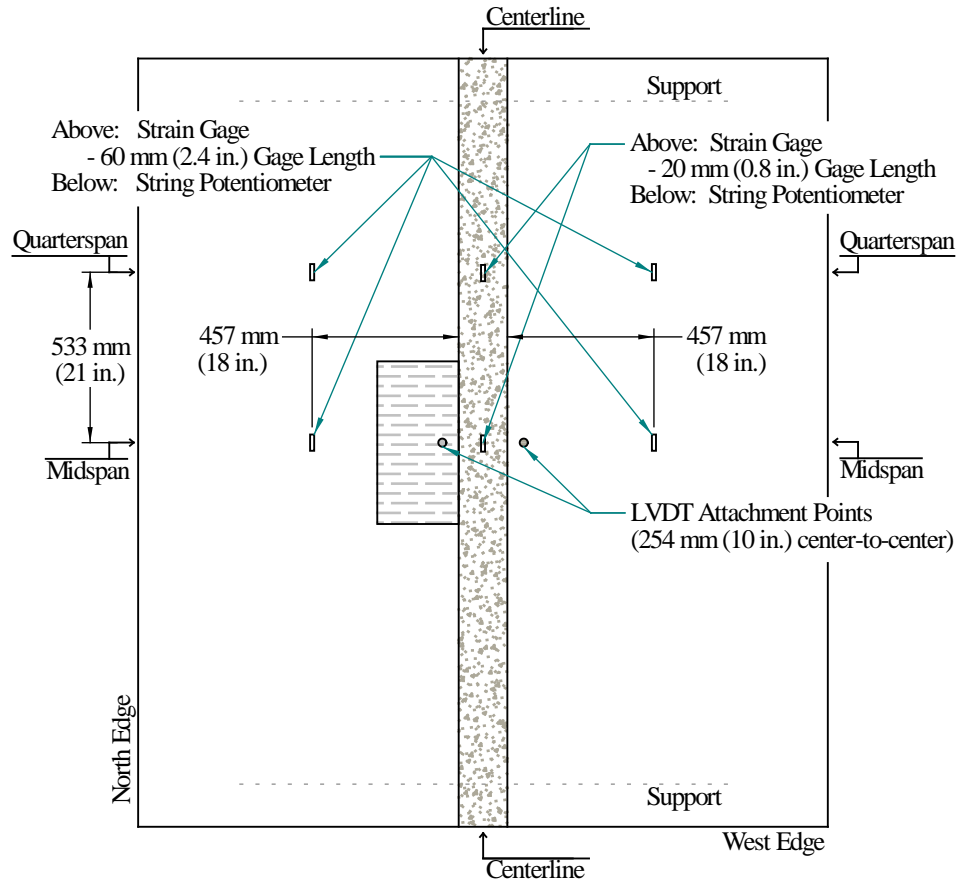


**Figure 20. Illustration. Instrumentation for static testing of panels 8H, 8E, 8G, and 8B.**

### **Specimen 8H**

Specimen 8H was designed and loaded to simulate the transverse connection between two full-depth bridge deck panels. The reinforcing details were described in Chapter 3 and are shown in Figure 8. Recall that the discrete reinforcement within the connection included two layers of headed reinforcing bars which were lapped across a 152 mm (6 inch) wide connection.

### ***Cyclic Testing***

The cyclic testing of this specimen was completed according to the process described previously. The testing was completed over the course of 4 weeks. The cyclic loading included 2,063,124 cycles with a sinusoidal applied load ranging from 9 to 71 kN (2 to 16 kips), followed by 5,110,275 cycles ranging from 9 to 95 kN (2 to 21.3 kips).

The structural response of the specimen as captured by the electronic gages is presented in Figure 21. This two part graph shows the stroke range of the hydraulic actuator and the strain per unit of applied load on the specimen as a function of the number of cycles of load applied. The data in this figure was generated by analyzing the response of the specimen as captured during the increasing load portion of periodic cycles throughout the test. The stroke range was calculated from the maximum and minimum displacement of the actuator piston during a cycle.

The strain per applied load was calculated through a best-fit approximation of the slope of the load-strain response over the load range from approximately 36 kN (8 kips) to approximately 90 percent of the peak applied load.

The results in Figure 21 show that the response of the specimen stabilized soon after the initiation of cyclic loading in each load range. The lone exception is the response of the strain gage on the tension face 457 mm (18 inch) north of the connection. This gage showed an increase of strain beginning at approximately 500,000 cycles. As will be discussed below, this response is indicative of first cracking of the specimen which occurred near this gage and was first visually observed after the conclusion of the cycling to 71 kN (16 kips).

The strain response of the specimen as captured at two representative timeframes during the test is presented in Figure 22 and Figure 23. These figures show the range of strain observed on the surface of the specimen at the strain gage locations. Figure 22 presents results from early in the loading after a total of 462,000 cycles had been completed. Figure 23 presents results from the end of cyclic testing after a total of 7,137,000 cycles had been completed.

Immediately prior to the start of cyclic loading, the specimen was checked for structural cracking that may have occurred during handling or test setup. No cracks were identified. Next, the specimen was statically loaded to 71 kN (16 kips) then unloaded to 9 kN (2 kips). Again, no cracks were identified. After the conclusion of cycling to 71 kN (16 kips), the specimen was again checked for cracks. Figure 24 illustrates the cracking which was apparent at this point in the testing. A tight intermittent crack was observed to run from the north side of the connection to a point near the north tension face strain gage. This crack was small but visible with the unaided eye. Three additional cracks were observed to run across the connection just west of midspan. These cracks were only visible through the use of an alcohol-based evaporative crack indicator. No interface cracks were observed. The cracks in the specimen were again assessed after the conclusion of the first cycle to 95 kN (21.3 kips). Additional cracking was noted and is also shown in Figure 24.

The cracking in the specimen was assessed two more times, once after 687,000 cycles to 95 kN (21.3 kips) and again after the conclusion of cyclic loading. These results are shown in Figure 25. This figure demonstrates that the cracking in the precast panels had essentially stabilized by the first assessment, while additional cracking in the field-cast UHPC continued to occur. The flexural cracking evident in the figure demonstrates both the post-cracking strain localization which typically occurs in conventional concrete and the post-cracking strain distribution which occurs in UHPC. The precast panels essentially have a single midspan flexural crack, while the UHPC connection displays 10 to 15 tightly spaced cracks near midspan.

No interface cracking was observed throughout the entire test. Also, no water leakage was observed at the interface or through the precast panels or UHPC.

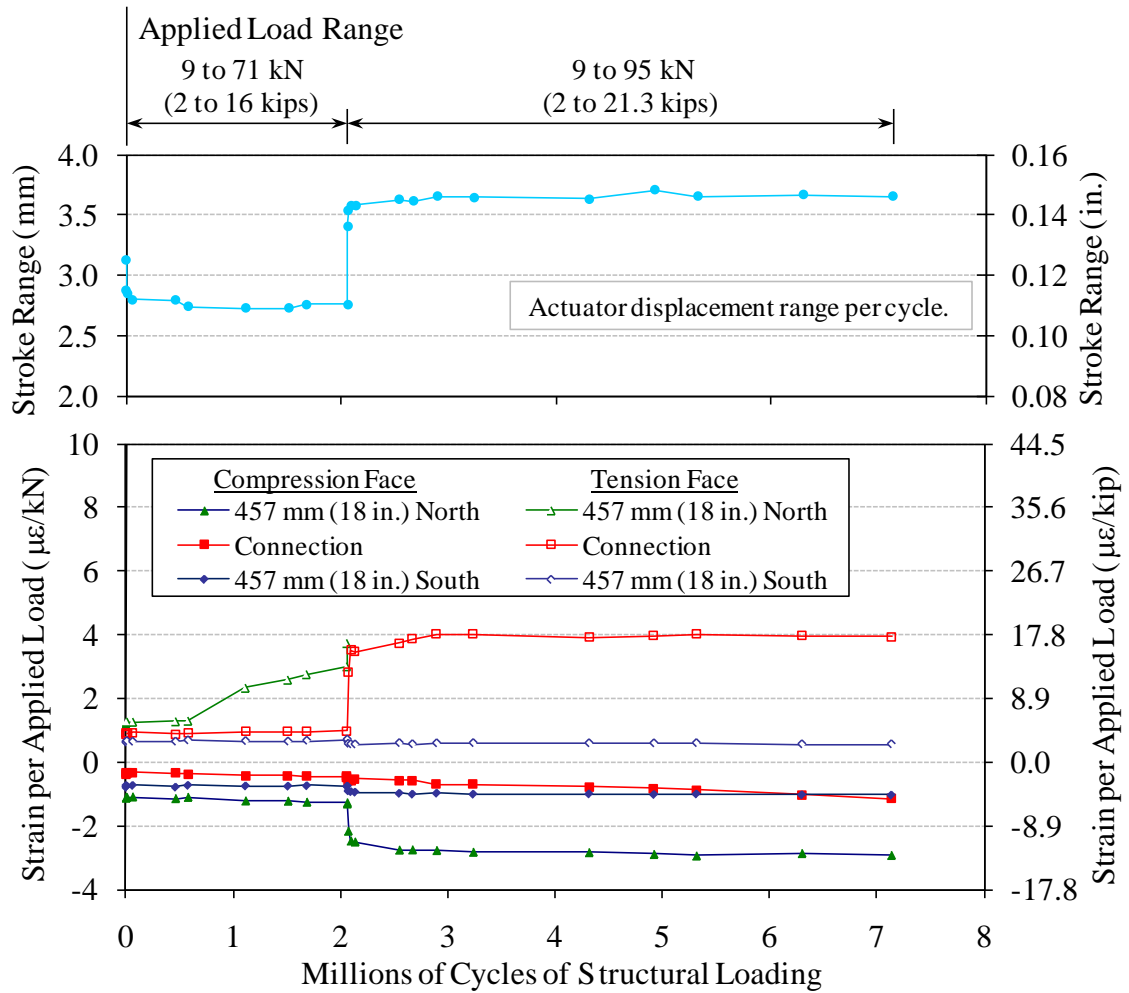


**Figure 21. Graph. Cyclic test results for panel 8H.**

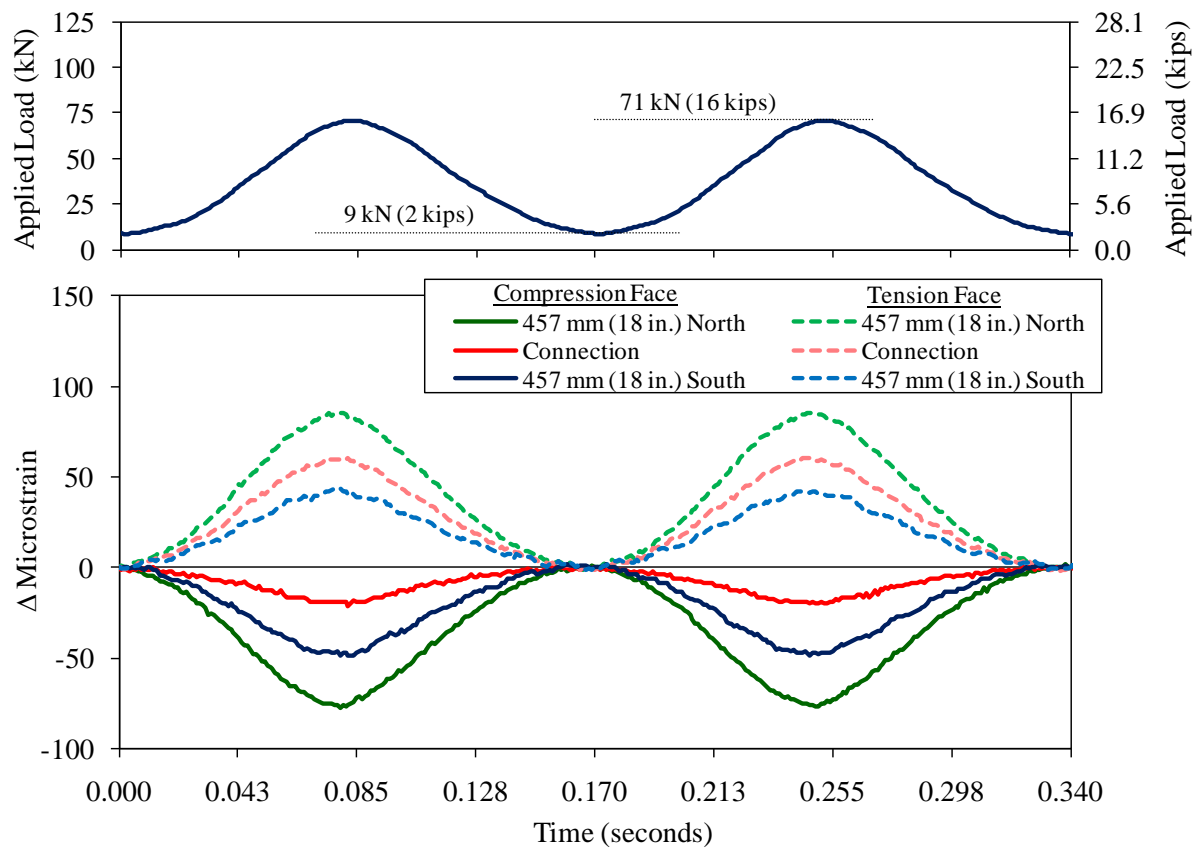


**Figure 22. Graph. Strain response for panel 8H after 462,000 cycles.**

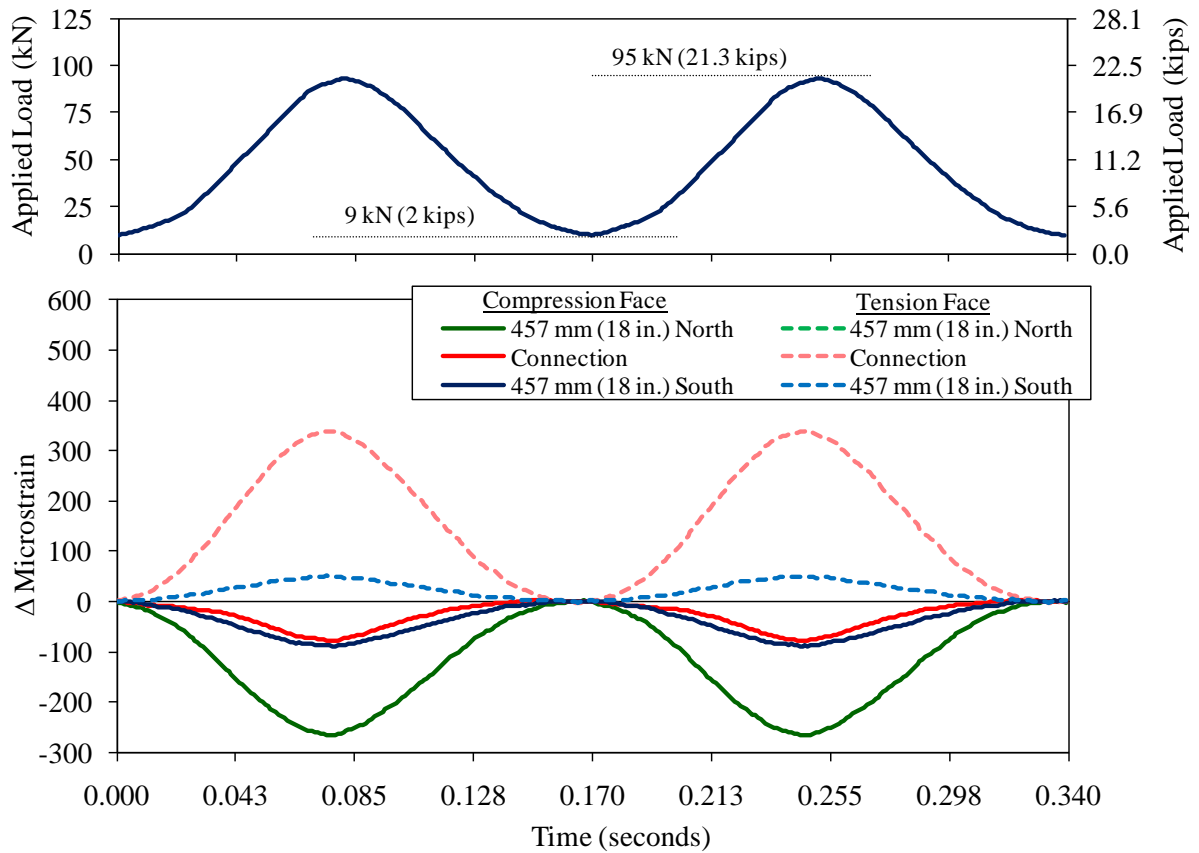


**Figure 23. Graph. Strain response for panel 8H after 7,137,000 cycles.**

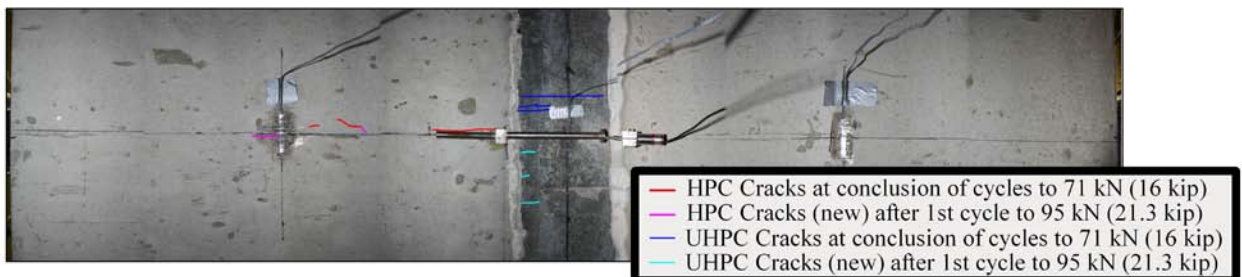


**Figure 24. Illustration. Cracking pattern observed on underside of panel 8H after the conclusion of 2.063 million cycles to 71 kN (16 kips), and additional cracks occurring during first cycle to 95 kN (21.3 kips).**

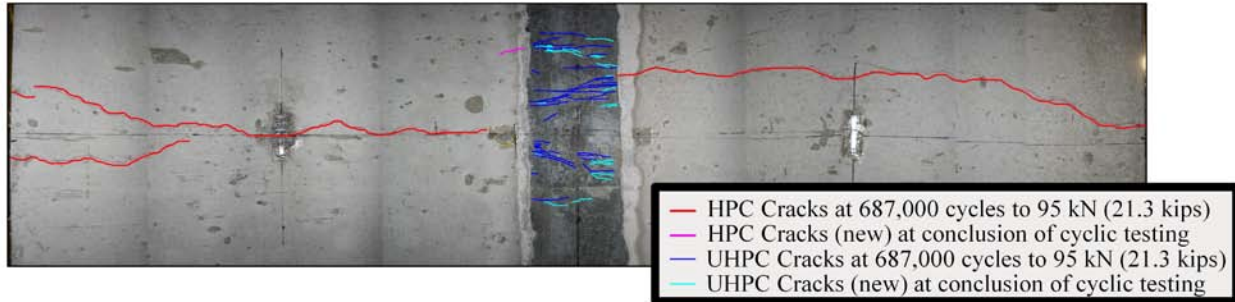


**Figure 25. Illustration. Cracking pattern observed on underside of panel 8H after 687,000 cycles to 95 kN (21.3 kips) and at the conclusion of cyclic testing.**

### *Static Testing*

The static testing of this specimen was completed according to the process described previously. The testing was completed over the course of 2 hours. The loading process included step-wise load application until approximately 400 kN (90 kips) of applied load was reached. After this the step-wise loading was changed to displacement control based on the midspan vertical displacement of the specimen. Recall that the cyclic loading of the specimen applied a peak load of approximately 95 kN (21.3 kips), which was sufficient to initiate inelastic behavior. As such, only loads greater than this level began to generate additional inelastic response.

The load-displacement results from the six potentiometers are presented in Figure 26. Similarly, the load-strain results from the six strain gages are presented in Figure 27. These results show that the inelastic cracking response of the specimen continued as the load increased to approximately 390 kN (85 kips). As the load increased above this level, the global response changed with significantly increased increments of displacement being observed. Complimentary behavior was displayed by the strain gages with increased strain per load increment being displayed at all three midspan gages. These behaviors are indicative of strain localization occurring in both the UHPC connection and in the precast panel, and the commensurate movement of the neutral axis toward the compression face of the specimen. This strain localization included pullout of the fiber reinforcement in the UHPC across a critical midspan crack as well as indications of yielding of the bottom mat of reinforcing steel at midspan. Figure 28 shows the underside of the specimen near midspan after a total of 40 mm (1.6 inch) of midspan centerline deflection had been imparted. Strain localization is apparent from the wide crack in the field-cast UHPC.

Failure of the specimen was defined as a decrease in ultimate load capacity concurrent with an increase in deflection. The specimen failed at a peak applied load of 503 kN (113 kips) at a measured midspan centerline displacement of 55 mm (2.16 inch). The failure was precipitated by the crushing of the concrete in the top of the specimen along midspan, primarily to the north of the load patch. Figure 29 provides a photograph of the specimen after failure, with the failed concrete clearly visible to the left of the load patch. There was no indication of debonding or other failure of the connection along either of the two connection interfaces. A photograph of the midspan centerline area on the underside of the specimen is provided in Figure 30.

After the completion of the test, the panel was inverted so that the cracking could be assessed and cataloged. Figure 31 illustrates the cracking that was observed. The cracks in the HPC precast panels were identified by eye. The cracks in the field-cast UHPC were identified with the aid of an alcohol-based spray. All cracks were marked on the surface of the specimen, photographed, then electronically traced and recorded with drawing software. The crack patterns clearly demonstrate the different behaviors exhibited by the two different types of concrete. In the HPC precast panels, a hypothetical line between the two supports would intersect between 10 and 20 discrete cracks. In the UHPC, a similar line would intersect between 120 and 140 discrete cracks. Aside from the single strain localization crack in the UHPC at midspan, the other cracks in the UHPC remained very tight after failure as a result of the elastic unloading of the fiber reinforcement bridging the cracks.

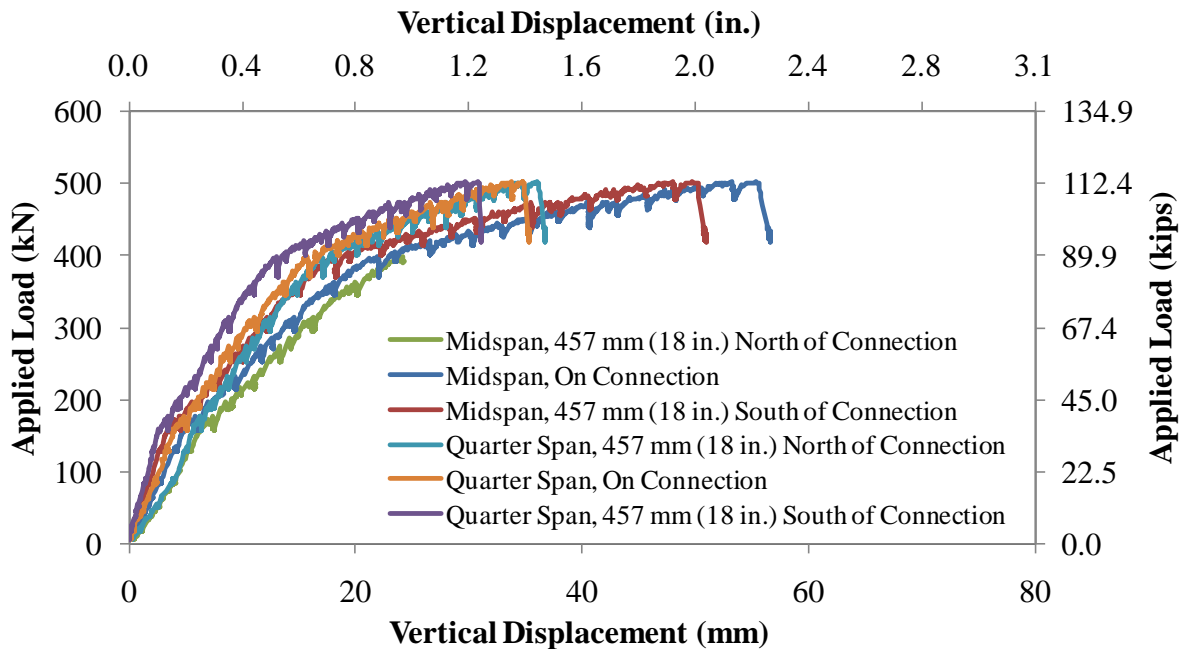


**Figure 26. Graph. Load-deflection response of panel 8H under step-wise loading to failure.**

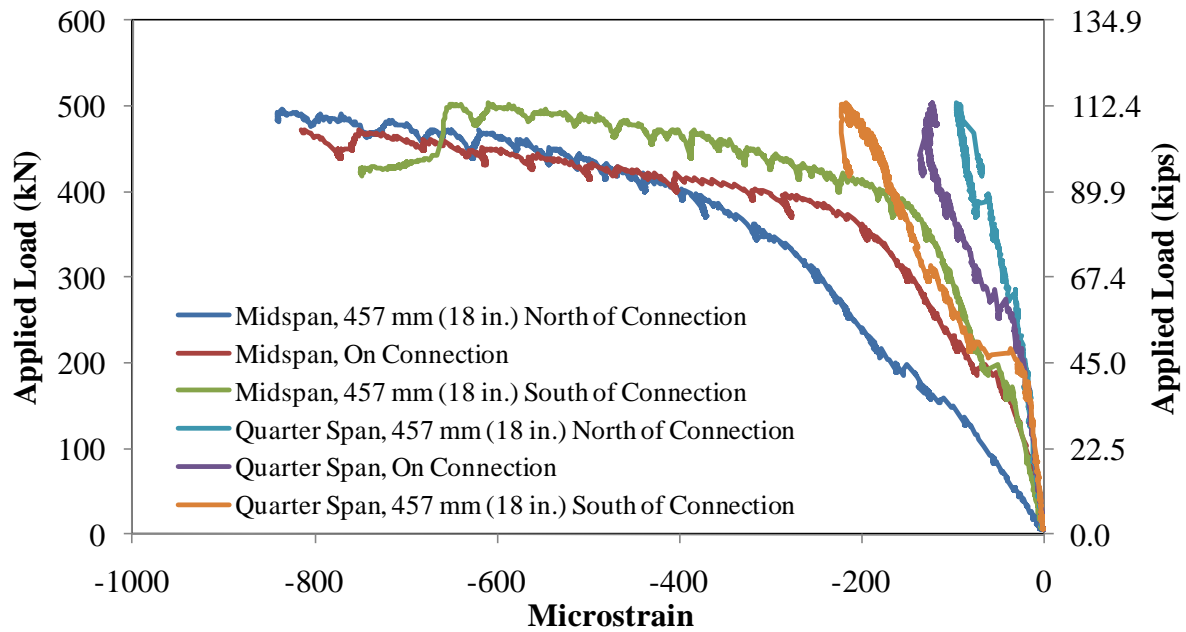


**Figure 27. Graph. Load-strain response of panel 8H under step-wise loading to failure.**

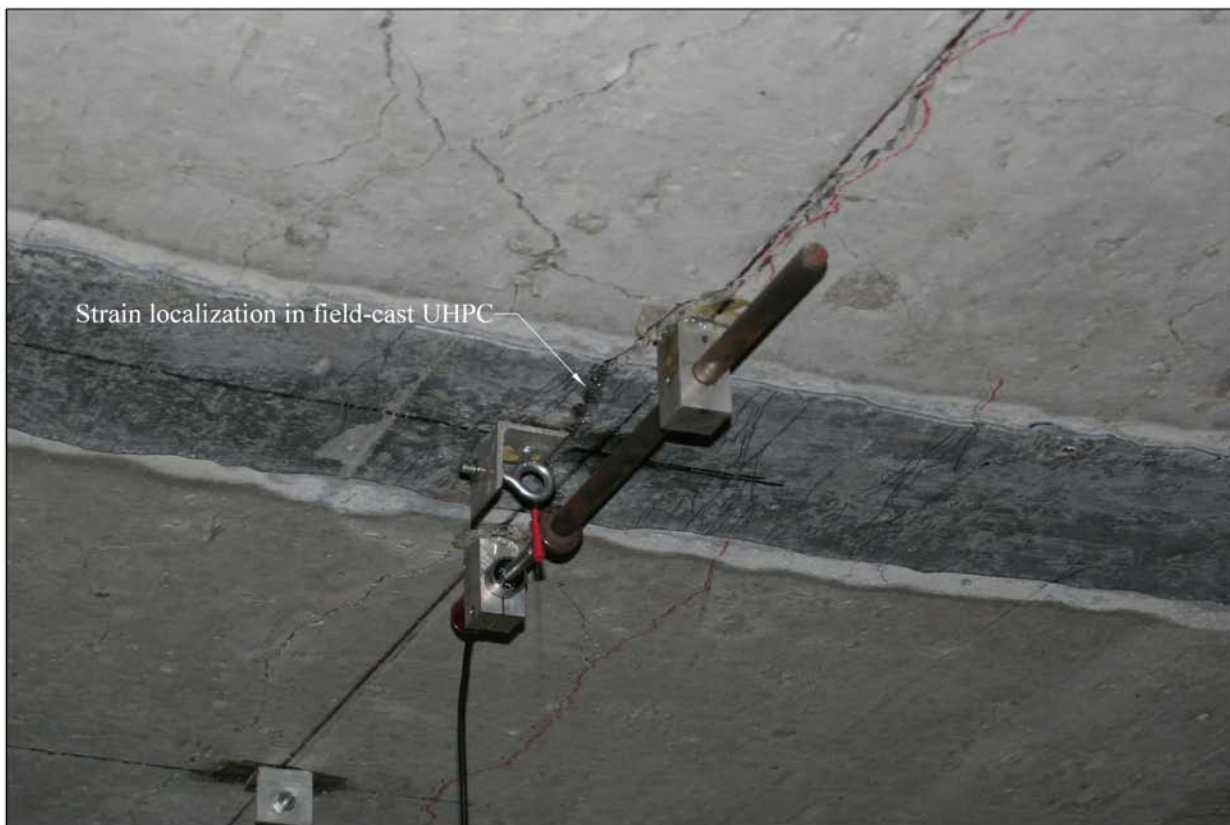


**Figure 28. Photograph. Underside of panel 8H near midspan after 40 mm (1.6 inch) of midspan centerline deflection.**

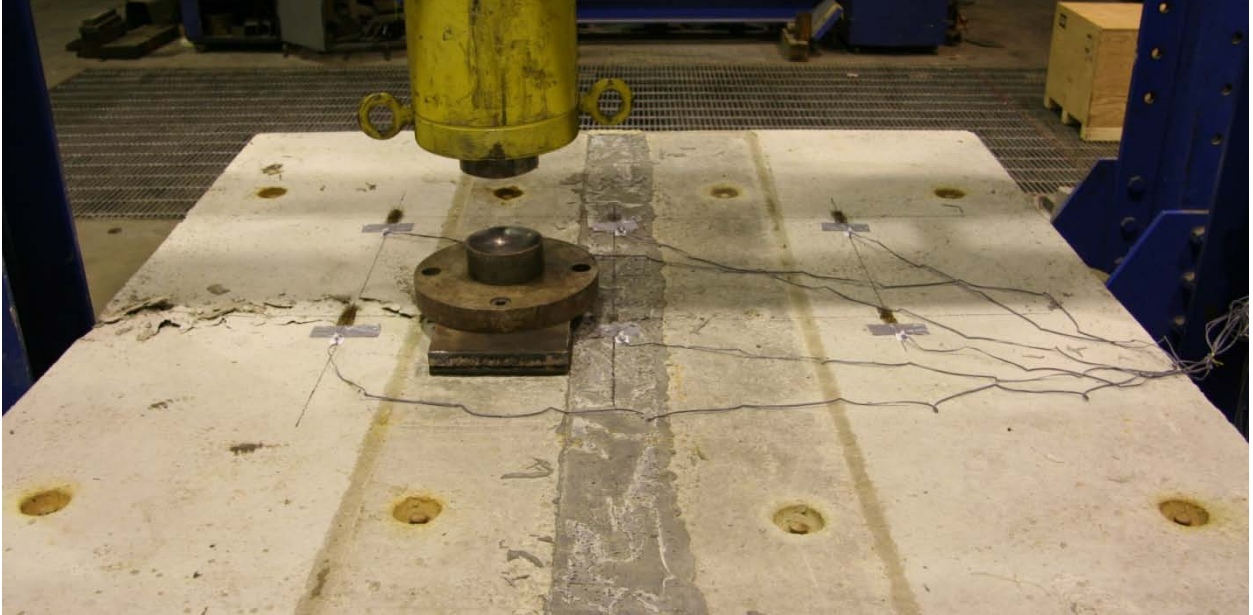


**Figure 29. Photograph. Top of panel 8H after flexural failure.**



**Figure 30. Photograph. Underside of panel 8H at midspan centerline location after flexural failure.**

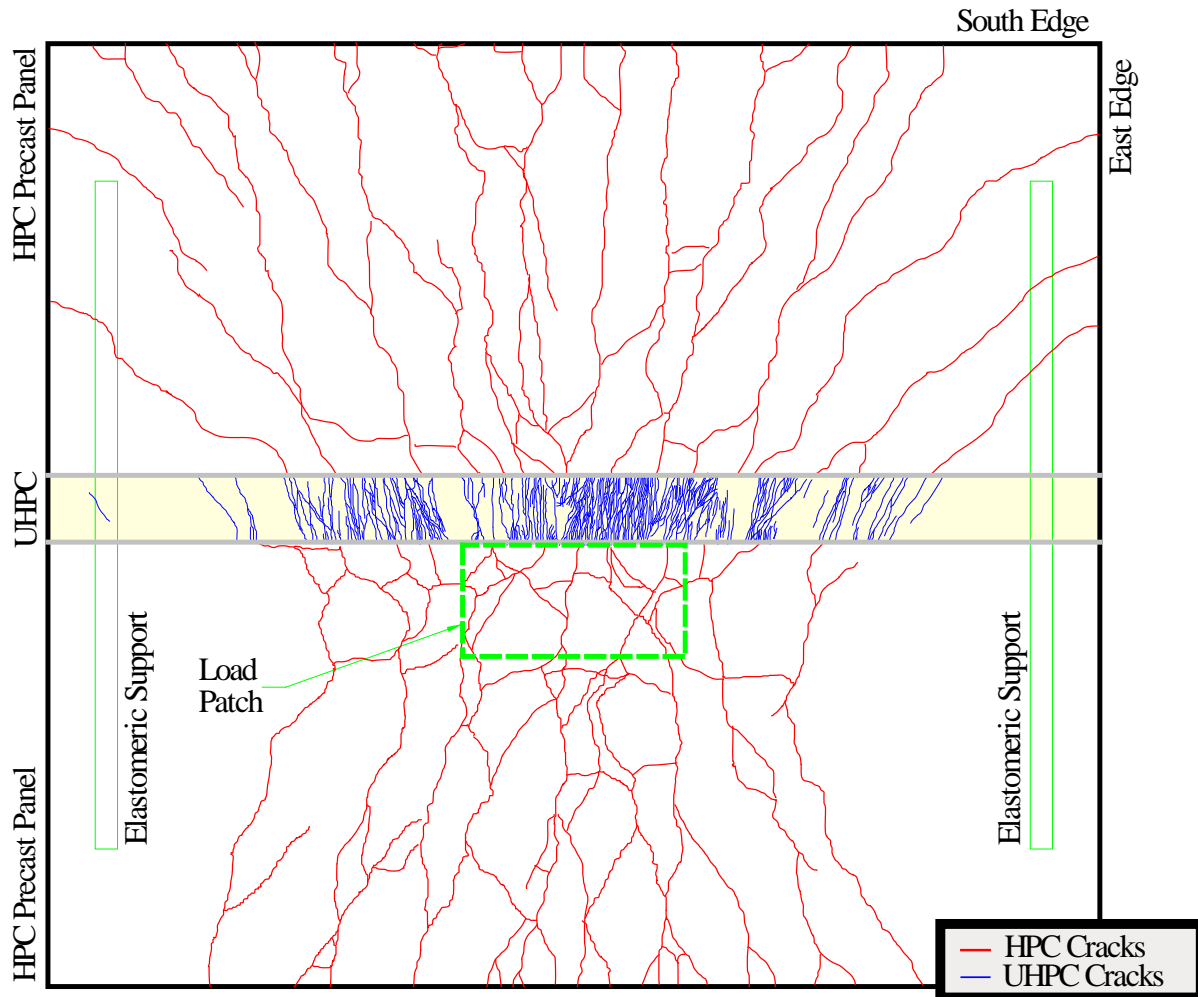


**Figure 31. Illustration. Cracking pattern observed on underside of panel 8H after conclusion of static test.**

### **Specimen 8E**

Specimen 8E was designed and loaded to simulate the transverse connection between two full-depth bridge deck panels. The reinforcing details were described in Chapter 3 and are shown in Figure 9. Recall that the discrete reinforcement within the connection included epoxy-coated hairpin reinforcement which was lapped across a 152 mm (6 inch) wide connection.

### ***Cyclic Testing***

The cyclic testing of this specimen was completed according to the process described previously. The testing was completed over the course of 3 months. The cyclic loading included 8,930,000 cycles with a sinusoidal applied load ranging from 9 to 71 kN (2 to 16 kips), followed by 5,222,000 cycles ranging from 9 to 95 kN (2 to 21.3 kips).

The structural response of the specimen as captured by the electronic gages is presented in Figure 32. This two part graph shows the stroke range of the hydraulic actuator and the strain per unit of applied load on the specimen as a function of the number of cycles of load applied. The data in this figure was generated by analyzing the response of the specimen as captured during the increasing load portion of periodic cycles throughout the test. The stroke range was calculated from the maximum and minimum displacement of the actuator piston during a cycle. The strain per applied load was calculated through a best-fit approximation of the slope of the load-strain response over the load range from approximately 36 kN (8 kips) to approximately 90 percent of the peak applied load. The results in Figure 32 show that the response of the specimen stabilized during the cyclic loading in each load range.

The strain response of the specimen as captured at a representative timeframe during the test is presented in Figure 33. This figure shows the range of strain observed on the surface of the specimen at the strain gage locations. These results pertain to strains observed after 5,824,000 cycles of loading to 71 kN (16 kips) had been completed.

Prior to the start of cyclic loading, the specimen was checked for structural cracking that may have occurred during handling or test setup. No cracks were identified. Next, the specimen was statically loaded to 71 kN (16 kips) then unloaded to 9 kN (2 kips). Again, no cracks were identified. After the conclusion of the 8.93 million cycles to 71 kN (16 kips), the specimen was again checked for cracks. No cracks were found.

Cracking in the specimen was assessed immediately after the first cycle to 95 kN (21.3 kips) was completed. A single flexural crack was observed to run from 50 mm (2 inch) north of the connection at midspan to the north edge of the specimen. This continuous crack in the precast panel was small but visible by the unaided eye. No cracking was observed in the UHPC connection or at the connection interface.

Cracking was assessed periodically throughout the remainder of the cyclic testing of this specimen. During the first one million cycles to 95 kN (21.3 kips), the midspan flexural crack on the north panel extended through the UHPC connection, into the south precast panel, and to the south edge of the specimen. No additional cracking was noted during the final 4.222 million cycles applied to this specimen. In the precast panels, the crack was a single crack nominally located at midspan. At the connection the single crack in the precast panels did not run directly into a single UHPC crack. Instead, it stopped at the interface then restarted as a set of nominally parallel cracks running across the connection. These UHPC cracks were only visible with the aid of a volatile, alcohol-based crack spray.

No interface cracking was observed throughout the entire test. Also, no water leakage was observed at the interface or through the precast panels or UHPC.

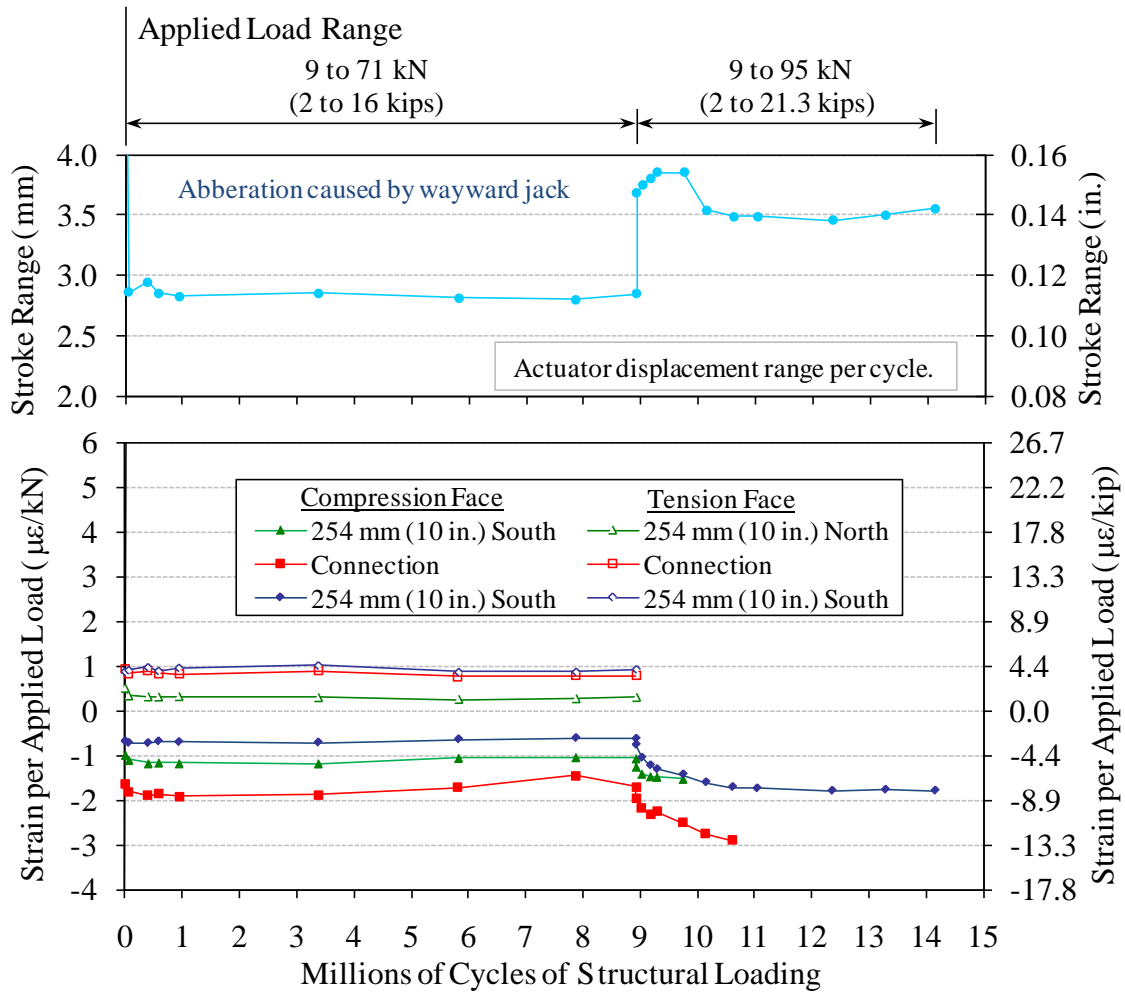


**Figure 32. Graph. Cyclic test results for panel 8E.**

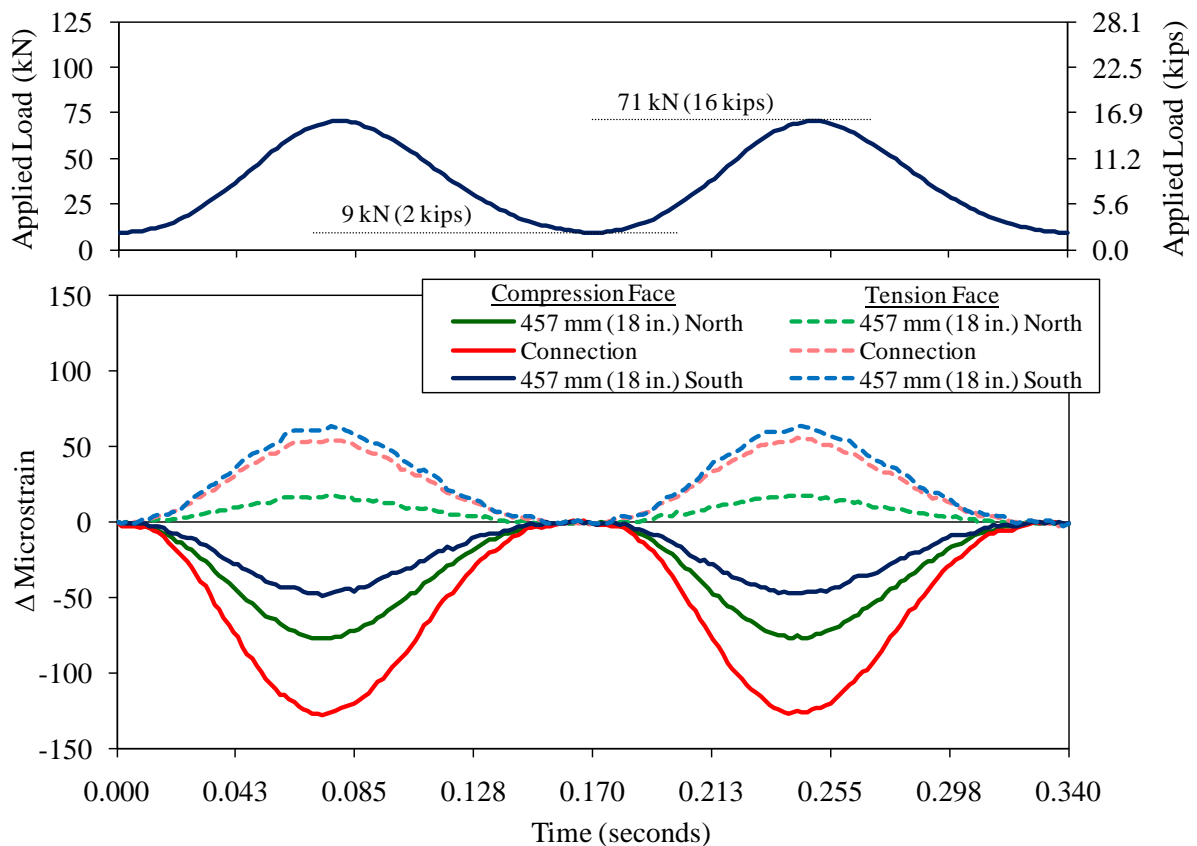


**Figure 33. Graph. Strain response for panel 8E after 5,824,000 cycles.**

### *Static Testing*

The static testing of this specimen was completed according to the process described previously. The testing was completed over the course of 2 hours. The loading process included step-wise load application until approximately 380 kN (85 kips) of applied load was reached. After this the step-wise loading was changed to displacement control based on the midspan vertical displacement of the specimen. Recall that the cyclic loading of the specimen applied a peak load of approximately 95 kN (21.3 kips), which was sufficient to initiate inelastic behavior. As such, only loads greater than this level began to generate additional inelastic response.

A data acquisition and storage failure resulted in the loss of the full data set collected from the electronic gages during the testing of this specimen. As such, only the backup electronic data set can be presented herein. This data set only included data collected as 16 of the loading steps were reached. This data was manually captured from the data acquisition readout during the test, and thus is significantly more sparse than the data collected during the other deck panel static tests.

The load-displacement results from the six potentiometers are presented in Figure 34. Similarly, the load-strain results from the six strain gages are presented in Figure 35. These results show

that the inelastic cracking response of the specimen continued as the load increased to approximately 340 kN (77 kips). As the load increased above this level, the global response changed with significantly increased increments of displacement being observed. Complimentary behavior was displayed by the strain gages with increased strain per load increment being displayed at two of the three midspan gages. These behaviors are indicative of strain localization occurring in both the UHPC connection and in the precast panel, and the commensurate movement of the neutral axis toward the compression face of the specimen. This strain localization included pullout of the fiber reinforcement in the UHPC across critical midspan cracks as well as indications of yielding of the bottom mat of reinforcing steel at midspan. Figure 36 shows the specimen after a total of 53 mm (2.1 inch) of midspan centerline deflection had been imparted.

Failure of the specimen was defined as a decrease in ultimate load capacity concurrent with an increase in deflection. The specimen failed at a peak applied load of 499 kN (112 kips) at a measured midspan centerline displacement of 74 mm (2.90 inch). The failure was precipitated by the crushing of the concrete in the top of the specimen along midspan, primarily to the north of the load patch. Figure 37 provides a photograph of the specimen after failure, with the failed concrete clearly visible to the left of the load patch. Aside from a short length in an area near the UHPC strain localizations, there was no indication of debonding or other failure of the connection along either of the two connection interfaces. A photograph of the midspan centerline area on the underside of the specimen is provided in Figure 38. The two major and one minor strain localization cracks, along with the short length of interface cracking, are annotated in the figure.

After the completion of the test, the panel was inverted so that the cracking could be assessed and cataloged. Figure 39 illustrates the cracking that was observed. The cracks in the HPC precast panels were identified by eye. The cracks in the field-cast UHPC were identified with the aid of an alcohol-based spray. All cracks were marked on the surface of the specimen, photographed, then electronically traced and recorded with drawing software. The crack patterns clearly demonstrate the different behaviors exhibited by the two different types of concrete. In the HPC precast panels, a hypothetical line between the two supports would intersect between 10 and 20 discrete cracks. In the field-cast UHPC, a similar line would intersect between 160 and 200 discrete cracks. Aside from the strain localization cracks in the UHPC at midspan, the other cracks in the UHPC remained very tight after failure as a result of the elastic unloading of the fiber reinforcement bridging the cracks.

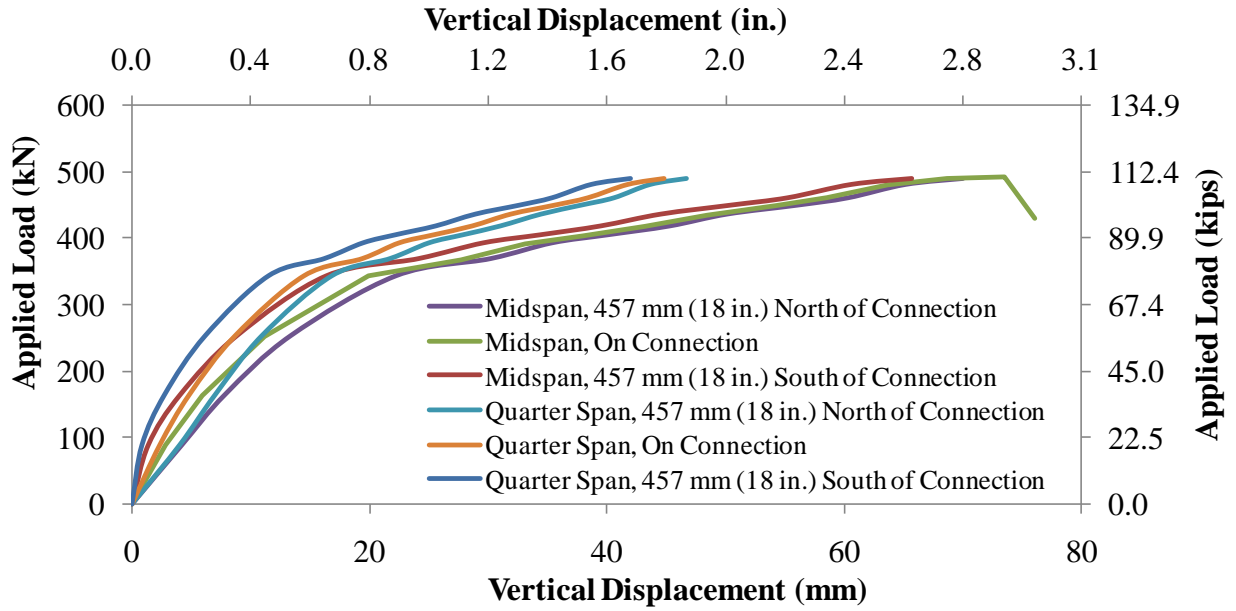


Figure 34. Graph. Load-deflection response of panel 8E under step-wise loading to failure.

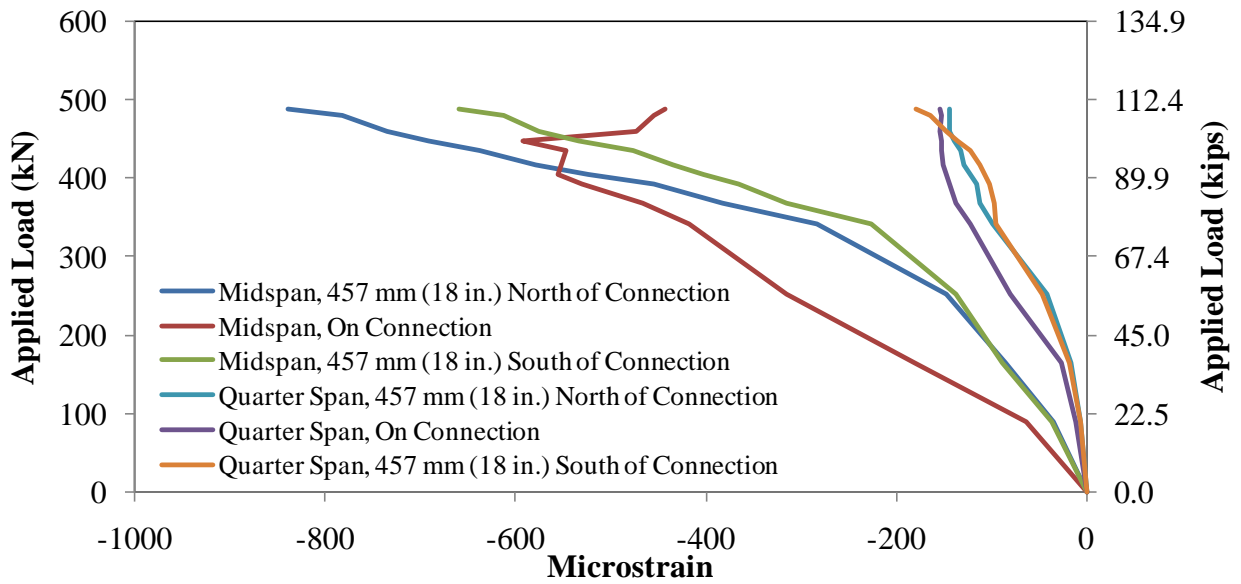


Figure 35. Graph. Load-strain response of panel 8E under step-wise loading to failure.



**Figure 36. Photograph. East side and top of panel 8E after 53 mm (2.1 inch) of midspan centerline deflection.**



**Figure 37. Photograph. Top of panel 8E after flexural failure.**

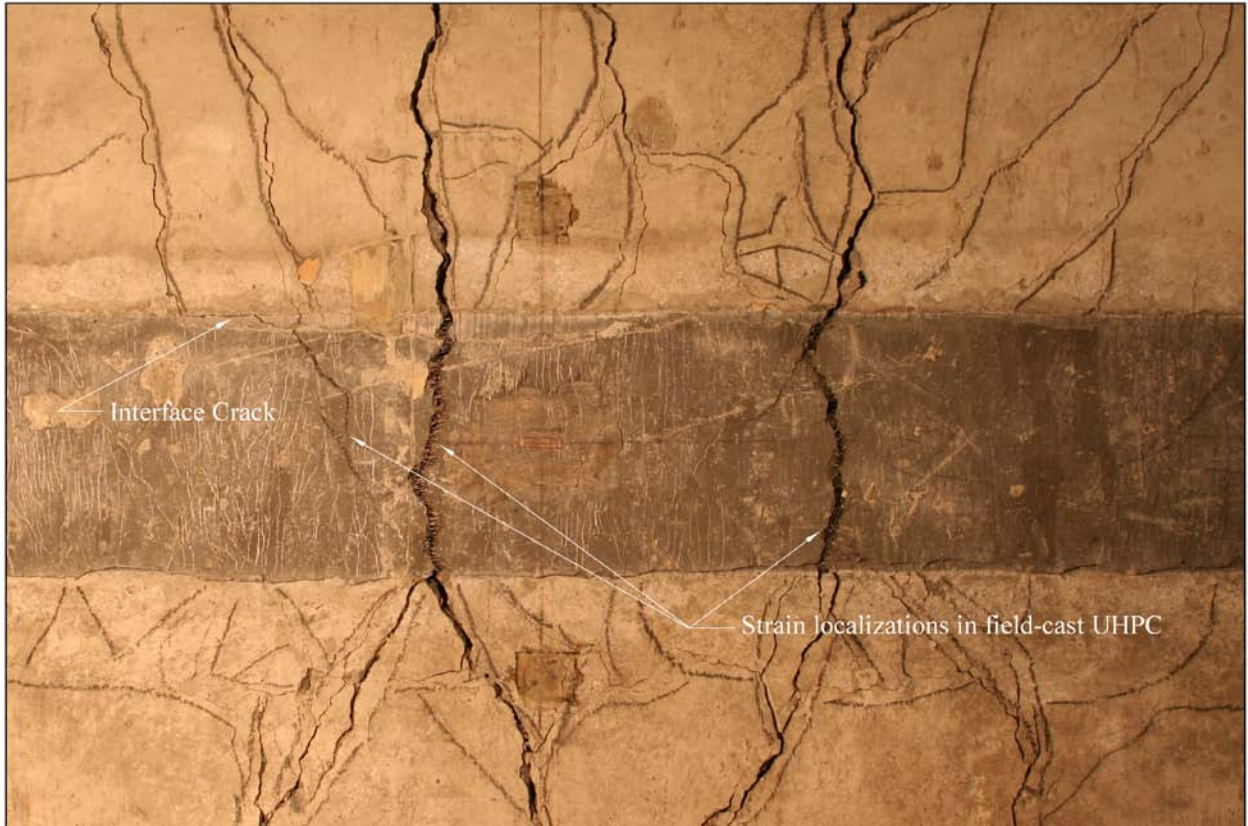


**Figure 38. Photograph. Underside of panel 8E near midspan centerline location after flexural failure.**

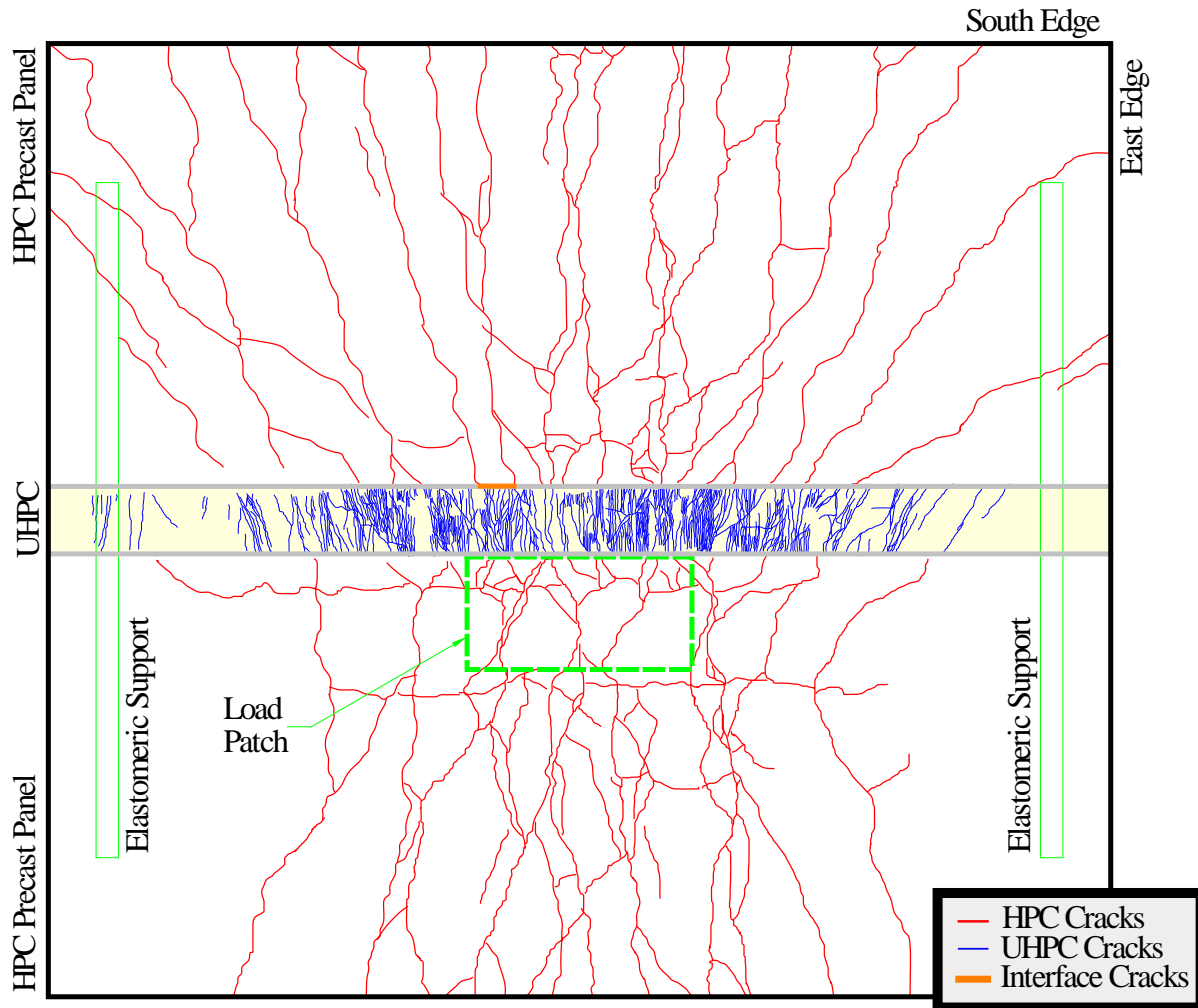


**Figure 39. Illustration. Cracking pattern observed on underside of panel 8E after conclusion of static test.**

## Specimen 8G

Specimen 8G was designed and loaded to simulate the transverse connection between two full-depth bridge deck panels. The reinforcing details were described in Chapter 3 and are shown in Figure 10. Recall that the discrete reinforcement within the connection included two layers of straight galvanized reinforcing bars which were lapped across a 152 mm (6 inch) wide connection.

### *Cyclic Testing*

The cyclic testing of this specimen was completed according to the process described previously. The testing was completed over the course of 4 weeks. The cyclic loading included 2,170,000 cycles with a sinusoidal applied load ranging from 9 to 71 kN (2 to 16 kips), followed by 5,621,018 cycles ranging from 9 to 95 kN (2 to 21.3 kips).

The structural response of the specimen as captured by the electronic gages is presented in Figure 40. This two part graph shows the stroke range of the hydraulic actuator and the strain per unit of applied load on the specimen as a function of the number of cycles of load applied. The data in this figure was generated by analyzing the response of the specimen as captured during the increasing load portion of periodic cycles throughout the test. The stroke range was calculated from the maximum and minimum displacement of the actuator piston during a cycle. The strain per applied load was calculated through a best-fit approximation of the slope of the load-strain response over the load range from approximately 36 kN (8 kips) to approximately 90 percent of the peak applied load. The results in the figure show that the response of the specimen stabilized soon after the initiation of cyclic loading in each load range.

The strain response of the specimen as captured at two representative timeframes during the test is presented in Figure 41 and Figure 42. These figures show the range of strain observed on the surface of the specimen at the strain gage locations. Figure 41 presents results from early in the loading after a total of 1,694,000 cycles had been completed. Figure 42 presents results from the end of cyclic testing after a total of 7,791,000 cycles had been completed.

Prior to the start of cyclic loading, the specimen was checked for structural cracking that may have occurred during handling or test setup. No cracks were identified. Next, the specimen was statically loaded to 71 kN (16 kips) then unloaded to 9 kN (2 kips). Again, no cracks were identified. After the conclusion of cycling to 71 kN (16 kips), the specimen was again checked for cracks. None were found.

Cracking in the specimen was again assessed immediately after the first cycle to 95 kN (21.3 kips) was completed. A single flexural crack was observed to run from 50 mm (2 inch) north of the connection at midspan to 200 mm (8 inch) from the north edge of the specimen. This continuous crack in the precast panel was small but visible with the naked eye. No cracking was observed in the field-cast UHPC or at the connection interface. The location of this crack is noted in Figure 43.

Following 73,000 cycles to 95 kN (21.3 kips), the cracking of the panel was assessed. The single crack in the north precast panel was observed to have extended 25 mm (1 inch) farther south as well as 200 mm (8 inch) north to the edge of the specimen. The crack did not reach the connection interface, and no cracks were observed in the UHPC, in the south precast panel, or along the connection interface.

Additional cracking occurred during the remainder of the cycling to 95 kN (21.3 kips). Figure 43 shows the full crack pattern which was observed on the underside of the panel after the conclusion of cyclic testing. The precast panel cracks ranged in width from 0.03 to 0.13 mm (0.001 to 0.005 inch). The UHPC cracks were far more numerous and tended to be clustered in locations near the interface terminations of the precast panel cracks. The widths of the UHPC cracks could not be measured with the available crack microscope, which was limited to measuring cracks larger than 0.013 mm (0.0005 inch).

No interface cracking was observed throughout the entire test. Also, no water leakage was observed at the interface or through the precast panels or UHPC.

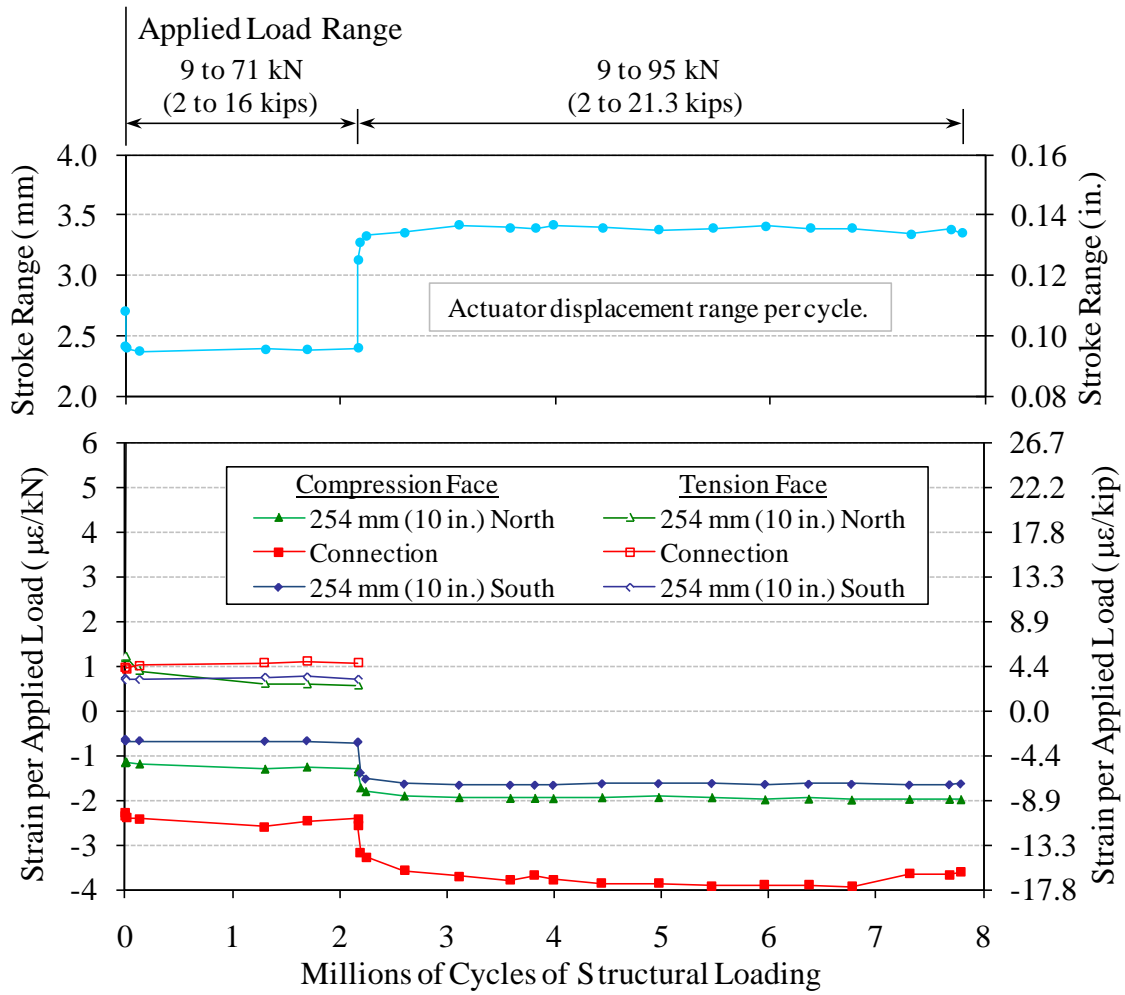


**Figure 40. Graph. Cyclic test results for panel 8G.**

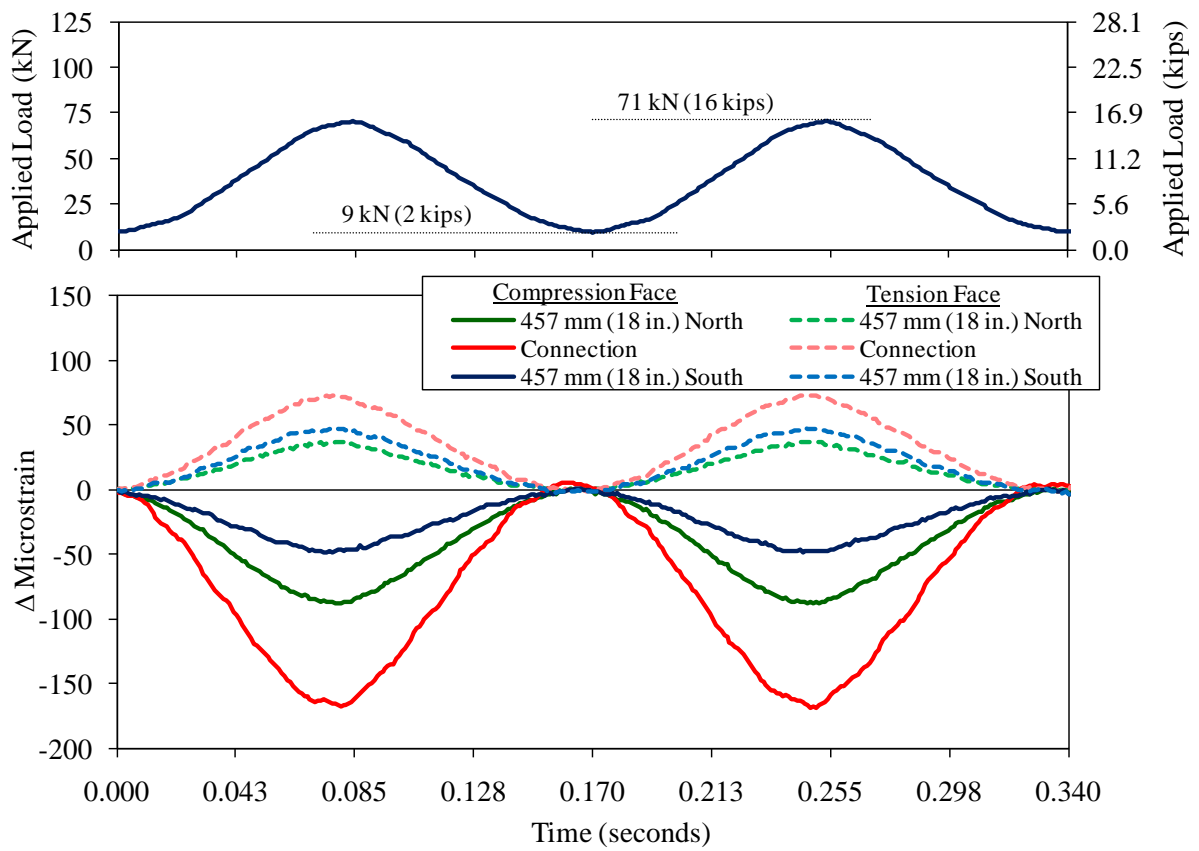


**Figure 41. Graph. Strain response for panel 8G after 1,694,000 cycles.**

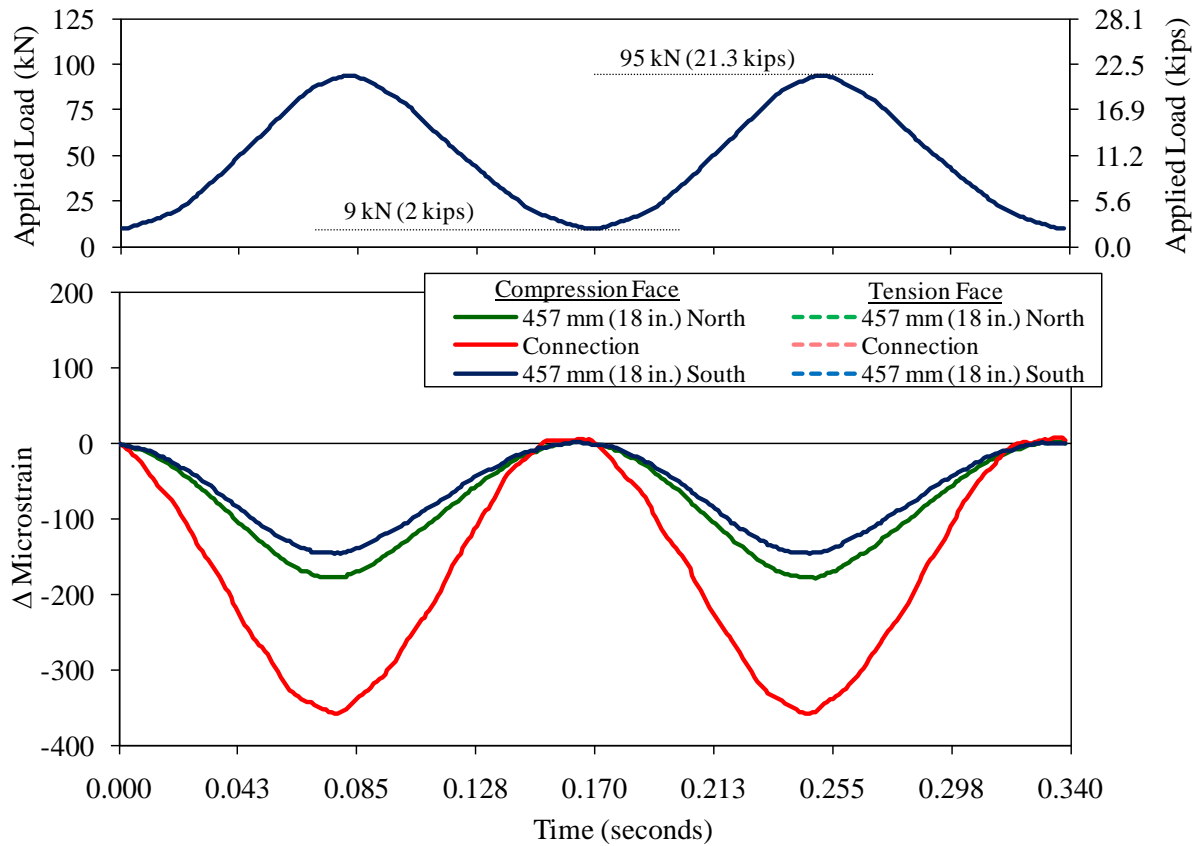


**Figure 42. Graph. Strain response for panel 8G after 7,791,000 cycles.**

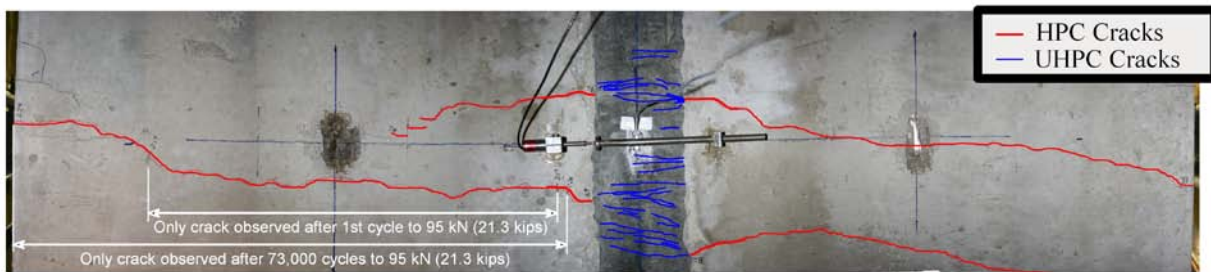


**Figure 43. Illustration. Cracking pattern observed on underside of panel 8G after the conclusion of cyclic testing.**

### **Static Testing**

The static testing of this specimen was completed according to the process described previously. The testing was completed over the course of 2 hours. The loading process included step-wise load application until approximately 360 kN (80 kips) of applied load was reached. After this the

step-wise loading was changed to displacement control based on the midspan vertical displacement of the specimen. Recall that the cyclic loading of the specimen applied a peak load of approximately 95 kN (21.3 kips), which was sufficient to initiate inelastic behavior. As such, only loads greater than this level began to generate additional inelastic response.

The load-displacement results from the six potentiometers are presented in Figure 44. Similarly, the load-strain results from the six strain gages are presented in Figure 45. These results show that the inelastic cracking response of the specimen continued as the load increased to approximately 385 kN (86 kips). As the load increased above this level, the global response changed with significantly increased increments of displacement being observed. Complimentary behavior was displayed by the strain gages with increased strain per load increment being displayed at two of the three midspan gages. These behaviors are indicative of strain localization occurring in both the field-cast UHPC and in the precast panel, and the commensurate movement of the neutral axis toward the compression face of the specimen. This strain localization included pullout of the fiber reinforcement in the UHPC across critical midspan cracks as well as indications of yielding of the bottom mat of reinforcing steel at midspan. The first visual indication of the strain localization on the underside of the UHPC connection was observed at a midspan centerline displacement of 25 mm (1.0 inch) corresponding to an applied load of 391 kN (88 kips).

Failure of the specimen was defined as a decrease in ultimate load capacity concurrent with an increase in deflection. The specimen failed at a peak applied load of 501 kN (113 kips) at a measured midspan centerline displacement of 65 mm (2.57 inch). The failure was precipitated by the crushing of the concrete in the top of the specimen along midspan. Figure 46 provides a photograph of the specimen after failure, with the failed concrete clearly visible to the left and right of the load patch. Aside from a short length in an area near the UHPC strain localizations on the underside of the specimen, there was no indication of debonding or other failure of the connection along either of the two connection interfaces. A photograph of the midspan centerline area on the underside of the specimen is provided in Figure 47. The two major and one minor localization cracks, along with the short length of interface cracking, are annotated in the figure.

After the completion of the test, the panel was inverted so that the cracking could be assessed and cataloged. Figure 48 illustrates the cracking that was observed. The cracks in the HPC precast panels were identified by eye. The cracks in the field-cast UHPC were identified with the aid of an alcohol-based spray. All cracks were marked on the surface of the specimen, photographed, then electronically traced and recorded with drawing software. The crack patterns clearly demonstrate the different behaviors exhibited by the two different types of concrete. In the HPC precast panels, a hypothetical line between the two supports would intersect between 10 and 20 discrete cracks. In the field-cast UHPC, a similar line would intersect between 160 and 200 discrete cracks. Aside from the strain localization cracks in the UHPC at midspan, the other cracks in the UHPC remained very tight after failure as a result of the elastic unloading of the fiber reinforcement bridging the cracks.

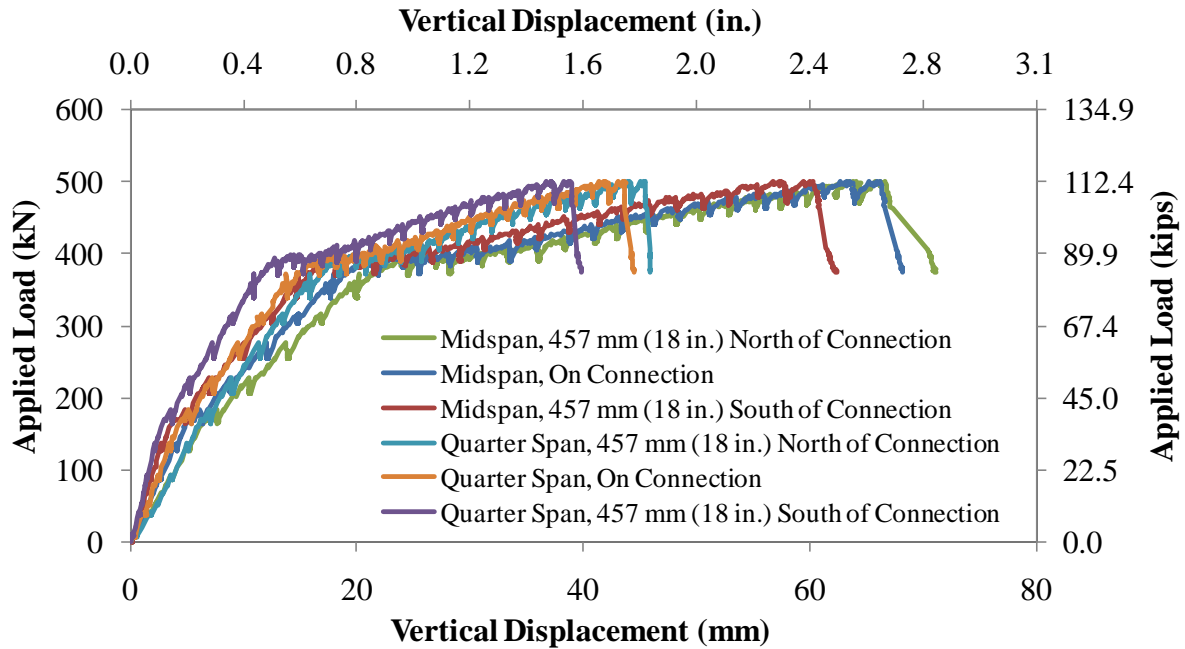


Figure 44. Graph. Load-deflection response of panel 8G under step-wise loading to failure.

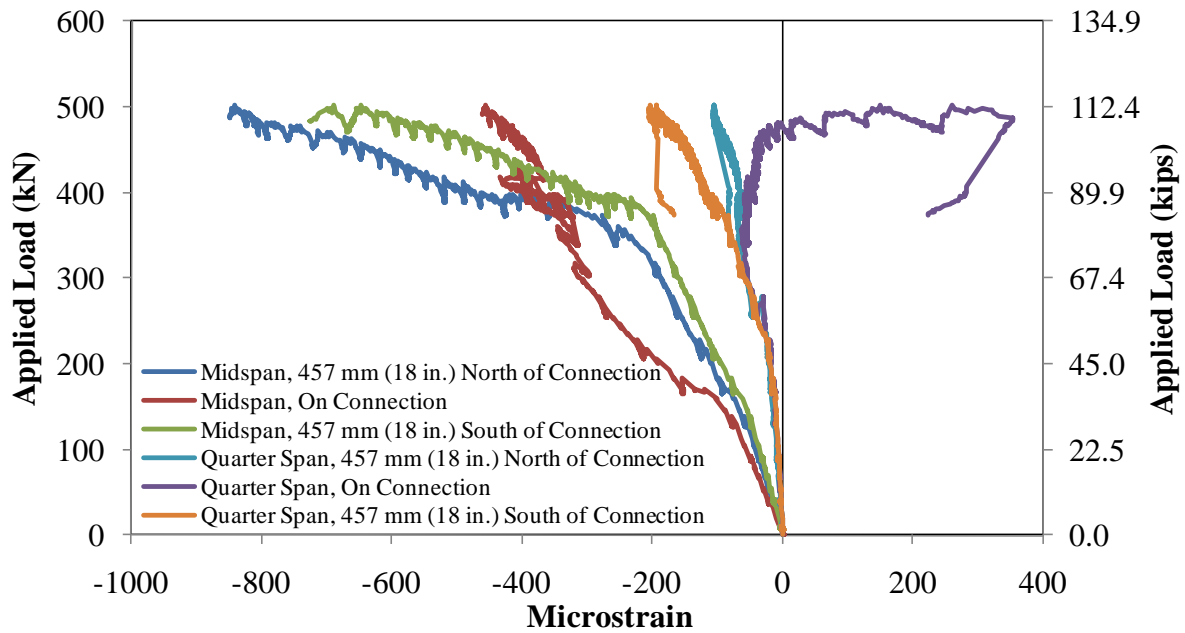
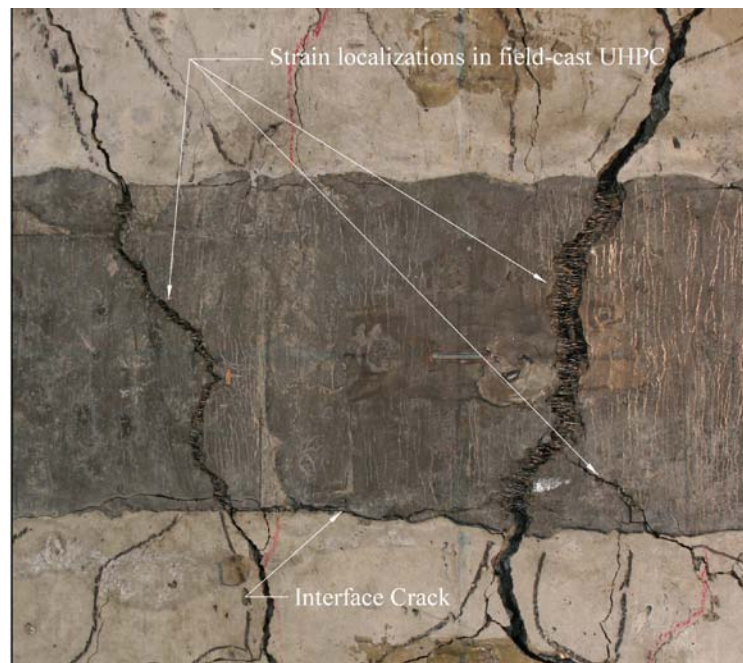


Figure 45. Graph. Load-strain response of panel 8G under step-wise loading to failure.



**Figure 46. Photograph. Top of panel 8G after flexural failure.**



**Figure 47. Photograph. Underside of panel 8G near midspan centerline location after flexural failure.**

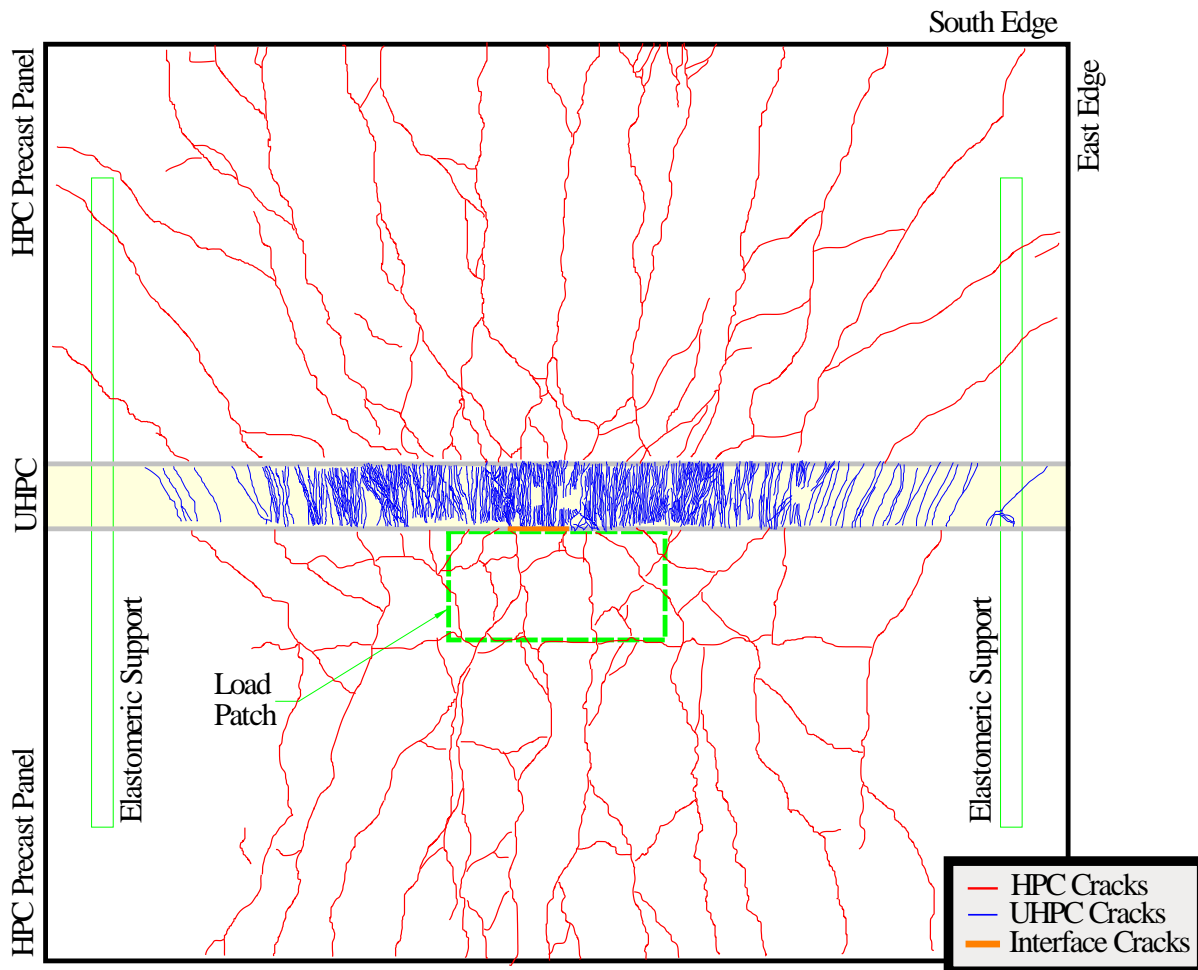


**Figure 48. Illustration. Cracking pattern observed on underside of panel 8G after conclusion of static test.**

### **Specimen 8B**

Specimen 8B was designed and loaded to simulate the transverse connection between two full-depth bridge deck panels. The reinforcing details were described in Chapter 3 and are shown in Figure 10. Recall that the discrete reinforcement within the connection included two layers of straight reinforcing bars which were lapped across a 152 mm (6 inch) wide connection.

### ***Cyclic Testing***

The cyclic testing of this specimen was completed according to the process described previously. The testing was completed over the course of 4 weeks. The cyclic loading included 2,117,239 cycles with a sinusoidal applied load ranging from 9 to 71 kN (2 to 16 kips), followed by 5,255,008 cycles ranging from 9 to 95 kN (2 to 21.3 kips).

The structural response of the specimen as captured by the electronic gages is presented in Figure 49. This two part graph shows the stroke range of the hydraulic actuator and the strain per unit of applied load on the specimen as a function of the number of cycles of load applied. The data in this figure was generated by analyzing the response of the specimen as captured during the increasing load portion of periodic cycles throughout the test. The stroke range was calculated from the maximum and minimum displacement of the actuator piston during a cycle. The strain per applied load was calculated through a best-fit approximation of the slope of the load-strain response over the load range from approximately 36 kN (8 kips) to approximately 90 percent of the peak applied load. The results in the figure show that the response of the specimen stabilized soon after the initiation of cyclic loading in each load range.

The strain response of the specimen as captured at two representative timeframes during the test is presented in Figure 50 and Figure 51. These figures show the range of strain observed on the surface of the specimen at the strain gage locations. Figure 50 presents results from early in the loading after a total of 1,608,000 cycles had been completed. Figure 51 presents results from the end of cyclic testing after a total of 7,372,000 cycles had been completed.

Prior to the start of cyclic loading, the specimen was checked for structural cracking that may have occurred during handling or test setup. No cracks were identified. Next, the specimen was statically loaded to 71 kN (16 kips) then unloaded to 9 kN (2 kips). Again, no cracks were identified. After the conclusion of cycling to 71 kN (16 kips), the specimen was again checked for cracks. None were found.

Cracking in the specimen was assessed immediately after one cycle and after 54,000 cycles to 95 kN (21.3 kips) were completed. No cracks were found. Cracking was again assessed after 169,000 cycles to 95 kN (21.3 kips) were completed. A single flexural crack was observed at midspan on the underside of the north precast panel. This crack stopped short of both the connection interface and the north edge of the specimen.

A further crack assessment was completed after 263,000 cycles to 95 kN (21.3 kips) were completed. The crack in the north precast panel was observed to have extended such that a midspan flexural crack now ran from the north to the south edge of the specimen.

A final crack assessment was completed after the conclusion of cyclic testing. The results of this crack assessment are shown in Figure 52. The single midspan flexural crack was observed to extend across the specimen. At the connection interfaces, the precast panel cracks were observed stop and multiple UHPC cracks were observed to begin. The figure shows that there were approximately 10 to 15 UHPC cracks running across the connection near the terminations of the precast panel cracks. The widths of the precast panel cracks were measured to be approximately 0.08 mm (0.003 inch) at the conclusion of cyclic loading. The UHPC cracks were only visible with the aid of an alcohol-based spray. The widths of the UHPC cracks could not be measured with the available crack microscope, which was limited to measuring cracks larger than 0.013 mm (0.0005 inch).

No interface cracking was observed throughout the entire test. Also, no water leakage was observed at the interface or through the precast panels or UHPC.

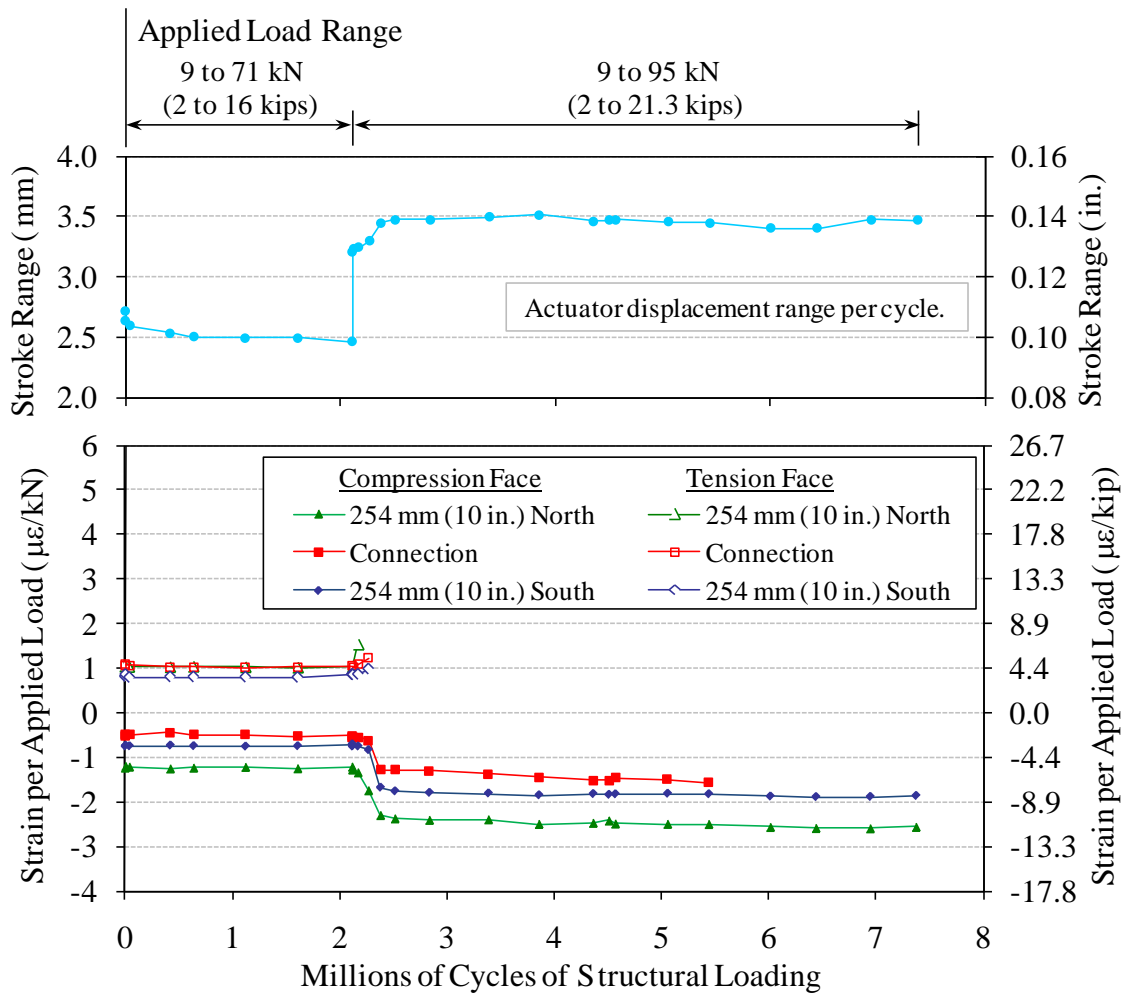


**Figure 49. Graph. Cyclic test results for panel 8B.**

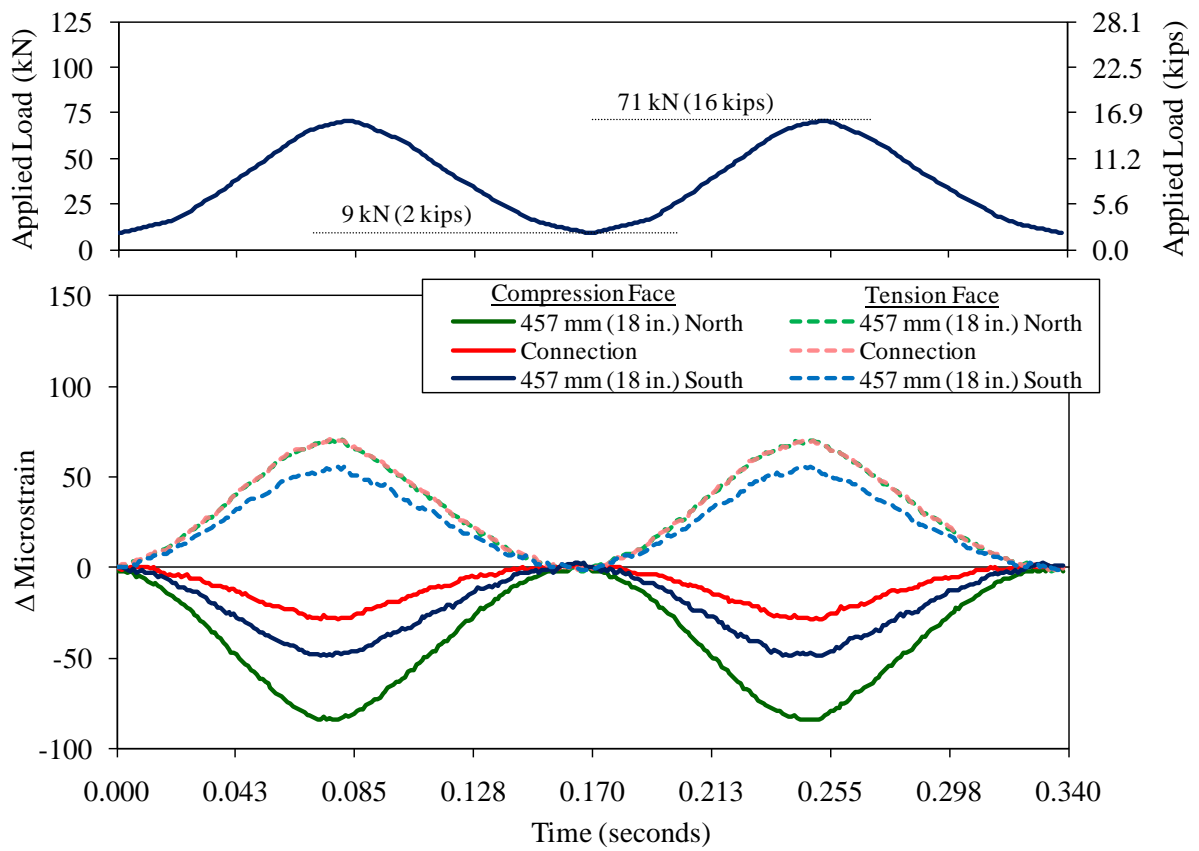


**Figure 50. Graph. Strain response for panel 8B after 1,608,000 cycles.**

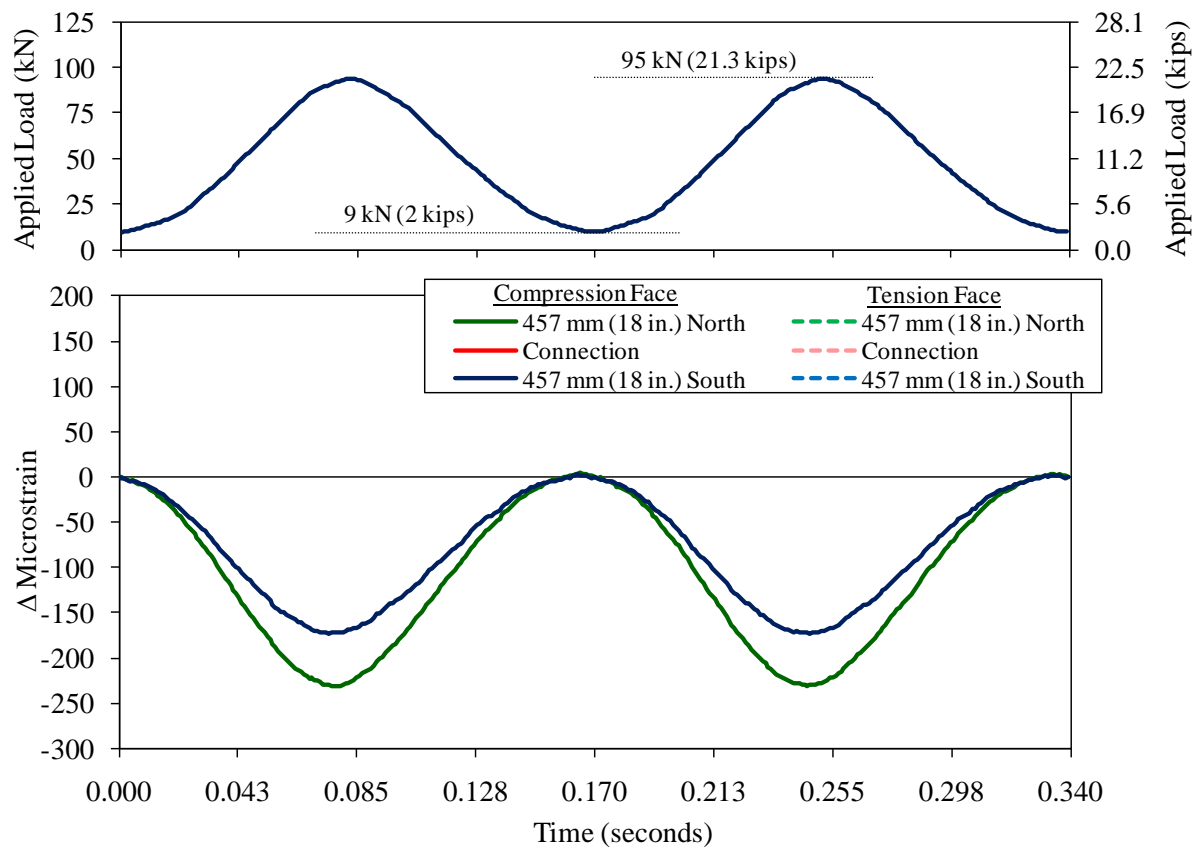


**Figure 51. Graph. Strain response for panel 8B after 7,372,000 cycles.**

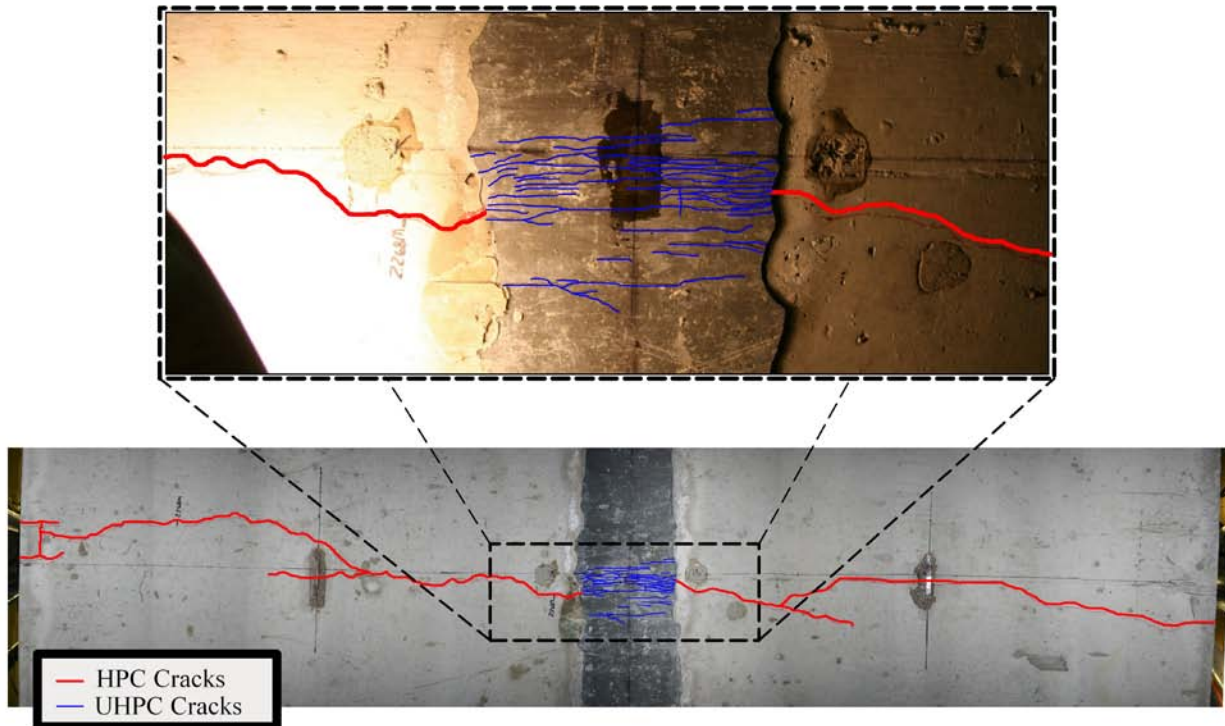


**Figure 52. Illustration. Cracking pattern observed on underside of panel 8B after the conclusion of cyclic testing.**

### *Static Testing*

The static testing of this specimen was completed according to the process described previously. The testing was completed over the course of 2 hours. The loading process included step-wise load application until approximately 360 kN (80 kips) of applied load was reached. After this the step-wise loading was changed to displacement control based on the midspan vertical displacement of the specimen. Recall that the cyclic loading of the specimen applied a peak load of approximately 95 kN (21.3 kips), which was sufficient to initiate inelastic behavior. As such, only loads greater than this level began to generate additional inelastic response.

The load-displacement results from the six potentiometers are presented in Figure 53. Similarly, the load-strain results from the six strain gages are presented in Figure 54. These results show that the inelastic cracking response of the specimen continued as the load increased to approximately 360 kN (81 kips). As the load increased above this level, the global response changed with significantly increased increments of displacement being observed. Complimentary behavior was displayed by the strain gages with increased strain per load increment being displayed by all three of the midspan gages. These behaviors are indicative of strain localization occurring in both the field-cast UHPC and in the precast panel, and the commensurate movement of the neutral axis toward the compression face of the specimen. This strain localization included pullout of the fiber reinforcement in the UHPC across critical midspan cracks as well as indications of yielding of the bottom mat of reinforcing steel at midspan. The first visual indication of the strain localization on the underside of the field-cast UHPC was observed at a

midspan centerline displacement of 26 mm (1.0 inch) corresponding to an applied load of 391 kN (88 kips).

Failure of the specimen was defined as a decrease in ultimate load capacity concurrent with an increase in deflection. The specimen failed at a peak applied load of 471 kN (105.9 kips) at a measured midspan centerline displacement of 58 mm (2.28 inch). The failure was precipitated by the crushing of the concrete in the top of the specimen along midspan. Figure 55 provides a photograph of the specimen after failure, with the failed concrete clearly visible in both the precast panel and the UHPC connection. Aside from a short length in an area near the UHPC strain localizations on the underside of the specimen, there was no indication of debonding or other failure of the connection along either of the two connection interfaces. A photograph of the midspan centerline area on the underside of the specimen is provided in Figure 56. The one major and one minor localization, along with the short length of interface cracking are annotated in the figure.

After the completion of the test, the panel was inverted so that the cracking could be assessed and cataloged. Figure 57 illustrates the cracking that was observed. The cracks in the HPC precast panels were identified by eye. The cracks in the field-cast UHPC were identified with the aid of an alcohol-based spray. All cracks were marked on the surface of the specimen, photographed, then electronically traced and recorded with drawing software. The crack patterns clearly demonstrate the different behaviors exhibited by the two different types of concrete. In the HPC precast panels, a hypothetical line between the two supports would intersect between 10 and 20 discrete cracks. In the field-cast UHPC, a similar line would intersect between 180 and 220 discrete cracks. Aside from the strain localization cracks in the UHPC at midspan, the other cracks in the UHPC remained very tight after failure as a result of the elastic unloading of the fiber reinforcement bridging the cracks.

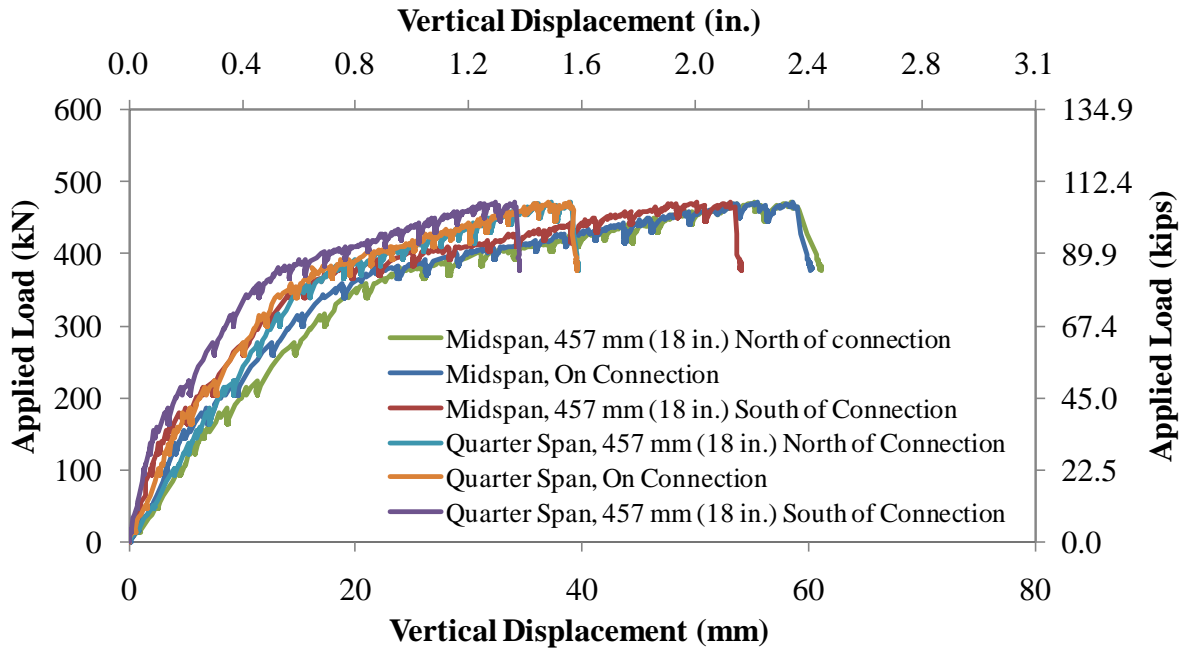


Figure 53. Graph. Load-deflection response of panel 8B under step-wise loading to failure.

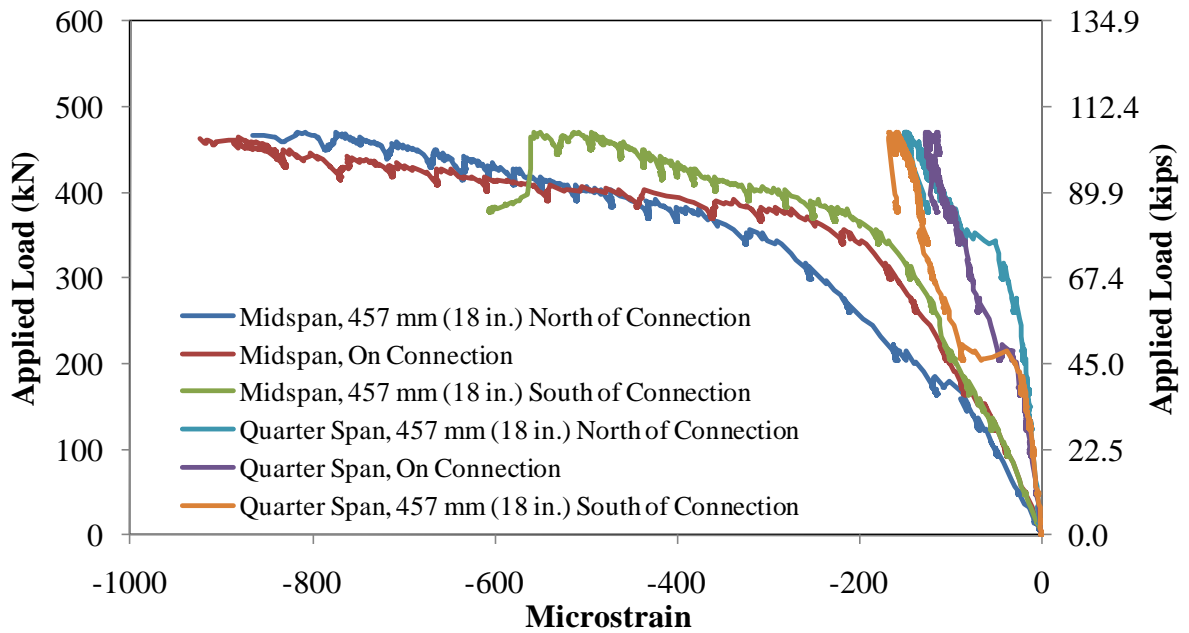


Figure 54. Graph. Load-strain response of panel 8B under step-wise loading to failure.



**Figure 55. Photograph. Top of panel 8B after flexural failure.**



**Figure 56. Photograph. Underside of panel 8B at midspan centerline location after flexural failure.**

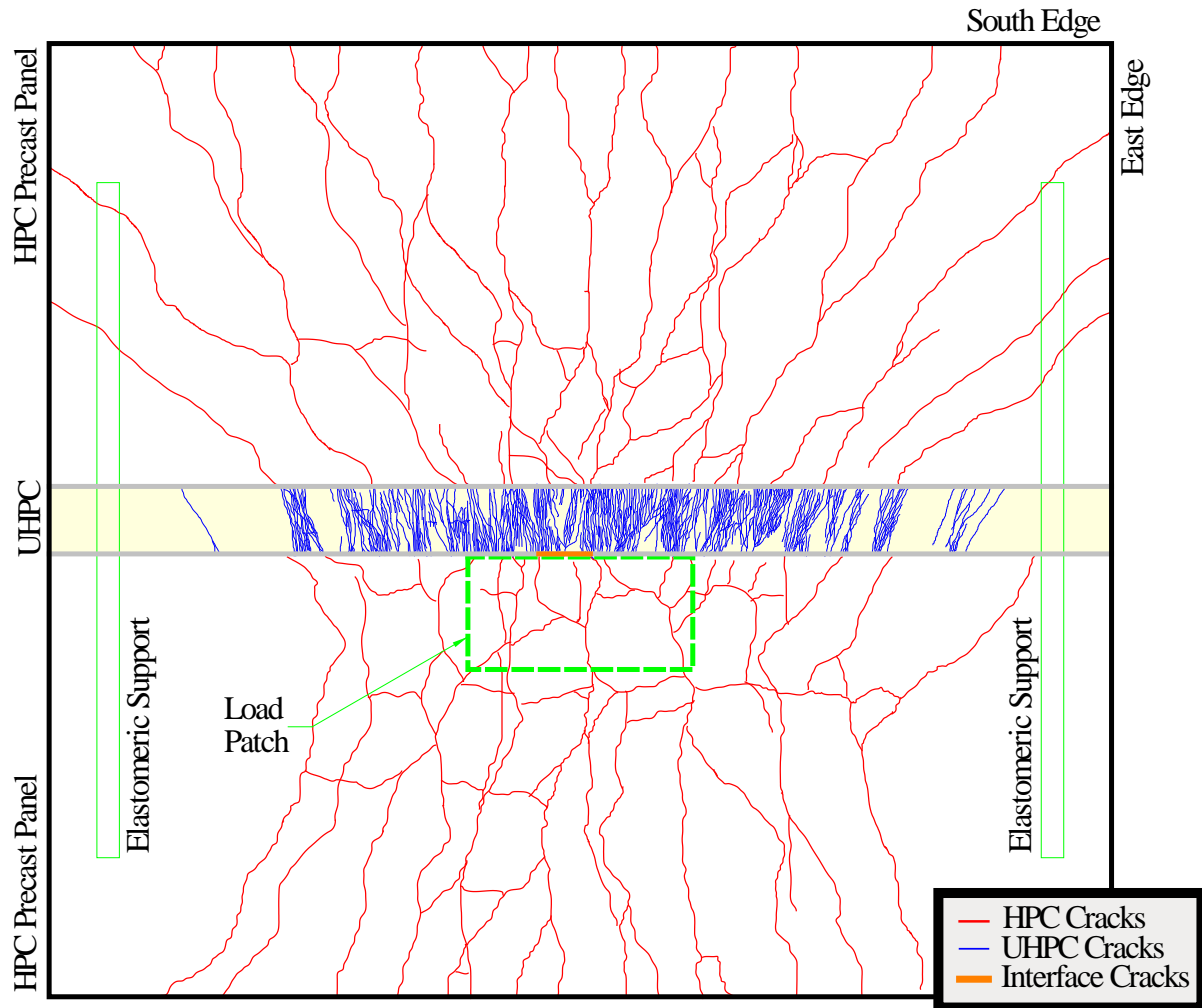


**Figure 57. Illustration. Cracking pattern observed on underside of panel 8B after conclusion of static test.**

## **SUMMARY OF TRANSVERSE CONNECTION TEST RESULTS**

The body of results generated through the four transverse connection tests can be summarized into a set of overall observations. These observations pertain to the general concept of using field-cast UHPC in transverse connections between precast concrete deck panels.

The connection designs investigated focused on testing four different discrete reinforcement configurations while maintaining a uniform connection geometry and using field-cast UHPC. In reinforced concrete, the discrete reinforcement is minimally engaged until after cracking of the surrounding concrete. The test setup and loadings applied in this program, although severe, did not result in any significant UHPC or interface cracks which were parallel to the connection. As such, none of the four discrete reinforcing details were engaged and thus no assessment of performance can be made. Note, however, that these types of connections can be subjected to flexural and tensile forces directly perpendicular to the connection on multi-span continuous

bridges. Indications of performance related to this type of loading can be extrapolated from the longitudinal connection tests which are presented later in this report.

The large structural loads applied throughout the test program caused flexural tensile cracking along midspan on the tensile face of the specimens. Given the test setup, these cracks are generally oriented perpendicular to the connection. At the locations where the cracks intersected the connection interfaces, the cracks continued in a generally straight direction across the connection and did not turn to run along interface. No interface cracking was observed in any of the specimens during cyclic loading. The static loading to failure caused one short length of interface cracking to occur in three of the four specimens in heavily cracked regions near midspan.

Single cracks in the HPC precast panels, when encountering the UHPC connection, became multiple, tightly-spaced cracks in the field-cast UHPC. After passing through the UHPC connection, the crack again became a single crack in the HPC precast panel. Crack widths were commensurate with the cracking behavior of the parent materials. In a general sense, an individual HPC panel crack of a given width will lead into a set of approximately ten cracks in the field-cast UHPC, each of which are on the order of ten times narrower than the adjacent HPC crack. Given that no debonding was observed along the connection interfaces during the applications of cyclic load, it is clear that strain compatibility was maintained between the precast components and adjacent field-cast UHPC. Thus, the approximately equivalent total width of a set of UHPC cracks as compared to an adjacent HPC crack is consistent with strain compatibility and the localization of strain in cracked concrete.

The cyclic testing demonstrated that the cracking load of these specimens was greater than 71 kN (16 kips) and less than 95 kN (21.3 kips). Cyclic application of structural loading for at least 2 million cycles to 71 kN (16 kips) demonstrated that the field-cast UHPC, the connected precast components, and the connection interfaces were not adversely affected by this cyclic loading.

Initial cycles to the 95 kN (21.3 kip) load level resulted in flexural cracking of the specimens. The cracking stabilized during the early portion of this cyclic loading. Cracking patterns and crack widths were not observed to be significantly affected by the continued application of cyclic loads through at least 5 million cycles.

The static loading of the specimens resulted in a global flexural failure of the simply-supported panels. The static behaviors of these specimens emulated the behaviors that would be anticipated to be observed from a monolithic deck panel subjected to similar loading conditions. Measurements and observations indicated that the following series events led to the failures in each of the specimens. First, during the cyclic loading each specimen was cracked in flexure resulting in an engagement of the mild-steel reinforcement in the HPC panels and an engagement of the fiber reinforcement in the field-cast UHPC connection. Next, the initial application of static loads resulted in additional cracking of the specimens. As the static loads increased, both the yielding strain of the reinforcing steel in the panels and the pullout tensile strain capacity of the fiber reinforcement in the field-cast UHPC were reached. Finally, this localization of strain along a single midspan crack led to hinging of the specimen and eventual crushing failure of the concrete above the localized crack at the peak applied load.

Due to the support and loading conditions applied to the subcomponent specimens, the cyclic loads applied generated stresses more severe than would traditionally be observed in a concrete bridge deck under similar magnitude wheel loads. The full scale testing reported in NCHRP Report 584 indicated that, for an 200-mm (8-inch) thick conventional concrete deck panel system connected to girders spaced at 6.1 m (20 feet) with wheel patch loads applied at the quarter points to a peak total applied load of 189 kN (42.6 kips), the observed elastic strain ranges on the uncracked tensile and compressive faces were 50 and 65 microstrain, respectively. In the present study, cyclic loads to 71 kN (16 kips) over a simply-supported 2.13 m (7 foot) span generated peak elastic tensile strains at midspan locations generally on the order of 60 to 90 microstrain. Simultaneously, peak elastic compressive strains at midspan locations were on the order of 80 to 130 microstrain. A simple analytical study completed herein suggests that the testing configuration implemented herein with loads peaking at 71 kN (16 kips) generated elastic stresses which are similar to the elastic stresses that might be observed in a conventional concrete deck spanning 3 m (10 feet) between adjacent girders and loaded to a peak wheel patch load of 125 kN (28 kips).

## **LONGITUDINAL CONNECTION TEST PROGRAM AND RESULTS**

Two of the deck panels were designed to simulate the longitudinal connection between the top flanges of adjacent decked girders. In order to simulate the types of stresses normally imparted into this type of connection, the test setup was arranged so that the specimens were loaded in three-point bending with a load adjacent to the connection. This setup generated primary flexural stresses across the connection.

Figure 58 shows the test setup that was used for the cyclic testing of the two test panels, namely 6B and 6H. Figure 59 shows the test setup used for the static testing to failure of specimen 6H. The cyclic and static set setups were identical aside from the change in the hydraulic jack and the type of cylindrical bearing attached thereto. The load application point was offset from the center of the panel toward the north such that the load was applied immediately adjacent to the connection. The load patch measured 254 x 508 mm (10 x 20 inch) and was oriented to mimic a truck wheel load driving on a bridge deck. Loads were applied to the deck through a 25 mm (1 inch) thick elastomeric pad which was backed by a 25-mm (1-inch) thick steel plate. Each specimen was supported by a pair of 152-mm (6-inch) diameter, 1219-mm (48-inch) long steel rollers. Figure 60 provides a photograph showing specimen 6H being subjected to cyclic loading.

It is recognized that, given the boundary conditions, this test setup does not simulate a subcomponent of a bridge which spans the full distance transversely between two adjacent girder webs. In a bridge structure, the top flanges of the decked girders are integral to the girders, thus allowing for limited rotations of the top flanges relative to the girder webs. The test setup employed here more closely represents the portion of the modular component system which spans transversely between two adjacent inflection points in the flexural response of the bridge deck. Additionally, this test setup did not emulate the axial restraint (i.e., “arching action”) which also can contribute a portion of the load carrying capacity of a bridge deck. As such, this test setup with the wheel patch loads applied was significantly more severe than that which this type of connection would typically experience under service loads.

The cyclic loads were applied through the use of a servo-hydraulic controlled actuator operated under load control. The maximum achievable frequency of loading was influenced by the stiffness of the specimen and reaction system. Prior to structural cracking of the deck panel specimen, the loading frequency was approximately 6 Hz. After cracking, the frequency was decreased such that the load peaks were reached and objectionable movement of the load frame did not occur. The sinusoidal cyclic loading of each panel was initially programmed to achieve peak applied loads of 9 and 17 kN (2 and 16 kips). This loading was continued for at least 2 million cycles. Subsequently, the load level was increased to achieve peak applied loads of 9 and 95 kN (2 and 21.3 kips). As with the transverse connection deck panel specimens, this loading program concluded the cyclic loading for specimen 6H. In contrast, the cyclic loading of specimen 6B included to additional higher load ranges, the last of which was continued until failure of the panel.

The structural response during the cyclic loading of the specimens was captured through the use of electronic instrumentation and visual/audible observations. The electronic instrumentation included five electrical resistance strain gages mounted on the concrete, one LVDT monitoring the opening of the underside of the connection, a load cell on the actuator to measure load, and an LVDT on the actuator to measure stroke. The locations for the five strain gages and the connection-opening LVDT are shown in Figure 61. The electronic data was captured during cyclic load application by a high speed data acquisition system. The rate of structural loading was not modified during the periodic data collection periods. The performance of the connection was also monitored through visual observations of water leakage through the connection. Water was ponded on the top of the connection throughout the cyclic tests, and the underside of each specimen was periodically checked for signs of water leakage. The ponding setup is shown in Figure 60.

The static loading of specimen 6H to failure was completed through the use of a pressure-actuated static hydraulic jack. The initial loading of the specimen was completed in a stair-step fashion with temporary holds occurring at approximately 22.2 kN (5 kip) intervals. After the initiation of inelastic behaviors, the steps were incremented on midspan displacement of the specimen.

The structural response during the static loading specimen 6H was captured through the use of electronic instrumentation and visual/audible observations. The electronic instrumentation included four electrical resistance strain gages mounted on the concrete, five string potentiometers to measure vertical deflection of the underside of the specimen, one LVDT monitoring the opening of the underside of the connection, a load cell on the actuator to measure load, and an LVDT on the actuator to measure stroke. The locations for the strain gages, potentiometers, and the connection-opening LVDT are shown in Figure 62.

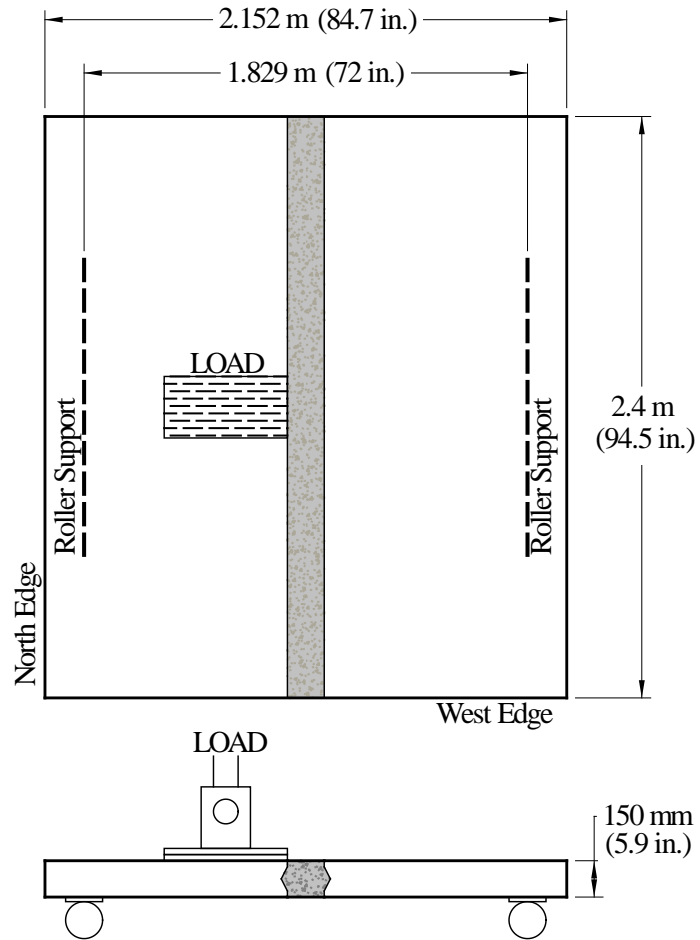


**Figure 58. Illustration. Test setup for cyclic loading of panels 6B and 6H.**



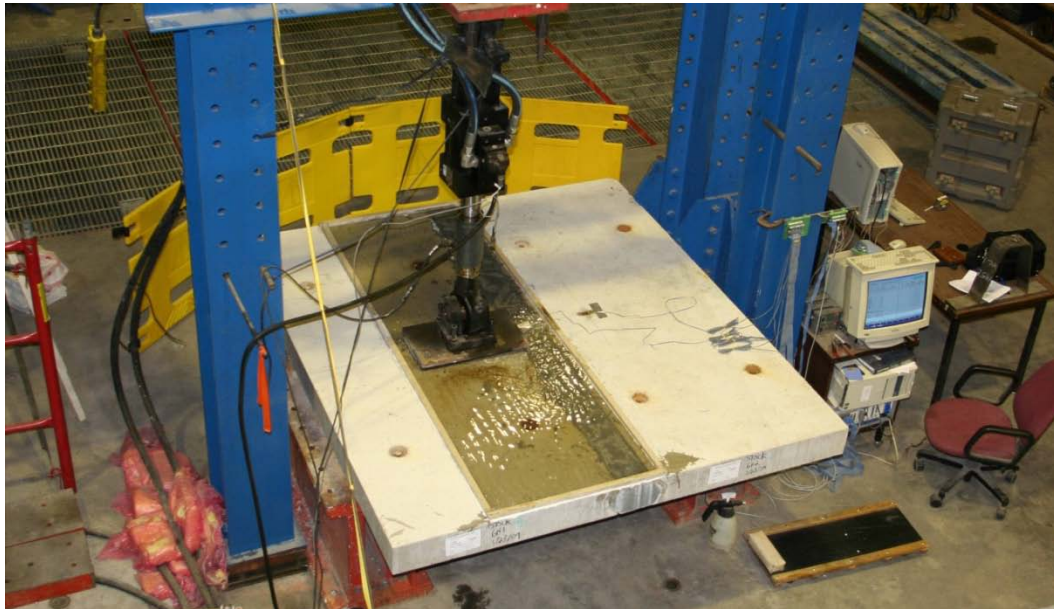


**Figure 60. Photograph. Overhead view showing cyclic test setup for panels 6B and 6H.**

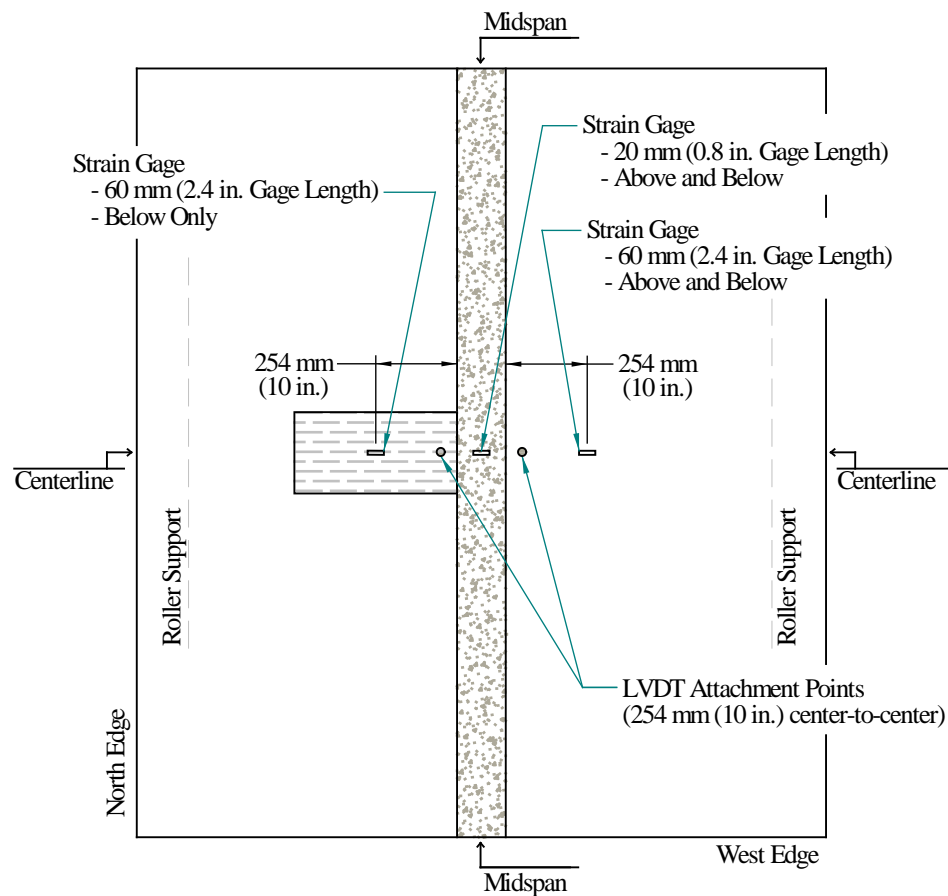


**Figure 61. Illustration. Instrumentation for cyclic testing of panels 6H and 6B.**

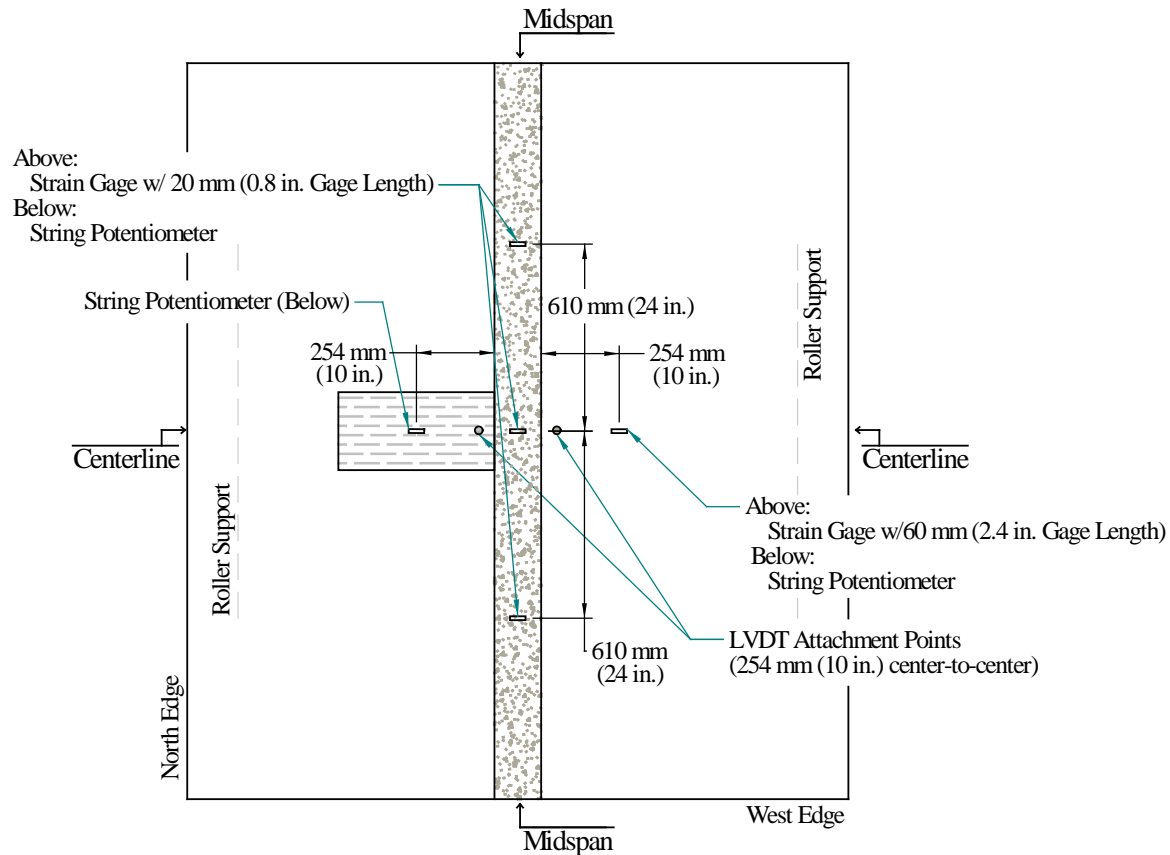


**Figure 62. Illustration. Instrumentation for static testing of panel 6H.**

### Specimen 6H

Specimen 6H was designed and loaded to simulate the longitudinal connection between the top flanges of two decked girders. The reinforcing details were described in Chapter 3 and are shown in Figure 11. Recall that the discrete reinforcement within the connection included two layers of headed reinforcing bars which were lapped across a 152-mm (6-inch) wide connection.

### *Cyclic Testing*

The cyclic testing of this specimen was completed according to the process described previously. The testing was completed over the course of 5 weeks. The cyclic loading included 2,031,500 cycles with a sinusoidal applied load ranging from 9 to 71 kN (2 to 16 kips), followed by 6,937,581 cycles ranging from 9 to 95 kN (2 to 21.3 kips).

The structural response of the specimen as captured by the electronic gages is presented in Figure 63. This two part graph shows the stroke range of the hydraulic actuator and the strain per unit of applied load on the specimen as a function of the number of cycles of load applied. The data in this figure was generated by analyzing the response of the specimen as captured during the increasing load portion of periodic cycles throughout the test. The stroke range was calculated from the maximum and minimum displacement of the actuator piston during a cycle. The strain per applied load was calculated through a best-fit approximation of the slope of the

load-strain response over the load range from approximately 36 kN (8 kips) to approximately 90 percent of the peak applied load.

The results in Figure 63 show that the response of the specimen stabilized soon after the initiation of cyclic loading in each load range. The lone exception is the response of the strain gages after the completion of approximately 7 million total cycles. The southernmost flexural cracking on the underside of the specimen occurred at this point and affected these strain readings.

The strain response of the specimen as captured at two representative timeframes during the test is presented in Figure 64 and Figure 65. These figures show the range of strain observed on the surface of the specimen at the strain gage locations. Figure 64 presents results from early in the loading after a total of 1,555,000 cycles had been completed. Figure 65 presents results from the end of cyclic testing after a total of 8,969,000 cycles had been completed.

Prior to the start of cyclic loading, the specimen was checked for structural cracking that may have occurred during handling or test setup. A set of flexural cracks were observed on the underside of the specimen. These cracks are identified within the annotation in Figure 66. It is not clear whether these cracks can be specifically attributed to an unintentional load applied during test setup; however, the crack pattern is consistent with that to be expected from the patch load and support configuration later used in the cyclic and static testing of this specimen. It is important to note that, aside from a 150 mm (3 inch) length on the west end of the north connection interface, these cracks ran parallel and adjacent to the connection interfaces within the precast panels. This cracking behavior indicates that the UHPC to HPC bond strength at the interface was greater than the HPC tensile strength in the precast panels.

Throughout the cyclic loading to 71 kN (16 kips), the specimen was monitored for additional cracking. None was identified. After the first load cycle to 95 kN (21.3 kips), the specimen was again checked for cracking. An existing crack connecting the northernmost precast panel flexural crack to the north support was noted to have extended to a termination at the precast panel crack just north of the connection interface. This crack was not observed to extend to the connection interface or into the field-cast UHPC. This crack is also identified in Figure 66.

Finally, the cracking observed in the panel after the completion of cyclic loading is also shown in Figure 66. An additional flexural crack was noted in the south precast panel. As noted above, strain readings and visual observations indicate that this crack appeared after approximately 7 million total cycles of loading. Throughout the entirety of the cyclic testing, no cracks were observed in the field-cast UHPC. Also, no water leakage was observed at the interface, through the precast panels, or through the UHPC.

An indication of the location of the flexural cracks through the depth of the specimen was obtained through viewing the exposed end surfaces of the specimen near the connection. Figure 67 and Figure 68 provide illustrations of the observed cracking on the east and west faces after the conclusion of cyclic loading. These observations clearly indicated that the cyclic loading had caused cracking through the full depth of the precast panels. These crack patterns also indicate that the cracks adjacent to the connection were not necessarily directly emanating from the stress concentration in the precast panels at the shear key's reentrant corner at panel middepth. On

both end faces, the crack immediately south of the connection remains at least 25 mm (1 inch) south of the connection throughout the depth.

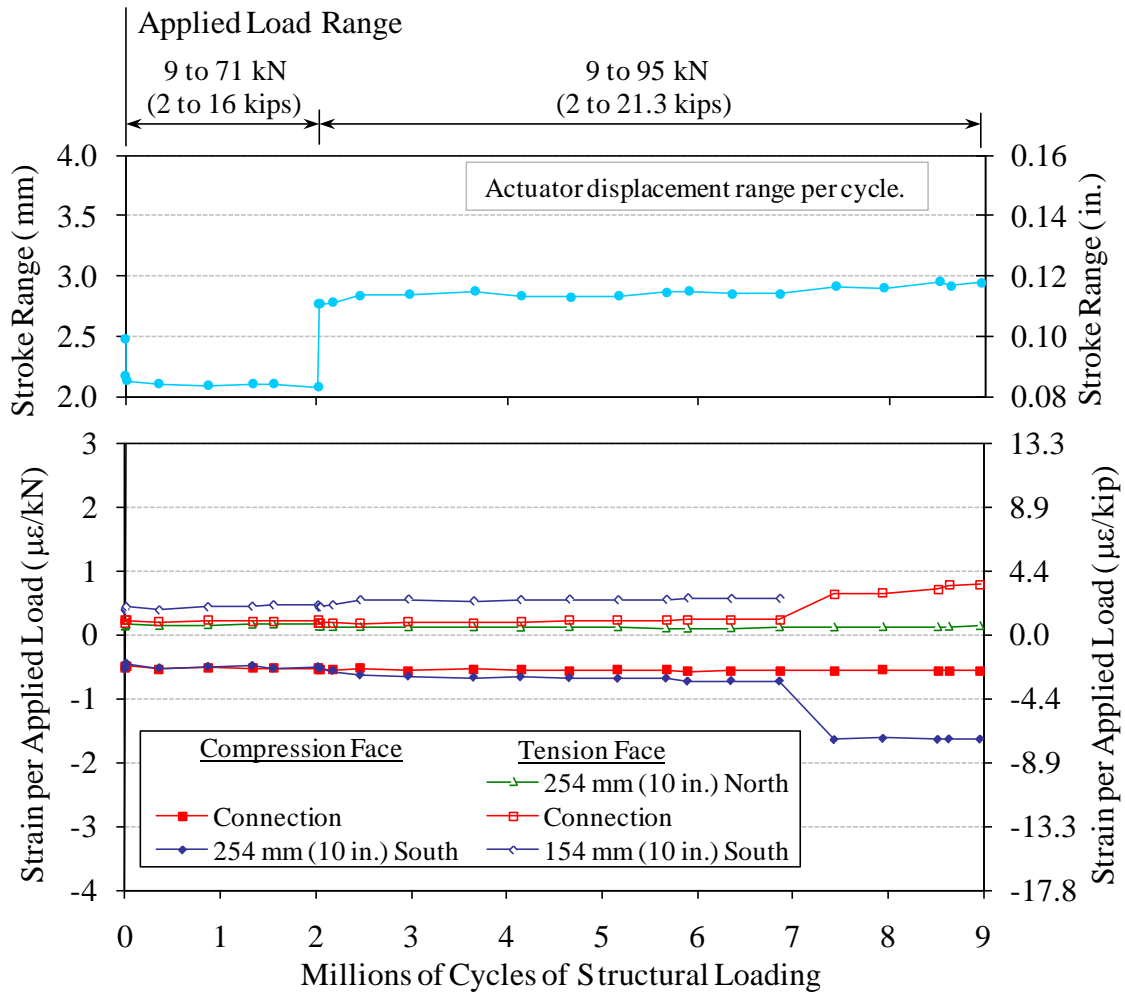


**Figure 63. Graph. Cyclic test results for panel 6H.**

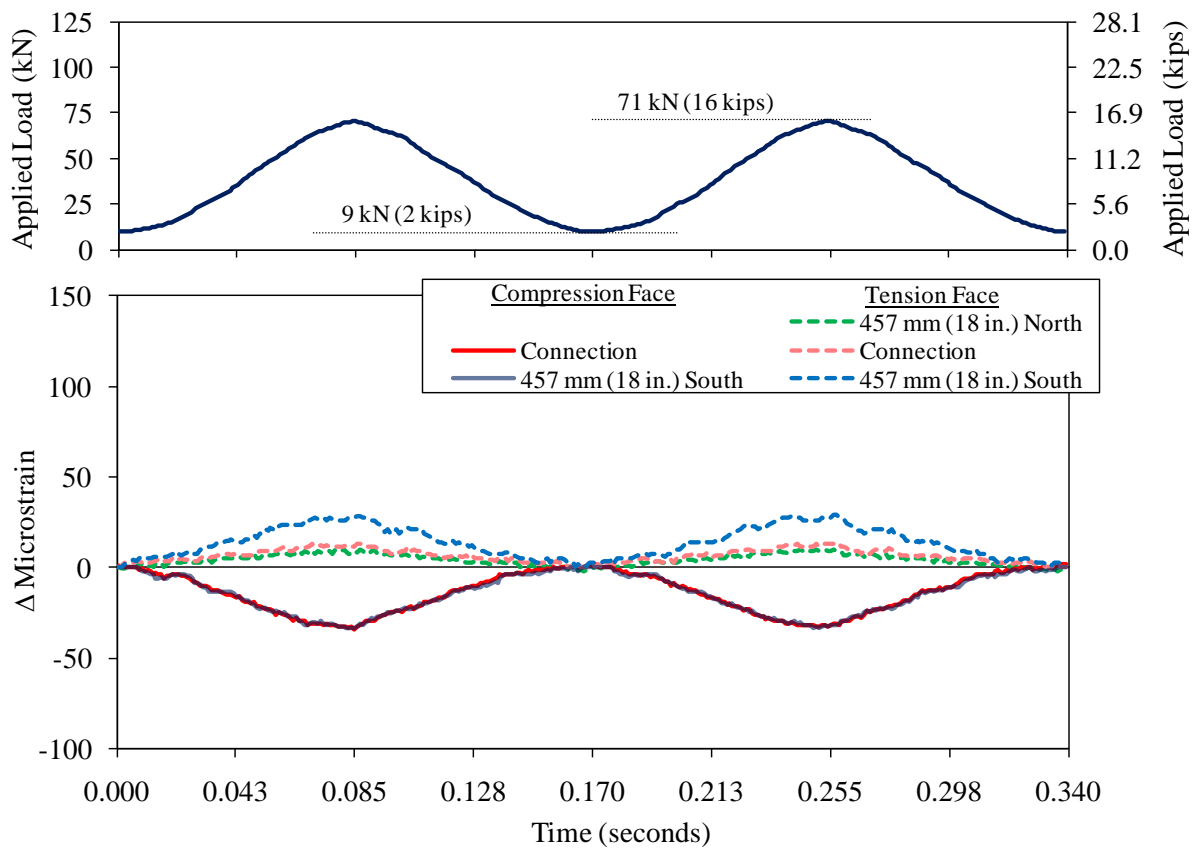


**Figure 64. Graph. Strain response for panel 6H after 1,555,000 cycles.**

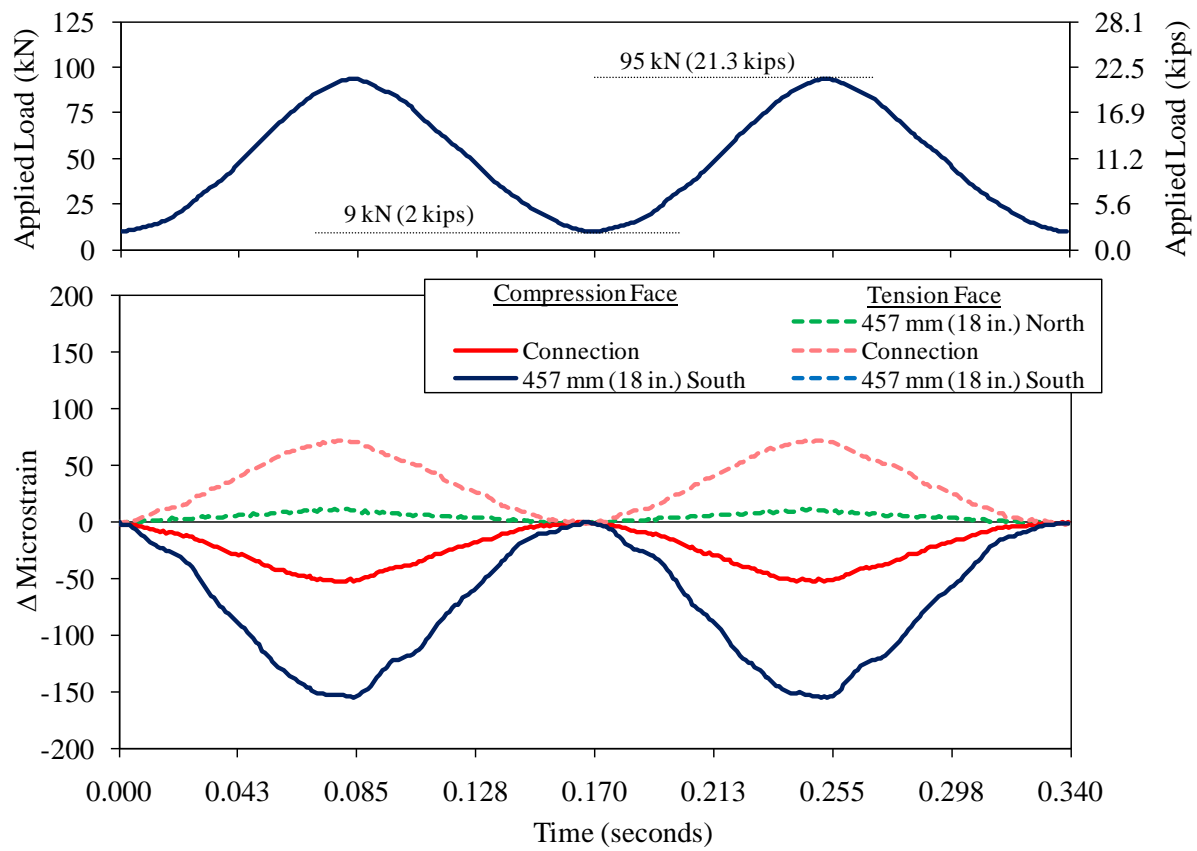


**Figure 65. Graph. Strain response for panel 6H after 8,969,000 cycles.**

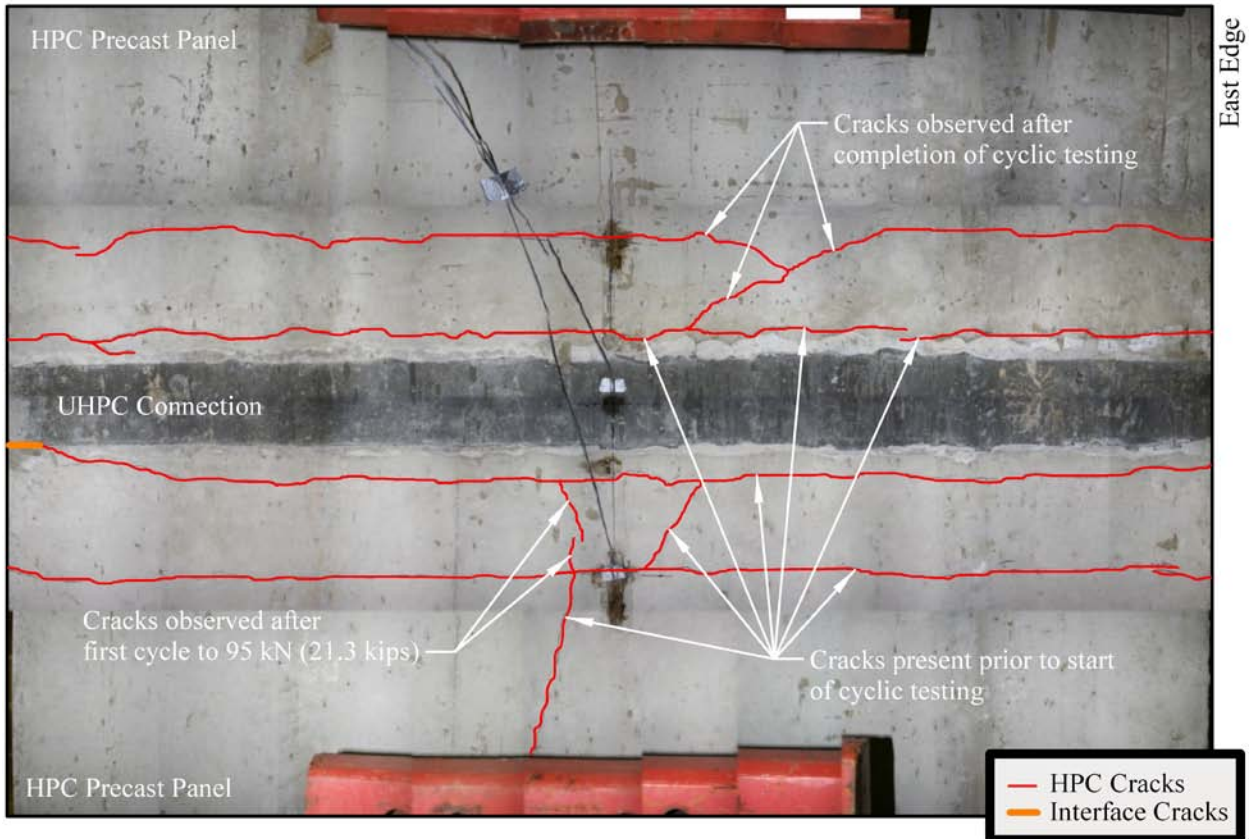


**Figure 66. Illustration. Cracking pattern observed on underside of panel 6H after conclusion of cyclic testing.**

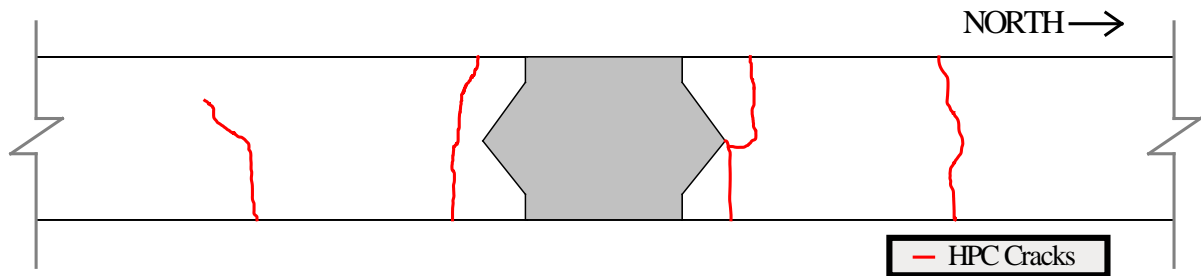


**Figure 67. Illustration. Cracking pattern observed on east face of panel 6H after conclusion of cyclic testing.**

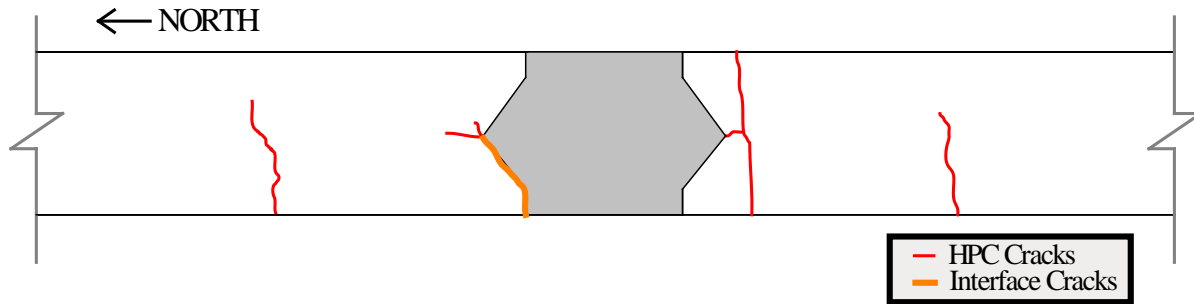


**Figure 68. Illustration. Cracking pattern observed on west face of panel 6H after conclusion of cyclic testing.**

### *Static Testing*

The static testing of this specimen was completed according to the process described previously. The testing was completed over the course of 3 hours. The loading process included step-wise load application until approximately 470 kN (106 kips) of applied load was reached. After this the step-wise loading was changed to displacement control based on the midspan vertical displacement of the specimen. Recall that this specimen was cracked by an unknown load prior to cyclic loading and that the cyclic loading applied a peak load of approximately 95 kN (21.3 kips). As such, only the application of loads higher than those already achieved resulted in additional inelastic response.

The load-displacement results from the five potentiometers are presented in Figure 69. Similarly, the load-strain results from the six strain gages are presented in Figure 70. These results show that the inelastic cracking response of the specimen became more apparent as the load increased beyond approximately 445 kN (100 kips). As the load increased above this level, the global response changed with significantly increased increments of displacement being observed. Complimentary behavior was displayed by the strain gages with increased strain per load increment being displayed by all three of the midspan gages. Finally, note that the largest vertical deflections were observed under the load point, followed by the midspan, centerline deflection.

Failure of the specimen was defined as a decrease in ultimate load capacity concurrent with an increase in deflection. The peak applied load was 520 kN (116.8 kips), occurring at a measured midspan centerline displacement of 30 mm (1.18 inch). The failure of the specimen was precipitated by a punching shear failure of the precast deck panel just beyond the north extent of the load patch. Figure 71 provides a photograph of the specimen after failure, with the arc of the punching shear failure visible to the right of the load patch. Based on this failure mechanism, it is clear that the spherical bearing between the actuator and the loading plate was unable to meet the rotation demand, resulting in a local overload of the concrete.

After the completion of the test, the panel was inverted so that the cracking could be assessed and cataloged. Figure 72 provides a photograph composed of a set of high resolution photographs showing the cracking apparent in the specimen after the conclusion of testing. Figure 73 illustrates the compilation of all of the cracking that was observed. The cracks in the

HPC precast panels were identified by eye. The cracks in the field-cast UHPC were identified with the aid of an alcohol-based spray. The tightly-spaced cracks in the UHPC, largely perpendicular to the primary flexural tensile forces, indicate that the panel was bending in two directions and distributing loads laterally along the connection interfaces. After failure and subsequent unloading the panel, the cracks in the UHPC remained very tight as a result of the elastic unloading of the fiber reinforcement bridging the cracks.

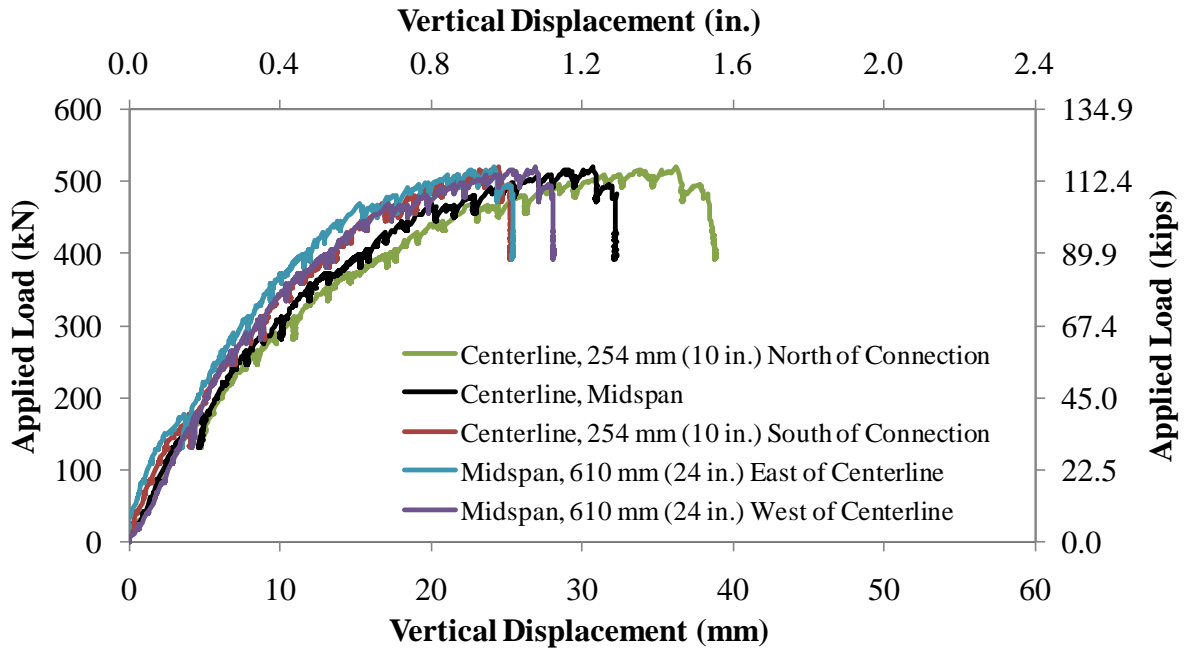
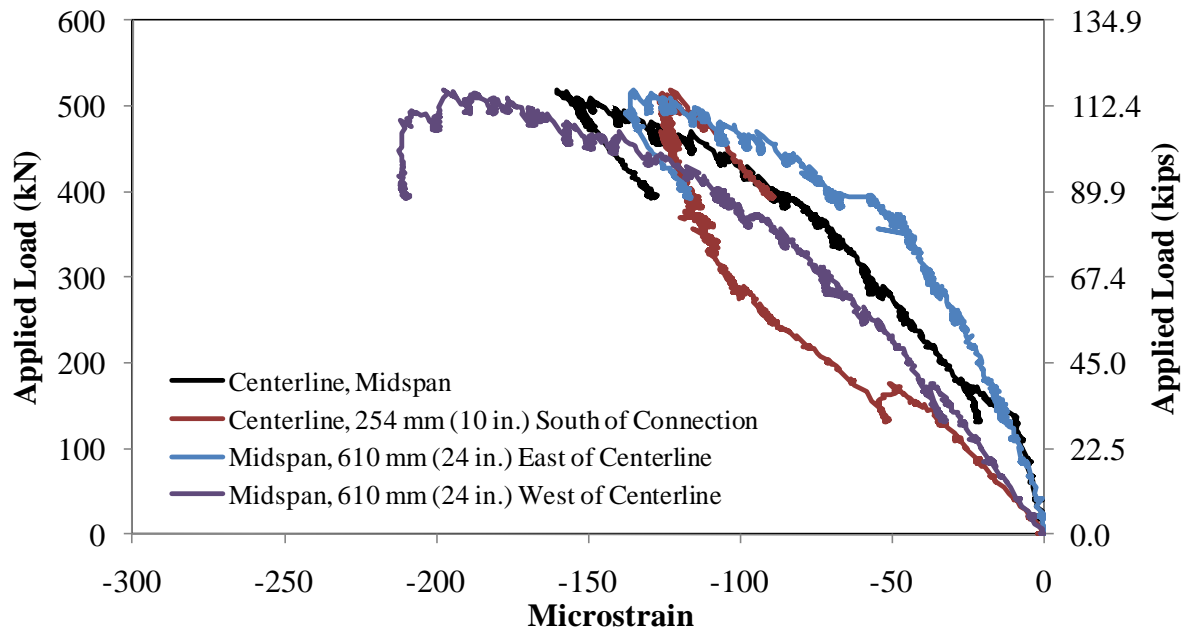


Figure 69. Graph. Load-deflection response of panel 6H under step-wise loading to failure.



**Figure 70. Graph. Load-strain response of panel 6H under step-wise loading to failure.**



**Figure 71. Photograph. Top of panel 6H after flexural failure.**



**Figure 72. Photograph. Underside of panel 6H along midspan after failure.**

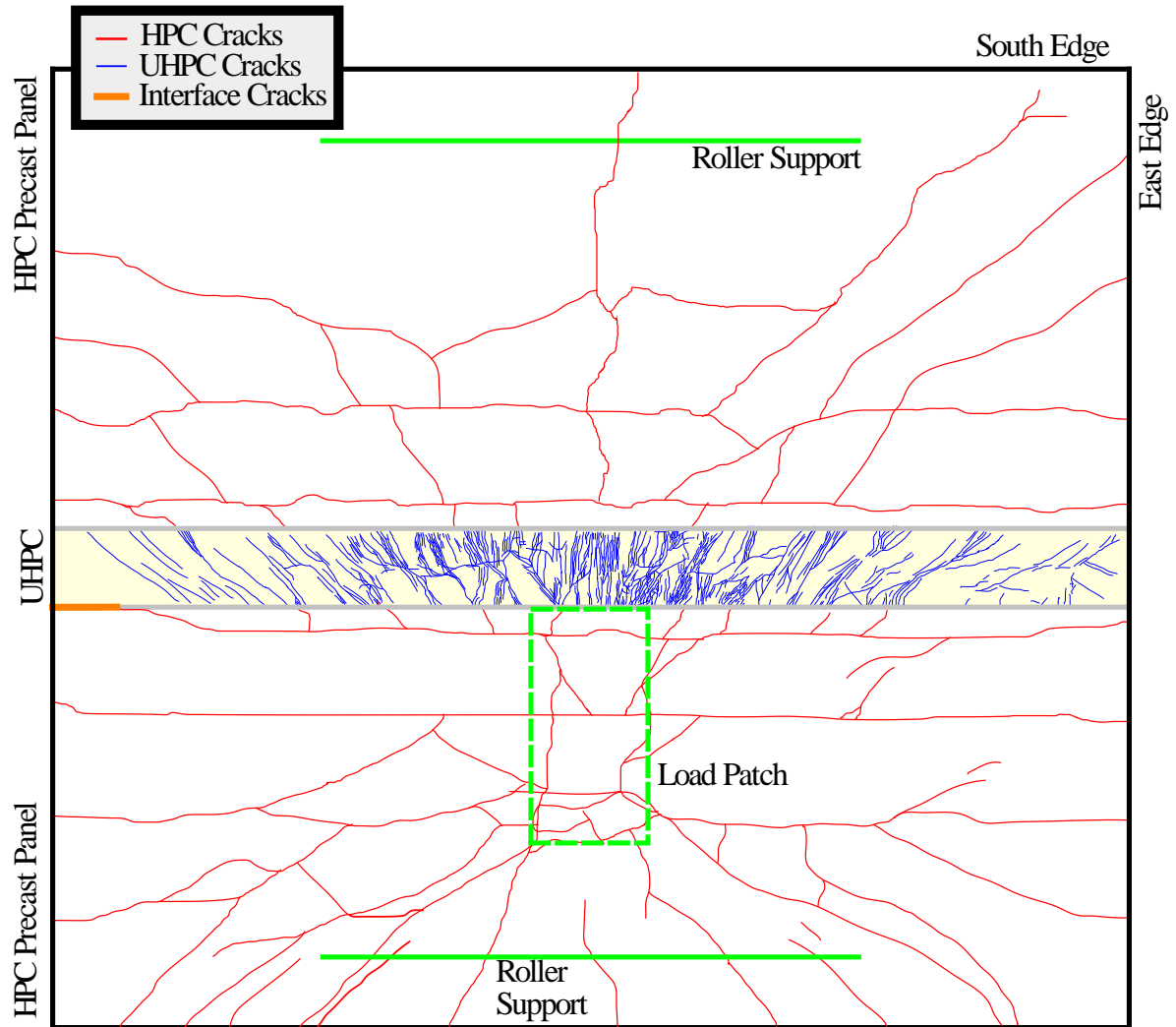


**Figure 73. Illustration. Cracking pattern observed on underside of panel 6H after conclusion of static test.**

## **Specimen 6B**

Specimen 6B was designed and loaded to simulate the longitudinal connection between the top flanges of two decked girders. The reinforcing details were described in Chapter 3 and are shown in Figure 12. Recall that the discrete reinforcement within the connection included two layers of straight reinforcing bars which were lapped across a 152 mm (6 inch) wide connection.

### ***Cyclic Testing***

The cyclic testing of this specimen was completed according to the process described previously, with the exception that two additional higher load levels were applied and the highest cyclic load level was continued until failure of the specimen occurred. The testing was completed over the course of 4 months. Given that the specimen failed at the conclusion of the cyclic testing, thus there was no subsequent static loading to failure.

The cyclic loading started with 57,369 cycles of sinusoidal applied load ranging from 9 to 71 kN (2 to 16 kips). After this cycle, an electronic control system malfunction resulted in an unintentional overload of the specimen to a maximum actuator capacity of 310 kN (70 kips). Subsequently, the cycling was restarted with 10,096,032 cycles ranging from 13 to 95 kN (3 to 21.3 kips), followed by 1,118,000 cycles ranging from 13 to 142 kN (3 to 32 kips), and finally 343,399 cycles ranging from 13 to 178 kN (3 to 40 kips). The cyclic loading of the specimen was halted at this point as the majority of the rebar crossing the north connection interface had fractured leaving the specimen nearly severed along this interface. The cyclic loading program is illustrated in Figure 74.

Prior to the start of testing, the panel was assessed to verify that it did not contain any significant cracking. Aside from tight, distributed shrinkage cracking in the precast panels, no cracking was observed in the specimen. The initial loading of the specimen covered a load range from 8.9 to 71.2 kN (2 to 16 kips). The first load applied over this range resulted in flexural cracking of the north precast panel. After removing the load, these three cracks were measured to have widths varying from 0.025 to 0.152 mm (0.001 to 0.006 inch). The locations of these cracks are illustrated in Figure 75. No cracks were observed in the UHPC or at the connection interface. No further crack assessments were completed prior to the unintentional overload.

The unintentional overload resulted in significant cracking of the specimen. The crack pattern observed on the underside of the specimen is presented in Figure 76. The extensive cracking observed included cracking in both precast panels, in the field-cast UHPC, and along the interface. The cracking in the HPC panels was measured to have widths in the vicinity of 0.25 to 0.51 mm (0.010 to 0.020 inch). Note that the flexural cracking along the connection interfaces was observed to extend along approximately 80 percent of the total interface length, with the remainder of the length being covered by cracks which diverged into the HPC panels.

The cracking of the specimen was assessed periodically throughout the cyclic loading to 95 kN (21.3 kips). No additional cracking was noted during this cycling and thus the crack pattern presented in Figure 76 also represents the cracking observed at the conclusion of this portion of the loading program. This lack of additional cracking is not unexpected as the peak cyclic load

is comparatively small relative to the overload. At the conclusion of the cyclic loading to 95 kN (21.3 kips), the connection interfaces remained water-tight.

Given that over 10 million cycles of loading had not resulted in any apparent progressive degradation of the connection, the load range was increased to cover the range from 13 to 142 kN (3 to 32 kips). The loading frequency was 3 Hz for a total of 1,118,000 cycles. Cracking was again assessed at the conclusion of these cycles. Although no additional significant cracking was observed, some HPC panel crack widths had increased. Also, the interface cracking had progressed up through the cross section and minor water leakage along cracks near the interface was observed.

The final load range, 13 to 178 kN (3 to 40 kips), was applied for a total of 343,399 cycles. During the final cycle, the specimen deflected excessively and the peak load could not be reached. The south interface from centerline to the west side of the specimen was observed to be fully disconnected. Cyclic loading was ceased and a static load was applied to pry the specimen apart along the south interface failure plane. Two rebar were audibly observed to fracture during this static loading. Another five rebar were manually cut with a torch in order to separate the north panel and field-cast UHPC from the south panel at the south interface. Figure 77 shows the east elevation of the panel after the conclusion of cyclic loading and prior to the cutting of the remaining rebar.

The structural response of the specimen as captured by the electronic gages is presented in Figure 78. This three part graph shows the connection opening as measured by the LVDT crossing the connection, the stroke range of the hydraulic actuator, and the strain per unit of applied load on the specimen, all as a function of the number of cycles of load applied. Note that this figure only presents the data captured after the unintentional overload. The data in this figure was generated by analyzing the response of the specimen as captured during the increasing load portion of periodic cycles throughout the test. The stroke range was calculated from the maximum and minimum displacement of the actuator piston during a cycle. The strain per applied load and connection opening per applied load were calculated through a best-fit approximation of the slope of the load-strain response over the load range from approximately 36 kN (8 kips) to approximately 90 percent of the peak applied load. Note that the connection opening per applied load is based on displacement measurements captured over a 254 mm (10 inch) center-to-center gage length which was inclusive of the entire connection at midspan as well as a portion of the precast panels. This measurement is inclusive both of connection opening at the interfaces and straining of included concrete.

The results in Figure 78 show that the response of the specimen stabilized during the application of the load range which peaked at 95 kN (21.3 kips). Although the number of cycles was significantly less, similar behavior was observed during the cycling whose loads peaked at 142 kN (32 kips). Different behavior is apparent in the results from the cyclic load application to 178 kN (40 kips) which resulted in progressive failure of the specimen. This behavior is most apparent in the connection opening results which show that the interface cracks adjacent to the connection were widening quickly, clearly indicating that the discrete reinforcement crossing these interfaces was failing.

The strain response of the specimen as captured at three representative timeframes during the test is presented in Figure 79, Figure 80, and Figure 81. These figures show the range of strain observed on the surface of the specimen at the strain gage locations. Figure 79 presents results captured after 9,743,000 cycles to 95 kN (21.3 kips) had been completed. Figure 80 presents results captured at the end of the 1,118,000 cycles to 142 kN (32 kips). Figure 81 presents results captured at the end of the 190,000 cycles to 178 kN (40 kips).

The failure of the specimen along the south interface of the connection was assessed through physical observation and analytical modeling. As discussed above, the connection opening measured in the middle of the specimen continually increased during the later cycles of the 178 kN (40 kips) cyclic load set. Failure along the south connection interface was visually apparent with the interface crack opening and the ponded water leaking through. By the final loading cycle, the entire western half of the south interface had become disconnected. After the cessation of cyclic loading, the separation of the northern remnant from the southern remnant allowed for an assessment of the discrete reinforcement crossing the failure plane. No evidence of debonding failure of the mild steel reinforcement was observed either in the rebar or in the surrounding UHPC.

Assessment of the reinforcing bars crossing the specimen failure plane provided a clear indication of the failure mechanism. Of the 18 rebar crossing the interface, five were torch cut and four were fractured with no indication of post-fracture impact by the mating rebar surface. The remaining nine rebar had fractured prior to the cessation of cyclic loading and showed signs of post-fracture impact with their mating rebar surface. This visual observation indicates that these rebar fractured under cyclic fatigue loading. Mating surfaces were observed on each side of the interface for every rebar, and there was no indication that any of the rebar debonded either within the field-cast UHPC or within the precast panel. Figure 82 shows the cross section of the failed connection interface with the rebar and the rebar failure mechanisms noted. This figure also shows photographs of twelve of the rebar tips. The seven easternmost rebar were either torch cut or were observed to fracture during the post-test loading of the specimen which was intended to separate the north and south parts at the interface. The rebar labeled 2, 3, 4, 5, 6, 7, 8, 9, and 12 showed evidence of having fractured prior to the completion of cyclic loading. Thus, none of these rebar exhibited a clean tensile fracture surface as would be expected, instead displaying blunted or “pounded” fracture surfaces indicative of impact between two mating surfaces after fracture. It is also important to note that the fracture locations were submerged within the field-cast UHPC, thus indicating the development length of the reinforcing bar may be less than the as-built lap length.

A cracked-section analysis of the specimen was completed to assess the stress range in the rebar at the connection during the cyclic loading. Given that the analysis assumed one-way bending and uniform distribution of load across the width of the specimen, the actual stresses in the bars near the middle of the deck were likely higher. During the loading which peaked at 95 kN (21.3 kips), the analysis indicated that the stress range in the bottom layer of rebar was 98 MPa (14.2 ksi). During the loading which peaked at 142 kN (32 kips), the corresponding stress range was 155 MPa (22.5 ksi). During the final cyclic loading to 178 kN (40 kips), the stress range in the bottom layer of rebar at the failure location was 197 MPa (28.6 ksi). Prior work on fatigue of mild steel reinforcing bar has indicated that stress range is the primary factor in tensile fatigue

fracture of rebar and that a stress range of 197 MPa (28.6 ksi) should result in a finite fatigue life<sup>(15)</sup>.

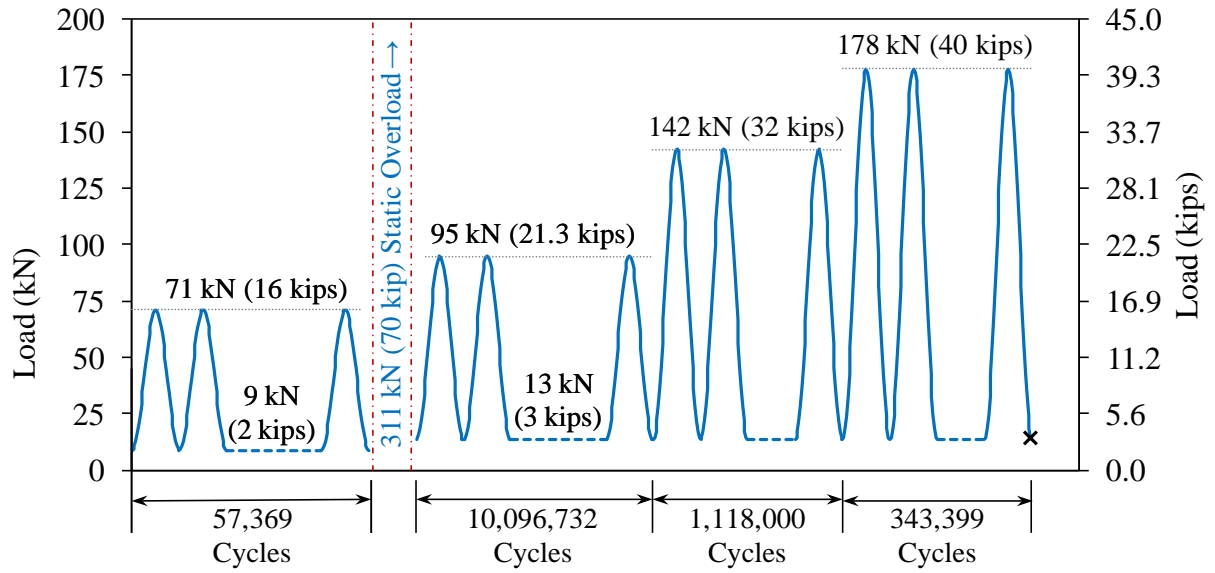


**Figure 74. Illustration. Cyclic test program for panel 6B.**

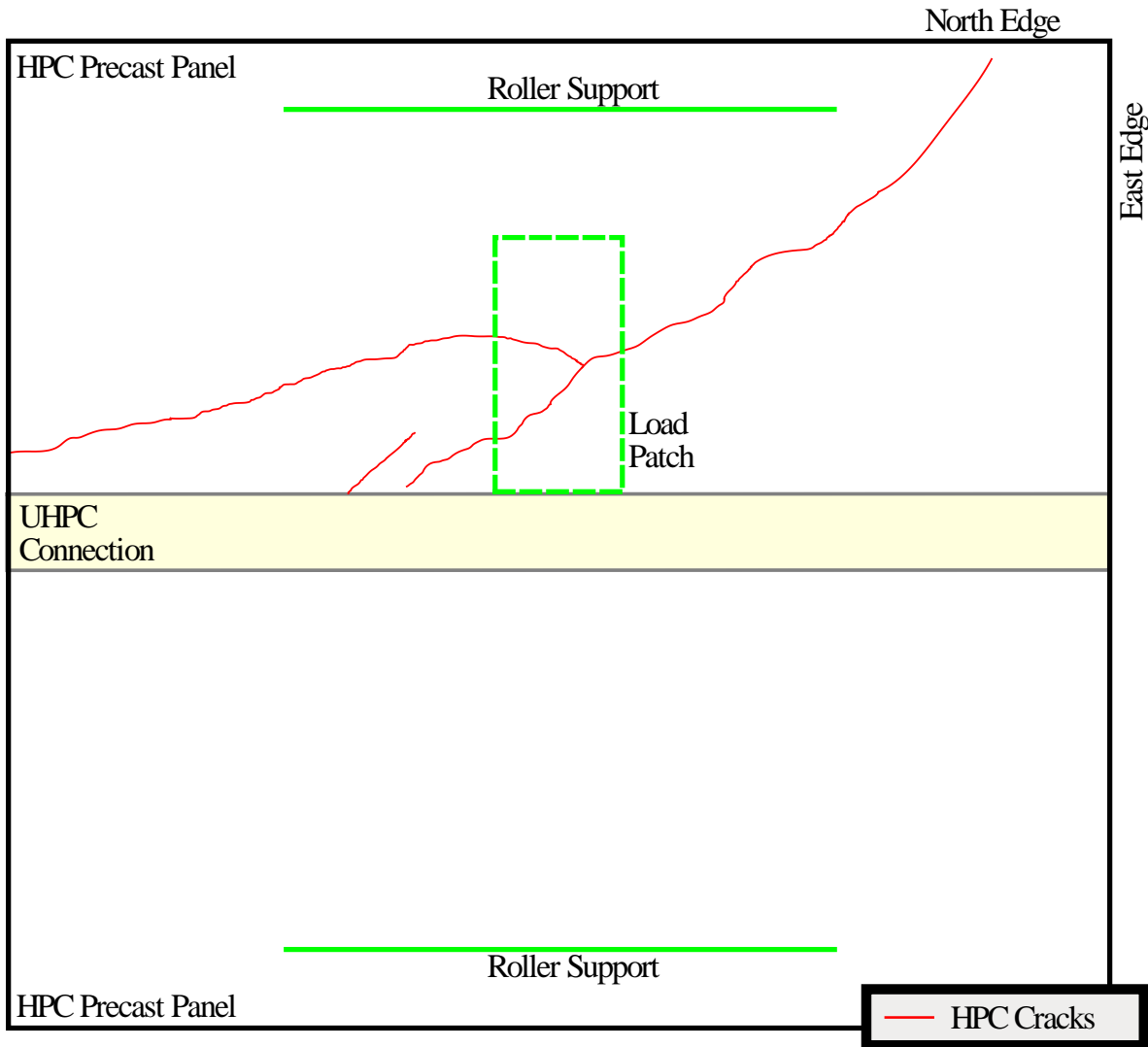


**Figure 75. Illustration. Cracking pattern observed on underside of panel 6B after the first cycle from 9 to 71 kN (2 to 16 kips).**

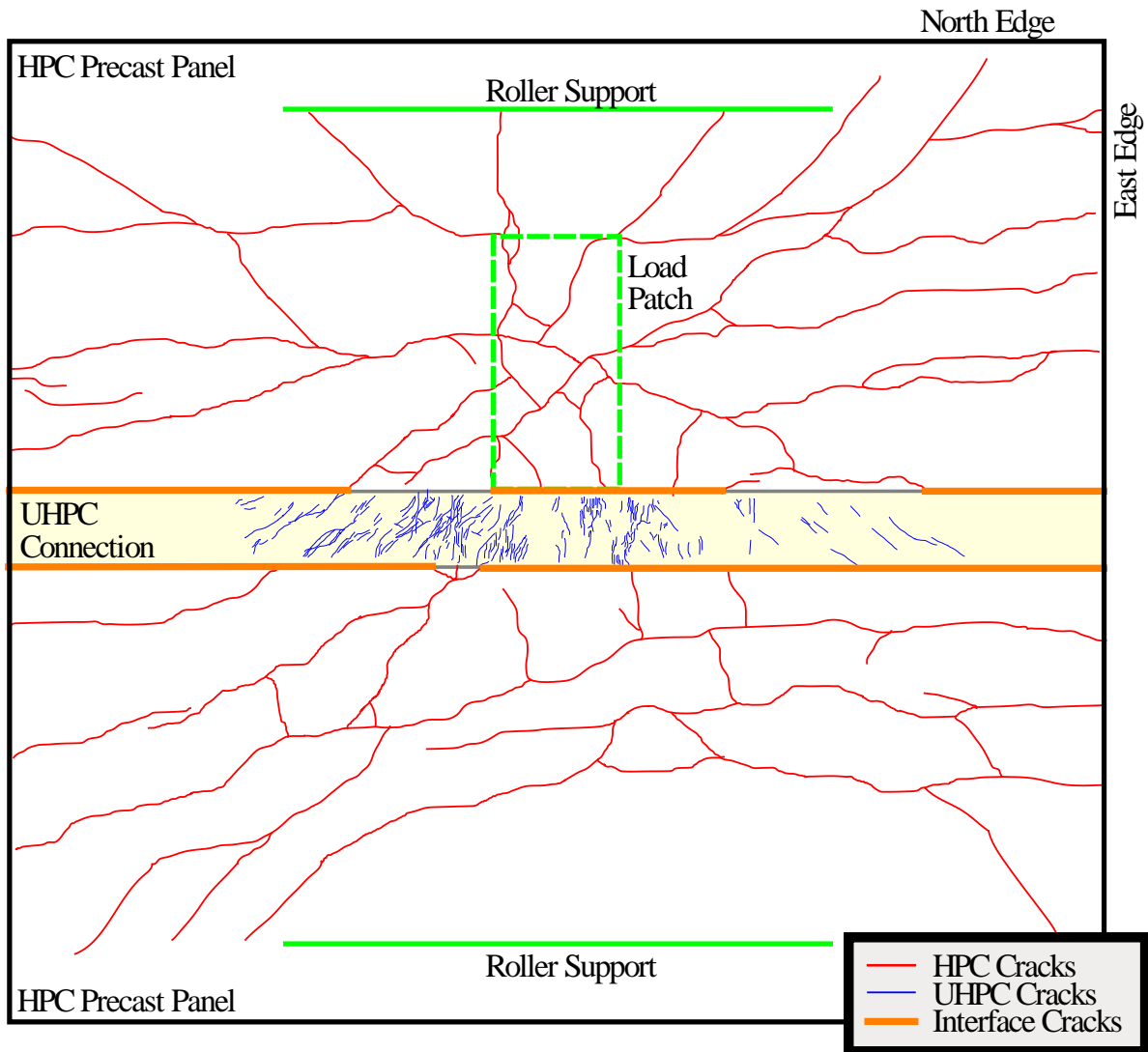


**Figure 76. Illustration. Cracking pattern observed on underside of panel 6B both after the initial overload and again after 10.1 million cycles of loading from 13 to 95 kN (3 to 21.3 kips).**



**Figure 77. Photograph. East side and top of panel 6B after the conclusion of cyclic loading.**

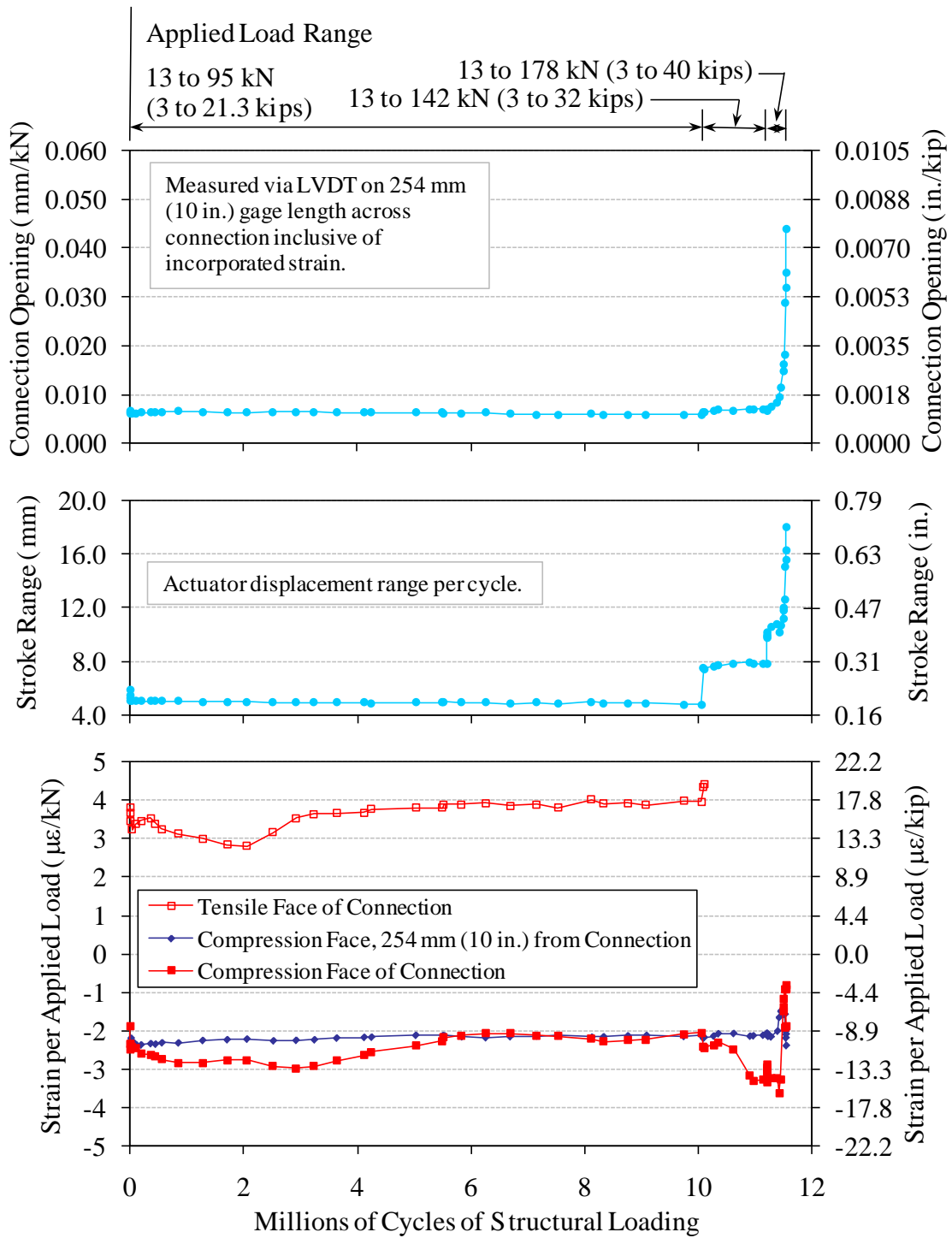


**Figure 78. Graph. Cyclic test results for panel 6B.**

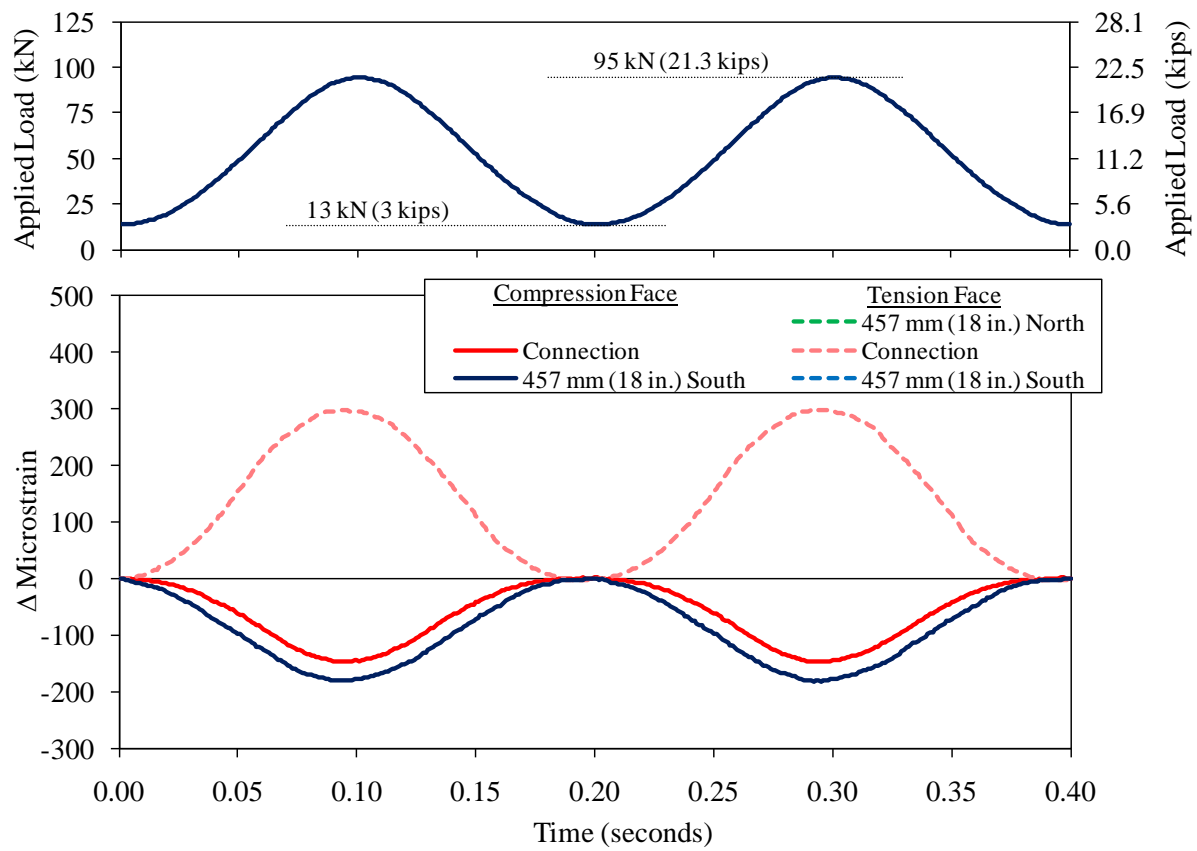


**Figure 79. Graph. Strain response for panel 6B after 9,743,000 cycles to 95 kN (21.3 kips).**

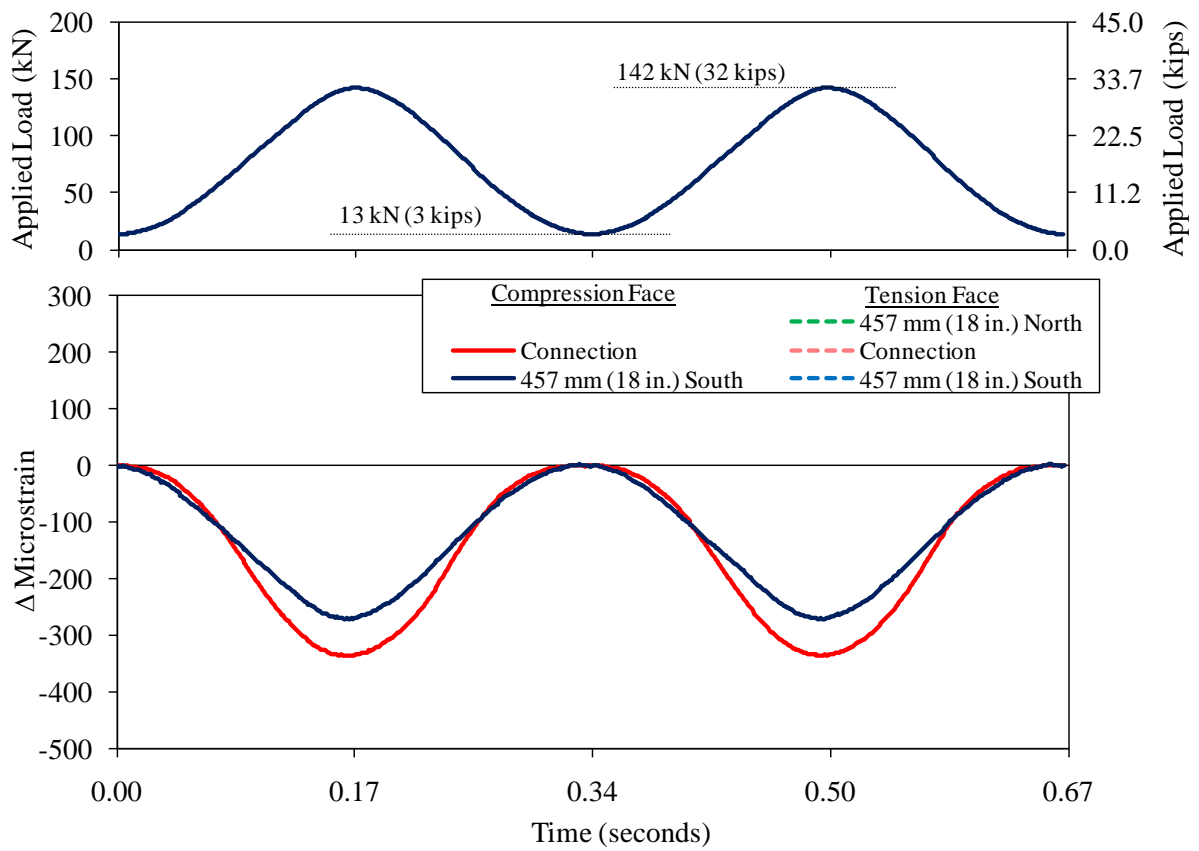


**Figure 80. Graph. Strain response for panel 6B after 1,118,000 cycles to 142 kN (32 kips).**

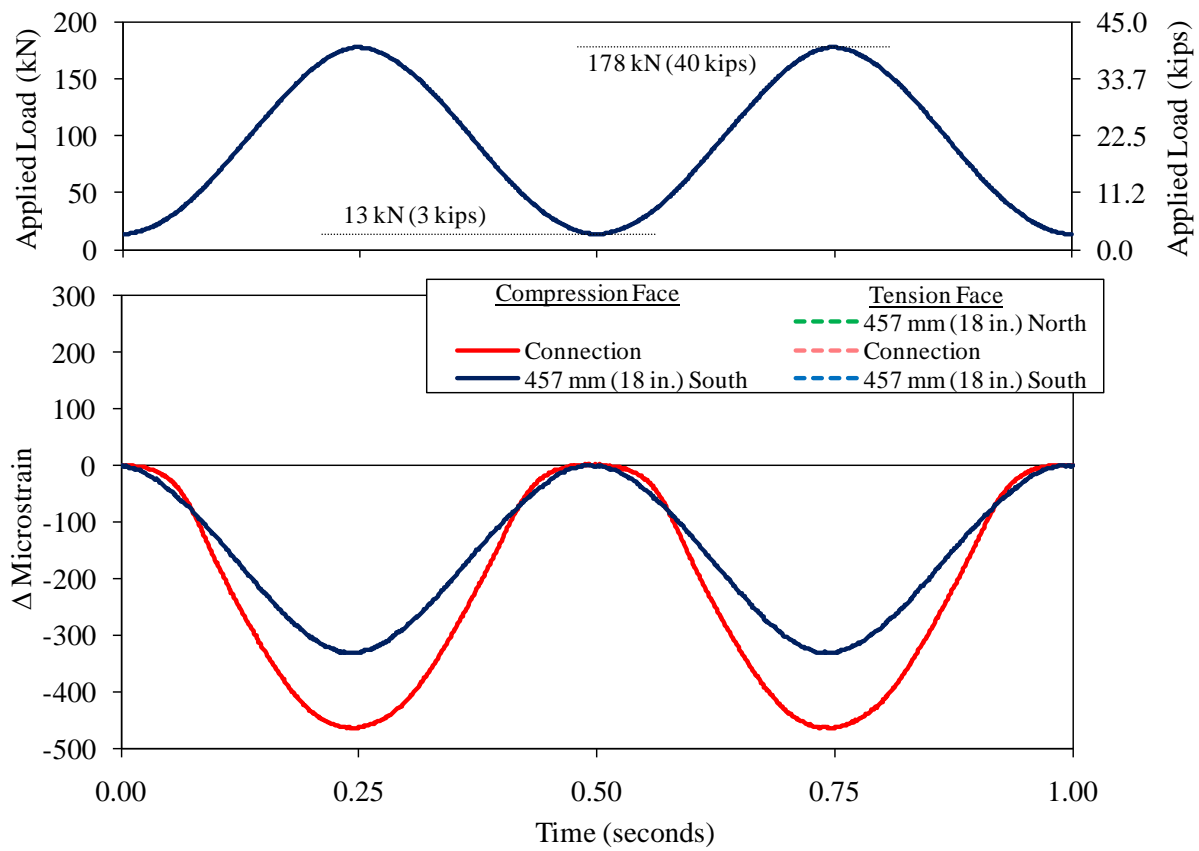
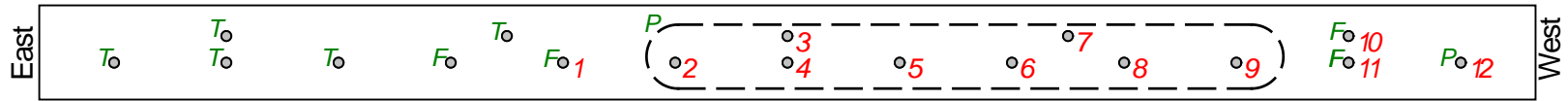
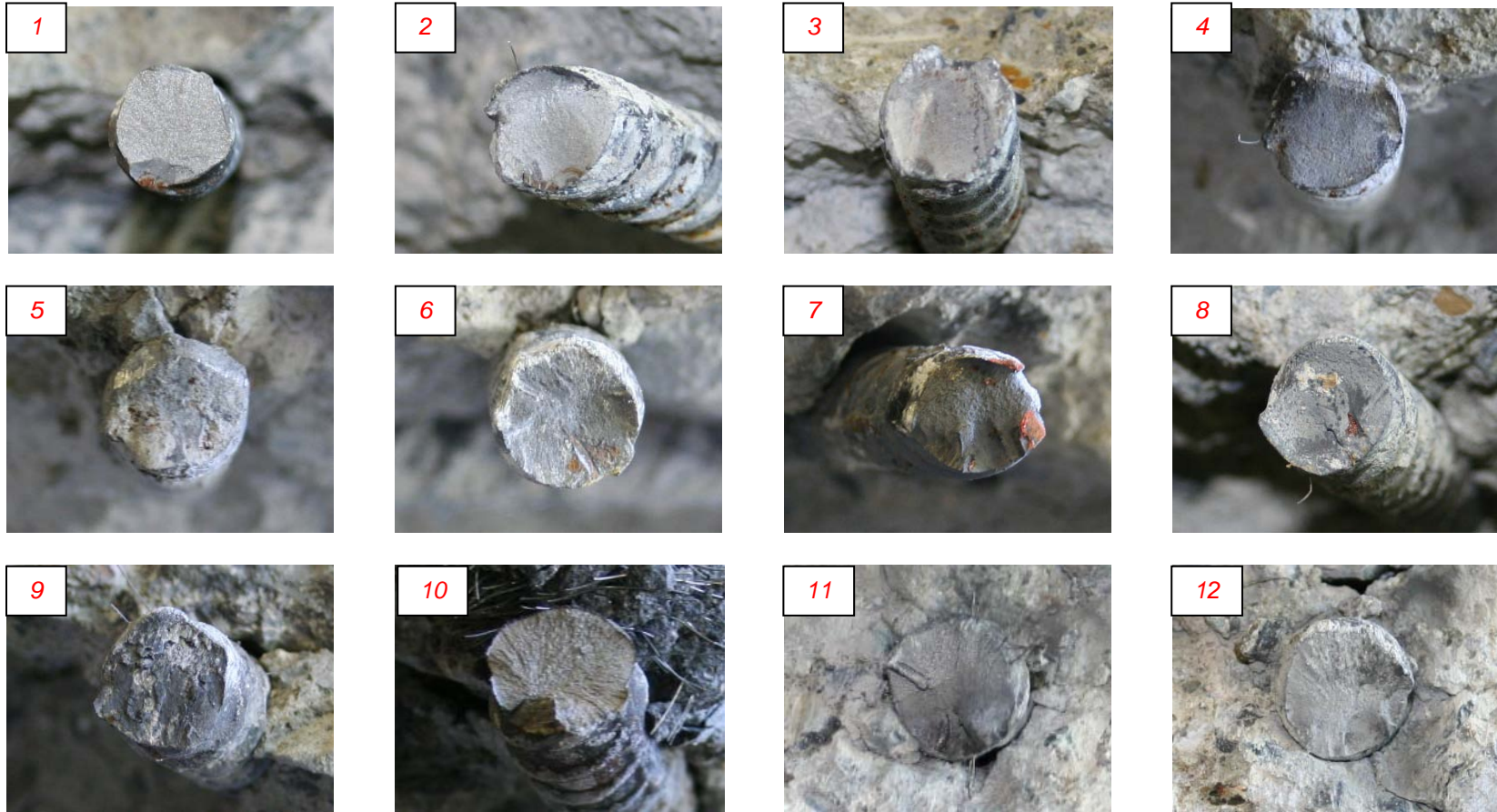


**Figure 81. Graph. Strain response for panel 6B after 190,000 cycles to 178 kN (40 kips).**



Note: Number adjacent to rebar (e.g., 1, 2, etc.) refers to photograph shown below.  
 General classification of rebar end condition indicated by *F* for fractured, *P* for fractured and pounded, and *T* for torched.



95

Figure 82. Illustration. Cross section at rebar failure plane for panel 6B including photographs of twelve of the rebar.

## LONGITUDINAL CONNECTION TEST COMPILATION OF RESULTS

The body of results generated through the two longitudinal connection tests can be summarized into a set of overall observations. These observations pertain to the general concept of using field-cast UHPC in longitudinal connections between precast concrete modular components.

Large flexural stresses oriented perpendicular to a field-cast UHPC connection will not necessarily result in debonding of the field-cast UHPC from the modular component HPC at the connection interface. In the two specimens tested, interface debonding was observed in one of the specimens, while HPC panel cracking was observed approximately 50 mm (2 inch) away from the connection in the other specimen. The different loading protocols followed for the two specimens may have influenced the observed results. Large, rapidly applied overloads may be more likely to cause interface cracking.

No evidence of rebar debonding was observed subsequent to the large overload which was applied to specimen 6B. During the subsequent 11.5 million cycles of structural loading at increasing load levels, there was no indication of lapped rebar debond within the field-cast UHPC connection. Aside from causing HPC, UHPC, and interface cracking, the overload, which caused significant structural damage to the specimen and was 60 percent of the ultimate capacity of the specimen as measured in the static testing of specimen 6H, was not observed to cause any fundamental change in the structural performance of the connection.

The development length of straight, black 16M (#5) mild steel reinforcing bars in this test program was demonstrated to be equal to or less than 150 mm (5.9 inch) when lapped within the field-cast UHPC connection. The cyclic loading of specimen 6B demonstrated that, when sufficiently large amplitude cyclic loads were applied, the stress range in the rebar was sufficient to force the rebar to fail via metal fatigue. The stress range conservatively calculated to exist in the rebar crossing the eventual failure interface was commensurate with the stress range known to cause metal fatigue failure in reinforcing bars.

No water leakage through the specimen was observed during the cyclic loading of specimen 6H or during the initial two cyclic load levels applied to specimen 6B. Water leakage along the interface and in the precast panels was observed near the conclusion of the 1.1 million cycles of loading to 142 kN (32 kips) applied to specimen 6B. This cyclically applied loading regime was sufficient to cause the tensile cracks observed on the underside of the specimen to extend to the top surface of the panel. Given the behavior of mild steel reinforced cast-in-place bridge decks, it is expected that wheel loads imparting flexural stresses larger than the tensile cracking strength of the concrete will cause cracking that extends to near the compression face of the member. Further extension of these cracks can be caused by many factors, including wheel loads applied in other nearby locations, thermal effects on the bridge, long-term dimensional instability in the deck or supporting elements, etc. Leakage through a deck, whether precast or cast-in-place, is symptomatic of global and local behaviors of bridge decks. Although a field-cast material which bonds well to precast components will alleviate one potential source of leakage, it cannot guarantee a leak-free deck.

In continuous bridge structures, negative moments can be induced in regions near supporting substructure elements resulting in nearly uniform tensile stresses through the depth of the bridge deck. Although not explicitly investigated in the present study, the type of results observed from the longitudinal connection testing can be informative in terms of the anticipated performance of transverse connections in these areas. The longitudinal connection test results demonstrated that reinforcing bars lapped for 150 mm (5.9 inch) across a connection can sustain large stresses that eventually may cause metal fatigue failure of the rebar; however, no debonding of these straight mild steel reinforcing bars from the surrounding field-cast UHPC would be anticipated.



## CHAPTER 5. CONCLUSIONS

### INTRODUCTION

The research program discussed herein focused on assessing the structural performance of field-cast UHPC connections for bridge deck components. Bridge deck components simulating both longitudinal and transverse connections were fabricated and tested under cyclic and static wheel patch loadings. The four transverse connection specimens simulated the connections between precast deck panels. These specimens were identical aside from the different discrete reinforcing details, which included straight lapped bars, headed bars, and intersecting hoop bars. The two longitudinal connection specimens simulated the connections between the top flanges of deck-bulb-tee girders. These two specimens were identical aside from the inclusion of two different discrete reinforcing details, namely straight lapped bars and lapped headed bars.

This loading program was designed to allow for the assessment of three critical behaviors. First, the cyclic loading below the cracking load allowed for the assessment of the cracking performance of the field-cast UHPC and the bonding performance of the UHPC to precast concrete interface. Second, the cyclic loading which generated stresses above the static cracking stress allowed for the assessment of the cracking performance of the system, including whether there was any uncontrolled, progressive cracking or any interface debonding. Finally, this loading program allowed for the assessment of the static overload performance of the system, thus providing an indication of whether the system effectively emulated the performance anticipated from a monolithic concrete deck.

Conclusions resulting from this study are presented below. A brief discussion of ongoing and future research related to this topic is presented immediately thereafter.

### CONCLUSIONS

The following conclusions are presented based on the research presented in this report.

1. Each of the four discrete reinforcement details tested in the transverse connection tests is anticipated to perform acceptably in the field. These details were not engaged during the cyclic loading program due to the good interface bonding between the precast HPC and the field-cast UHPC. The test setup and loadings applied in this program, although severe, did not result in any UHPC or interface cracks which were parallel to the connection. The performance of longitudinal connection specimen 6B containing straight lapped bars indicates that a simple detail such as that contained in transverse connection specimen 8B should exhibit acceptable structural performance in the field.
2. The structural behavior of the transverse connections tested herein emulated or surpassed the behaviors that would be anticipated from a monolithic concrete bridge deck. The cyclic responses demonstrated favorable cracking behavior with no interface debonding. The static loadings to failure resulted in global flexural failure of the simply-supported panels. The field-cast UHPC connections provided a limited additional amount of strength and stiffness due to the enhanced UHPC mechanical properties during elastic and early inelastic behaviors. Subsequently, the specimens behaved as passively

reinforced concrete slabs, with behaviors progressing through cracking, rebar yielding, and eventual concrete crushing.

3. The discrete reinforcing details included in the UHPC connections tested in this study are not susceptible to debonding from the UHPC under loads such as applied in this test program. No evidence of rebar debonding was observed in any of the longitudinal or transverse connection specimens. The most heavily stressed specimen, 6B, was subjected to a large static overload followed by 11.5 million subsequent cycles of structural loading at increasing load levels. The overload and subsequent cycling were not observed to cause any debonding of the straight lengths of rebar in the non-contact lap splice connection.
4. The development length of straight, black 16M (#5) mild steel reinforcing bars in this test program was demonstrated to be equal to or less than 150 mm (5.9 inch) when lapped within a field-cast UHPC connection and subjected to flexural tensile loads. The cyclic loading of specimen 6B demonstrated that, when sufficiently large amplitude cyclic loads are applied, the stress range in the rebar can be sufficient to force the rebar to fail via metal fatigue.
5. Structural cracks oriented perpendicular to a field-cast UHPC connection tend to follow straight across the connection and do not turn to run along the interface. In the tests simulating transverse connections between precast components, the structural loads applied throughout the test program caused flexural tensile cracking perpendicular to the connection along midspan on the tensile face of each of the specimens. No interface cracking was observed in any of the transverse connection specimens during cyclic loading. The static loading of these specimens to failure caused minor secondary cracking along the interface in some specimens in heavily cracked regions under the wheel patch load.
6. Single cracks in conventional concrete precast panels, when encountering the UHPC connection, became multiple, tightly-spaced cracks in the field-cast UHPC. After passing through the UHPC connection, the crack again became a single crack in the HPC precast panel. Crack widths were commensurate with the cracking behavior of the parent materials. In a general sense, an individual HPC panel crack of a given width will lead into a set of approximately ten cracks in the field-cast UHPC, each of which are on the order of ten times narrower than the adjacent HPC crack.
7. The cracking behavior of the precast panels and the field-cast UHPC is not significantly affected by the repeated applications of loads near, but below, the static cracking load. In transverse connection tests, the cracking load of the specimens was demonstrated to be greater than 71 kN (16 kips) and less than 95 kN (21.3 kips). Cyclic application of structural loading for at least 2 million cycles to 71 kN (16 kips) did not result in any structural cracking in three of the four specimens, while the fourth specimen developed minor intermittent flexure cracks. The first subsequent loading cycle to 95 kN (21.3 kips) caused clear, discrete flexural cracking in each of the specimens.

8. The repeated application of structural loading just above the cracking load does not significantly affect the structural performance of the field-cast UHPC connection. First application of a load peaking at 95 kN (21.3 kips) generally caused flexural cracking of the transverse connection test specimens. The cracking stabilized during the early portion of this cyclic loading. Cracking patterns and crack widths were not observed to be significantly affected by the continued application of cyclic loads through at least 5 million cycles to this load level.
9. Due to the support and loading conditions applied to the subcomponent specimens, the cyclic loads applied generated stresses more severe than would traditionally be observed in a concrete bridge deck under similar magnitude wheel loads. A simple analytical study focused on the behavior of the transverse connection specimens suggests that the testing configuration implemented herein with loads peaking at 71 kN (16 kips) generated elastic stresses which are similar to the stresses that might be observed in a conventional concrete deck spanning 3 m (10 feet) between adjacent girders and loaded to a peak wheel patch load of 125 kN (28 kips).
10. Large flexural stresses oriented perpendicular to a field-cast UHPC connection will not necessarily result in debonding of the field-cast UHPC from the modular component HPC at the connection interface. In the two longitudinal connection specimens tested, interface debonding was observed in one of the specimens, while HPC panel cracking was observed approximately 50 mm (2 inch) away from the connection in the other specimen.
11. Precast panels connected by field-cast UHPC connections are neither susceptible nor immune to water leakage through the deck. The favorable bond performance observed between the precast panels and the field-cast UHPC in transverse connection tests indicates that this bridge decking system is not likely to leak along the connection interface under cyclic service loads or static overloads. The longitudinal connection tests indicate that the connection interface may or may not crack under loads which surpass the one-way bending flexural cracking capacity of the panel. Regardless of the connection orientation, structural loadings which surpass the flexural cracking strength of the deck will likely cause cracks which extend up to near the top surface of the deck and create a situation wherein eventual water leakage is likely. This behavior is identical to that observed in conventional cast-in-place concrete bridge decks. Leakage through a deck, whether precast with connections or cast-in-place, is symptomatic of global and local behaviors of bridge decks. Although a field-cast material which bonds well to precast components will alleviate one potential source of leakage, it cannot guarantee a leak-free deck.

## **ONGOING AND FUTURE RESEARCH**

The results of this study demonstrate that advanced cementitious composite materials provide a viable solution for completing the field-cast connection between prefabricated bridge elements. Further study of this topic is currently underway within the FHWA Structural Concrete Research Program. A research program aimed at facilitating the widespread deployment of modular component bridge construction/reconstruction technologies was initiated in 2010. Modular

components can provide higher quality, accelerated, and safer construction; however, greater offsite prefabrication of bridge components necessitates an increased reliance on the long-term performance of field-installed connections. Of foremost interest is the performance of deck-level connections for decked girder and deck panel components. Connections have often proved lacking, resulting in less than desirable overall system performance. Enhancing the performance of deck level connections will be the focus of this study.

Deck-level connections have been installed on the U.S. highway system, analyzed for in service performance, and researched for decades. This study is intended to build upon these prior efforts by engaging the state-of-the-practice and the state-of-the-art in a broad effort aimed at advancing the use of modular components. The study may overlap other ongoing work around the U.S., as State Departments of Transportations and other funding agencies promote this important field of study. The advancements developed through other studies are being carefully considered for inclusion in the study.

The study will focus on many aspects of connection design, construction, and performance, thus revealing areas that need improvement. Material testing on a range of field-cast cementitious materials will include traditional as well as emulative tests. Significant effort will be focused on full-scale testing of connections to realistically assess the structural performance. Component-scale testing will likely be included in the study when a clear link is identified between the component and the full-scale performance.

This research project can be divided into two phases which are already underway, and a third phase which is being developed. The first two phases are intended to lay the groundwork for an expanded, flexible third phase which specifically addresses existing shortcomings and develops field-deployable solutions.

The first phase of the research focuses on the materials used between precast bridge components. This part of the study is looking into seven different materials for use in precast construction. This includes a typical deck concrete, two different non-shrink cementitious grouts, ultra-high performance concrete, epoxy grout, magnesium ammonium phosphate grout, and post-tensioning cable grout. Each material will undergo a series of tests, including standard ASTM tests on compressive strength, shrinkage, modulus of elasticity, and tensile strength, and non-standardized tests focusing on early age strength gain and shrinkage rates. In addition, tests focusing on the bond strength between the materials and the deck concrete will be conducted. The outcome of these tests will be a direct comparison of the relevant properties of the seven different materials.

The second phase of research focuses on the rebar bond within a closure pour during staged construction. The longitudinal closure pour between two prefabricated sections of a bridge may undergo differential movement due to traffic loads. While the closure pour connection is setting, these movements may affect the connection strength between the two precast parts. The bond strength within closure pours is being tested with a series of bond pull-out tests. These tests will investigate the frequency and magnitude of vibrations within the connection. A variety of materials will also be tested to determine if the fluidity and set time affect the bond. The results from the tests will be compared to the bond results from a standard deck concrete with no vibrations applied.

The third phase of the research is aimed at investigating the performance of the best available field-cast closure pour materials in full scale structural tests of bridge components. The connections between full depth precast panels are the first item of study. The focus will be on cast-in-place connections that can be easily and quickly assembled. A series of connections will be assembled on a full scale two girder, two span system. This will provide information on the connections on simple spans and continuous spans. Both the deck-level connections between components and composite connections to supporting superstructure elements will be investigated. The systems will be tested under cyclical truck loads to determine long term behavior.

A second part of this third phase will likely focus on the longitudinal connections between bulb tees and box girders. Full size, single span systems will be constructed and tested. Both cast-in-place and post-tensioned methods may be investigated. A series of connecting methods will be tested in the longitudinal and lateral direction under cyclical loading.

Expansion or modification of the study beyond the specific items listed above is possible. The goal of the program is to develop, verify, and prepare for deployment a set of connection details which remedy existing concerns associated with the use of modular construction.



## REFERENCES

1. Graybeal, B., "Material Property Characterization of Ultra-High Performance Concrete," Federal Highway Administration, Report No. FHWA-HRT-06-103, August 2006, 186 pp.
2. Aarup, B., J. Karlsen, and G. Lindström, "Fiber Reinforced High Performance Concrete for In-Situ Cast Joints," *Proceedings, PCI/FHWA/FIB International Symposium on High Performance Concrete*, Orlando, Florida, September 2000, 9 pp.
3. Hansen, L., and B. Jensen, "A New Building System Using Joints of Ultra High-Strength Fibre Reinforced Concrete," *Innovation in Concrete Structures: Design and Construction*, 1999, pp. 543-552, Dundee.
4. Nielsen, C., J. Olesen, and B. Aarup, "Effects of Fibres on the Bond Strength of High Strength Concrete," BHP96 Fourth International Symposium on Utilization of High-Strength/High-Performance Concrete, May 1996, Paris, France.
5. Aarup, B., and B. Jensen, "Bond Properties of High Strength Fiber Reinforced Concrete," *Bond and Development of Reinforcement*, ACI Publication SP-180, 1998, pp. 459-472.
6. Broo, H., and M. Broo, "Fog av högpresterande fiberbetong i prefabricerad brobanaplatta," examensarbete 97:2, Chalmers Tekniska Högskola, avd. för Betongbyggnad. (in Swedish, "Joint of High Performance Fiber Reinforced Concrete in Precast Bridge Slabs")
7. Harryson, P., "Böjprovning av fog i högpresterande fiberbetong för prefabricerade brobanepaltor, statisk belastning," rapport 99:1, Chalmers Tekniska Högskola, avd. för Betonbyggnad. (in Swedish, "Bending Test of Joint in High Performance Fiber Reinforced Concrete for Precast Bridge Slabs, Static Loading")
8. Harryson, P., "Utmattningsprovning av fog i högpresterande fiberbetong för prefabricerade brobanepaltor," rapport 00:2, Chalmers Tekniska Högskola, avd. för Betongbyggnad. (in Swedish, "Fatigue Test of Joint in High Performance Fiber Reinforced Concrete for Precast Bridge Slabs")
9. National Cooperative Highway Research Program, "Full-Depth Precast Concrete Bridge Deck Panel Systems," NCHRP Report 584, Transportation Research Board, Washington DC, 2008.
10. Li, L., J. Ma, and R. Oesterle, "Improved Longitudinal Joint Details in Decked For Accelerated Bridge Construction: Concept Development," *ASCE Journal of Bridge Engineering*, V. 15, No. 3, May-June 2010, p. 327-336.
11. Li, L., J. Ma, and R. Oesterle, "Improved Longitudinal Joint Details in Decked For Accelerated Bridge Construction: Fatigue Evaluation," *ASCE Journal of Bridge Engineering*, V. 15, No. 5, September-October 2010, p. 511-522.
12. National Cooperative Highway Research Program, "Cast-in-Place Concrete Connections for Precast Deck Systems," Transportation Research Board, Washington DC, report under review.
13. ASTM C39, "Standard Test Method for Compressive Strength of Cylindrical Concrete Specimens," American Society for Testing and Materials Standard Practice C39, Philadelphia, PA, 2001.

14. ASTM C469, "Standard Test Method for Static Modulus of Elasticity and Poisson's Ratio of Concrete in Compression," American Society for Testing and Materials Standard Practice C469, Philadelphia, Pennsylvania, 2002.
15. Helgason, T., J. Hanson, N. Somes, W. G. Corley, and E. Hognestad, "Fatigue Strength of High-Yield Reinforcing Bars," Portland Cement Association Research and Development Bulletin RD045.01E, 1976.